Università Politecnica delle Marche
Corso di Dottorato di Ricerca in Ingegneria Civile, Ambientale, Edile e Architettura
Curriculum in Ingegneria Civile, Ambientale, Edile e Architettura

---

External Dissipative Rocking System

Ph.D. Dissertation of:

Laura Gioiella

Advisor:

Prof. Fabrizio Gara

Co-Advisor:

Alessandro Balducci

Curriculum Supervisor:

Prof. Stefano Lenci

XXIX cycle

Università Politecnica delle Marche
Corso di Dottorato di Ricerca in Ingegneria Civile, Ambientale, Edile e Architettura
Curriculum in Ingegneria Civile, Ambientale, Edile e Architettura

---

External Dissipative Rocking System

Ph.D. Dissertation of:

Laura Gioiella

Advisor:

Prof. Fabrizio Gara

Co-Advisor:

Alessandro Balducci

Curriculum Supervisor:

Prof. Stefano Lenci

XXIX cycle

Università Politecnica delle Marche
Dipartimento di Ingegneria, Civile, Edile e Architettura
Via Brecce Bianche — 60131 - Ancona, Italy

Acknowledgments

I wish to thank Professor Andrea Dall'Asta and PhD Enrico Tubaldi for their time and patience and for the great opportunity to work with them during these years.

I am thankful to Professor Fabrizio Gara for his support during all my PhD activity.

I would like to thank Professor Luigino Dezi and Alessandro Balducci for giving me the chance to accomplish this PhD course.

Finally, I would like to thank all the staff of the Department I.C.E.A for supporting me through these years.

I am grateful to Marco, this work is for him.

Contents

List of Figures

List of Tables

Abstract

In this thesis the seismic performance of existing buildings frames coupled with an external dissipative rocking system is investigated; the arrangement consists of a steel truss, hinged at the foundation level, whose rocking motion promotes the dissipation of energy via viscous dampers located at the base. Under the assumption of linear elastic behaviour of both the frame and the dissipative structure, the equation of motion of the system are presented, together with a generalized Single Degree of Freedom (S-DOF) approximation of the system. This way, analysis through time-domain and frequency-domain are allowed for the investigation of the system dynamic behaviour.

Time-domain analysis, based on a state space approach, leads to the complex modal analysis of the coupled system, which allows the evaluation of the influence of the added damping and of the displacements linearization, promoted by the external dissipative rocking system, on both the dynamic behaviour and the seismic response. In particular, the proposed formulation permits to evaluate separately the contribution of each of the complex vibration modes of the system to the global seismic response. On the other hand frequency-domain analysis is particularly useful for the problem under investigation because it allows to work with an algebraic system rather than a differential one. Furthermore by representing the seismic input in terms of a stationary stochastic process, a relation can be established between the Power Spectral Density (PSD) of the input and that of the response parameters of interest via harmonic analysis of the system.

The performance of two case studies is evaluated by means of parametric analysis, involving added damping and stiffness, either through time- and frequency-domain. Finally, some aspects which need a deeper investigation are presented. Among them the evaluation and comparison between linear and non-linear fluid viscous dampers, dimensioned through dissipated energy criterion. The performance of the analyzed dissipative system, is compared with an alternative retrofitting configuration, consisting in the coupling with external stiff contrasting structure, known in literature as mass proportional damping system. At the end a first insight on the effects of Soil-Structure-Interaction (SSI), through the substructure approach, is provided.

Keywords: Passive Seismic Protection, External Seismic Retrofit, Rocking Motion, Fluid Viscous Dampers, Dissipative Tower.

Sommario

Questa tesi ha l'obiettivo di indagare il comportamento dinamico e sismico di edifici esistenti protetti con un sistema esterno di dissipazione basato sul rocking; esso è costituito da una struttura reticolare in acciaio, incernierata a livello di fondazione, il cui movimento oscillante attiva la dissipazione di energia, per mezzo di smorzatori viscosi situati alla base. Nell'ipotesi di comportamento elastico lineare sia del telaio, che della struttura dissipativa, vengono presentate l'equazione del moto del sistema accoppiato ed una generalizzazione del sistema ad un grado di libertà. Per risolvere il problema dinamico è possibile condurre analisi sia nel dominio del tempo, che in quello delle frequenze.

La soluzione nel dominio del tempo si basa su una formulazione alle variabili di stato che, tramite analisi modale complessa del sistema telaio da proteggere-struttura esterna di protezione passiva, permette di valutare l'influenza, sia sul comportamento dinamico che in termini di risposta sismica, dello smorzamento e della linearizzazione degli spostamenti forniti dalla struttura dissipativa. In particolare, la formulazione proposta, consente di valutare separatamente il contributo di ciascuno dei modi di vibrazione complessi del sistema sulla risposta sismica globale. Le analisi armoniche nel dominio delle frequenze, invece, sono particolarmente utili in quanto consentono di lavorare con un sistema algebrico piuttosto che differenziale. Inoltre, scegliendo di rappresentare l'input sismico come un processo stocastico stazionario, è possibile stabilire una relazione tra la densità spettrale di potenza (PSD) dell'input esterno e quella dei parametri di risposta di interesse, tramite analisi armonica del sistema.

Le prestazioni di due casi di studio sono valutate mediante analisi parametriche, riguardanti diversi livelli di smorzamento e rigidezza del sistema di protezione, sia con analisi nel tempo che in frequenza. Infine vengono presentati alcuni aspetti che necessitano di ulteriore approfondimento. Tra di essi la valutazione ed il confronto della performance sismica di smorzatori viscosi a comportamento lineare e non, dimensionati attraverso il criterio di uguaglianza dell'energia dissipata. Le prestazioni del sistema di protezione passiva indagato, vengono confrontate con un'altra configurazione esterna, che prevede l'accoppiamento del telaio con una struttura rigida di contrasto, nota in letteratura come sistema di smorzamento proporzionale alle masse. Infine viene condotta una prima analisi degli effetti dell'interazione terreno-struttura (SSI), mediante l'approccio alle sottostrutture.

Keywords: Sistemi Passivi di Protezione Sismica, Adeguamento Esterno, Moto di Rocking, Dissipatori Viscosi, Torri Dissipative.

Introduction

The challenge of gaining the seismic protection of both new and existing structures is a very current problem nowadays in Italy; not only for recent frequent seismic crises (L'Aquila 2009, Emilia 2012, central Italy 2016) with related losses in terms of human beings, but above all for the poor quality of a large part of the building heritage. Within it r.c. frame buildings built without seismic standards or with details inadequate to modern codes can be considered. In case of severe earthquakes, the poor quality of many structures can leads to more losses in terms of lives and of architectural and historical goods and to high socio-economic costs related to factories downtime. Hence the necessity of doing interventions towards seismic protection is a very fascinating target.

Towards the goal of the achievement of the seismic protection Performance Based Design Approach has become the design philosophy in the last few years. This method relates the performance objectives of a structure to the probability of occurrence of earthquakes, therefore different Limit States (LS), as a function of the importance of the facility itself; the aim is to avoid catastrophic failures, loss of lives and keep the construction costs under control. This means that strategical structures, like hospitals, fire stations or schools are expected to remain functional immediately after a severe earthquake, while basic facilities must still be able to sustain gravity loads even though they can undergo severe damages to the frame members. Hence structures are evaluated also through an economic point of view, in terms of costs for the society, keeping in mind that, for mission-critical structures, the structural cost it is just a small percentage of the overall cost, which also accounts for contents and non structural components. The performance achievement can be guaranteed through many techniques, which can be either traditional, Capacity Design, or more recent, like Seismic Isolation and/or Passive Supplemental Damping. In the recent past, many studies have proven the efficiency of passive control systems (Soong and Dargush 1997, Soong and Spencer 2002, Christopoulos and Filiatrault 2006).

Within Passive Supplemental Damping field there are many structural configurations available based on the use of different devices, that can be grouped into three main categories: hysteretic dampers, viscous and visco-elastic dampers and recentering systems (smart materials or post-tensioned mechanisms based on rocking motion). Traditionally passive damping devices are installed within a building frame in either diagonal or chevron brace configurations connecting adjacent storeys; dynamic properties of the damped system

and design methods have been implemented through many studies (e.g. Whittle et al. 2012, Di Cesare et al. 2012, Ponzo et al. 2012 Hwang et al. 2013, Lavan et al. 2013, Dall'Asta et al. 2016). Nevertheless this type of damping system may present some disadvantages, especially when employed for the retrofit of existing buildings, like the increase of internal actions in the columns with induced premature local failures (Freddi et al. 2012), the need of localized strengthening of foundations and the indirect costs related to the interruption and/or relocation of internal activities, which are significant especially for relevant structures. Therefore the use of external passive control system is becoming more and more frequent thanks to the fact that their interferences with existing frames, internal activities and related indirect costs, are notably reduced. Among the external intervention possibilities there is also the coupling of two adjacent buildings by placing dampers between them; the efficiency of this solution is guaranteed if the two structures have strongly different dynamic behaviours (Gattulli et al. 2013, Tubaldi et al. 2014, Tubaldi 2015).

This thesis seeks to investigate the dynamic behaviour of an alternative retrofit configuration, which can be called external dissipative rocking system. The proposed system, permits to gain the seismic protection of an existing frame building by exploiting the rocking motion of a stiff brace hinged at the foundation level to activate fluid viscous dampers (FVD), located at the base, for the energy dissipation. The rocking configuration can be used either in planar and spatial arrangements. Recently, some applications of such kind of systems have been developed (Roia et al. 2013, Roia et al. 2014) and are known as "dissipative towers", which is a patented solution (Balducci 2005).

Even if spherical hinges and viscous dampers are already widely employed in civil engineering applications and rocking motion is usually associated to recentering systems, the main objective of this thesis is to investigate the dynamic behaviour and the seismic response of frame buildings protected by means of the external dissipative rocking system. To reach this target the analysis of the dynamic performance in terms of modal properties is conducted, with a separate evaluation of stiffness and damping contribution. It is important to specify that the stiffness addition has to be intended only in terms of linearization of the displacements distribution. The seismic response is evaluated via modal decomposition method, through the monitoring of relevant engineering demand parameters (EDPs). With the aim to provide some useful tools necessary to the design of the system, which are already available for traditional retrofitting techniques, it is necessary to identify an optimal tower-to-frame stiffness ratio range, which is a meaningful parameter of the effectiveness of the linearization of displacements distribution. For what concern damping contribution it is important to check if the estimate of damping ratio obtained by employing approximate formula reported in current codes, can be valid also for the design of devices located at the base of the dissipative system. Moreover it is also necessary to identify the range in which the damping provided by the rocking system is effective.

Once defined the thesis objectives it is necessary to identify the way to reach them; for this purpose a formulation involving the coupling with the external dissipative rocking system is proposed and the related equation of motion is stated in matrices form. It is noteworthy that the proposed formulation is defined in general terms, therefore can be useful also for other external passive control systems. To find a solution to the dynamic problem, two alternative ways are shown, the first one is through time-domain, while the second is through frequency domain.

The thesis dissertation is organized in seven chapters, Chapter 1 provides an overview of the seismic passive control systems available. A brief recall on principal damping devices preludes to the possible structural configurations description and related state of the art. Finally the investigated system, external dissipative rocking system, is introduced.

In Chapter 2 the main features of the analyzed system are shown. The effects of added stiffness are explained in terms of linearization of displacements distribution along the building height, before and after the coupling, for two limit configurations: a shear-type structure and a cantilever frame. The problem formulation is stated in matrix forms and the equation of motion are presented, assuming that the existing frame and the external dissipative rocking structure exhibit a linear elastic behaviour. Moreover, proposed formulation accounts for the non-classical damped nature of the coupled system due to the concentrated location of the dampers at the base of the dissipative system. The equation of motion for a generalized SDOF approximation, dealing with the limit case of coupling with an infinitely stiff rocking system, is shown. For this particular configuration the displacements field is constrained through the base rotation of the bracing. Two ways to find a solution for the dynamic problem are introduced, the first one deals with Time-domain analysis and is presented in terms of a state-space formulation; the second one deals with Frequency domain analysis. Finally an alternative formulation, proposed by Chu et al. 2009, which provides an extension to the concept of participant mass ratios related to underdamped complex and conjugate modes and over damped modes, is introduced.

In Chapter 3 two case studies are analyzed to exhibit the capability of the proposed formulation to investigate the dynamic behaviour of the coupled system existing building external dissipative rocking bracing. The first one is a seven storey benchmark structure, Van Nuys Building, already used as a testbed by the Pacific Earthquake Engineering Research Center (PEER) and widely analyzed thanks to the fact that this building was equipped with accelerometers and recording instruments since 1971 and it was struck by several earthquakes (e.g. San Fernando 1971 and Northridge 1994). The second case study is a five storey r.c. frame structure, representative of many buildings built in Italy during the '80s without seismic detailing, which is assumed to be located in Camerino, a small town in central Italy very close to the epicentre of the Marche-Umbria 1997 and central Italy 2016 earthquakes, therefore representative of an area characterized by an high seismic hazard. For both the two case studies modelling criteria and seismic hazards are introduced.

In Chapter 4 the modal properties of the coupled system, existing frame plus external dissipative rocking system, are highlighted for the two case studies and the variations of both the contributions, that is stiffness and damping, are separately analyzed. First of all the effect of added stiffness is shown on the interstorey drifts distribution and on the shear action resisted by the frame along the building height. Parametric analysis are also performed by varying the tower-to-frame stiffness ratio. The effects of increasing level of added damping are also evaluated through the monitoring of deformed shapes and damping ratios associated to each vibration mode.

In Chapter 5 the seismic responses of the two analyzed case studies are shown and their performance is evaluated through monitoring of engineering demand parameters (EDP's), i.e. displacements and interstorey drifts, which are representative of the structural and non structural damages; shear actions distribution, for the monitoring of new and existing foundations; velocities and absolute accelerations whose monitoring is important for the contents. Moreover everything dealing with viscous dampers (displacements, velocities, axial actions and viscous bending moment) which are representative of their costs and

necessary for the design of the external bracings foundations. The higher order modes contribution on the overall responses are also evaluated.

Chapter 6 illustrates a frequency domain analysis of the seismic problem. This type of analysis is particularly useful for the problem at hand because it allows to work with an algebraic system rather than a differential one. Another advantage of working in the frequency domain is that by representing the seismic input in terms of a stationary stochastic process, a relation can be established between the Power Spectral Density (PSD) of the input and that of the response parameters of interest via harmonic analysis of the system.

Chapter 7 deals with further issues, involving the analyzed system, required for a complete analysis of its potentialities. Preliminary results of the main open problems are shown. Among them the performance of non-linear fluid viscous dampers, dimensioned through equating dissipated energy criterion, for a given Limit State (LS). A comparison of the performance of an alternative external configuration is evaluated for the Van Nuys building case study, by assuming the same contribution of added damping (ξ=30%). The alternative solution consists in the coupling with external stiff contrasting structure, known in literature as mass proportional damping system. Finally a first insight on the effects of Soil-Structure-Interaction (SSI), through the substructure approach, is provided for the Van Nuys building case study.

Chapter 1

Seismic Passive Control Systems

The achievement of the seismic protection of both new and existing structures is an important target for structural engineers, since it permits to avoid catastrophic losses and guarantee human beings protection. Moreover, in the last thirty years the awareness that the question does not involve only structural engineers, but also owners and the overall community is becoming more and more strong.

When a severe earthquake hits a country the cost is not only related to loss of life, but also to loss of architectural and historical goods and even to high socio-economic costs related to services and factories downtime and moreover to the cost of repair, which could be extremely high. Thus the concepts of performance and, more in detail, expected performance have been introduced, together with a design philosophy known as Performance Based Design.

Performance Based Design approach is a general philosophy according to which design criteria of structures are expressed as stated performance to reach for stated probabilities of occurrence of earthquakes. The performance target can be represented by any response parameter related to a certain threshold, because a single design parameter may not provide an adequate control of all the performance objectives for structural and non-structural components. The Performance Based Design method arises from the evaluation and upgrade process for existing buildings and its origin derives from Applied Technology Council ATC-33 project, sponsored in the USA by the Federal Emergency Management Agency (FEMA), for the development of a national guidelines for the seismic retrofit of buildings, then adopted and extended to the design of new buildings by Structural Engineers Association of California (SEAOC) in its Vision 2000 project. This approach aims not only to relate performance objectives of both structural and non structural elements, expressed as acceptable levels of damage, with the earthquake occurrence probability, but also to adjust them as a function of the importance of the structure in itself. The result is a performance-based design matrix shown in Figure 1-1 and adapted from the Vision 2000, SEAOC. Table 1-1 derives from the same document and relates performance levels to interstorey drift ratios and structural and non-structural damages description. Similarly, Table 1-2 reports the earthquake classification based on the definition of both return period as the average time span between shaking intensity that is equal to or greater

than a specified value, and probability of exceedance, which is the annual frequency of exceeding a given intensity.

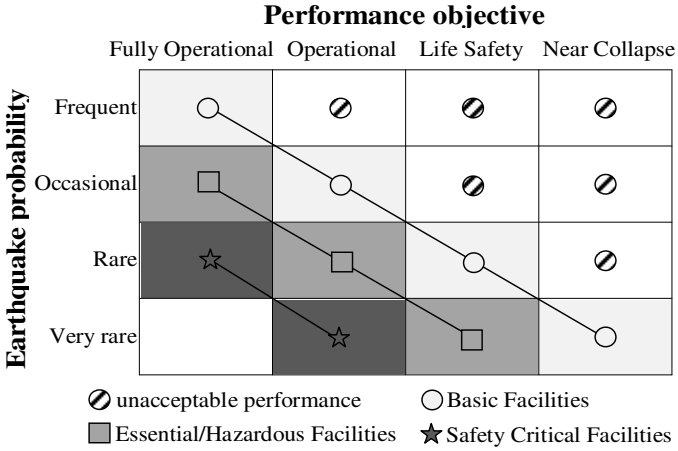

Figure 1-1 Performance Based Design matrix

Table 1-1 Interstorey drift-performance level relationship from Vision 2000 SEAOC

Performance level	*Drift %*	*Description*
Fully Operational	0.2	Continuous service. Negligible structural and non-structural damage.
Operational	0.5	Most operations and functions can resume immediately. Structure safe for occupancy. Essential operations protected, non-essential operations disrupted. Repair required to restore some non-essential services. Damage is light.
Life Safety	1.5	Damage is moderate, but structure remains stable. Selected building systems, features or contents may be protected from damage. Life safety is generally protected. Building may be evacuated following earthquake. Repair possible, but may be economically impractical.
Near Collapse	2.5	Damage severe, but structural collapse prevented. Non-structural elements may fall.

Table 1-2 Earthquake hazard levels from Vision 2000 SEAOC

Earthquake classification	*Return Period* [years]	*Probability of exceedance*
Frequent	43	50% in 30 years
Occasional	72	50% in 50 years
Rare	475	10% in 50 years
Very rare	970	5% in 50 years

Hence it is observable that strategical structures, like hospitals, fire stations or schools are expected to remain functional immediately after a severe earthquakes, while basic facilities must still be able to sustain gravity loads even though they can undergo severe damages to the frame members, therefore their repair is not convenient. This leads also to an economical evaluation of structures in terms of overall cost, keeping in mind that, for essential structures, the structural cost it is just a small percentage of the overall cost. Taghavi and Miranda proposed an accurate evaluation of this concept in their report *Response assessment of non-structural building elements* (PEER 2003) from which Figure 1-2 derives. The comparison of the structural, non structural and contents cost is provided for three kind of structures, an office, an hotel and an hospital. In general, the structural cost is limited into 20% and the percentage is even more reduced for the hospital case, where the cost of contents is highly significant. It is noteworthy that the non structural components represent the major cost (nearly higher than 50%).

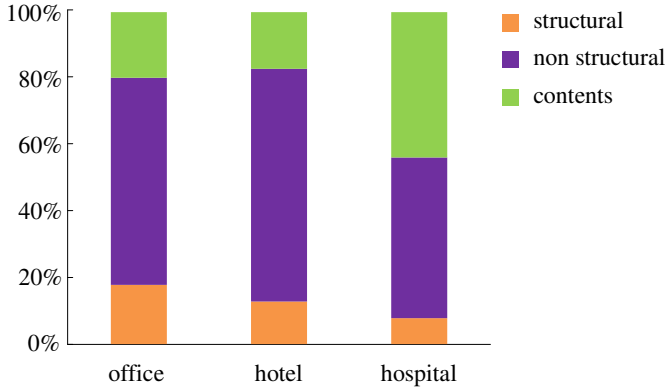

Figure 1-2 Cost components comparison among offices, hotels and hospitals proposed by Taghavi and Miranda 2003

The seismic protection of structures can be guaranteed through traditional techniques, like Capacity Design, or other solutions like Passive Control Systems, which do not need of external power sources to provide their contributions. Among them:

1 Seismic Isolation;
2 Passive Supplemental Damping.

Capacity Design is a design approach wherein the structure is configured to concentrate yielding and inelastic behavior in specific locations, plastic hinges, where elements are detailed to reliably exhibit such behavior, and which, through their ductile behavior, limit the demands on other portions of the structure that are designed with sufficient strength to remain essentially elastic during earthquake response, as shown by the sketch of Figure 1-3 (a). Capacity Design technique is usually related to the seismic design of basic facilities, while for the design and retrofit of strategic structures, like hospitals or schools, which must exhibit higher levels of performance (operational or fully operational for a rare earthquakes) the use of seismic isolation or passive supplemental damping is expected. Supplemental damping devices and/or seismic isolation are thought to be able to dissipate energy introduced in a system by seismic actions, instead of the frame members. Figure 1-3 (b) shows a possible configuration for supplemental damping devices, which are activated by the frame movement, while Figure 1-3 (c) depicts schematically seismic isolators, which

are located among the foundations and the superstructure, and whose task is to decouple motion between the ground and the frames.

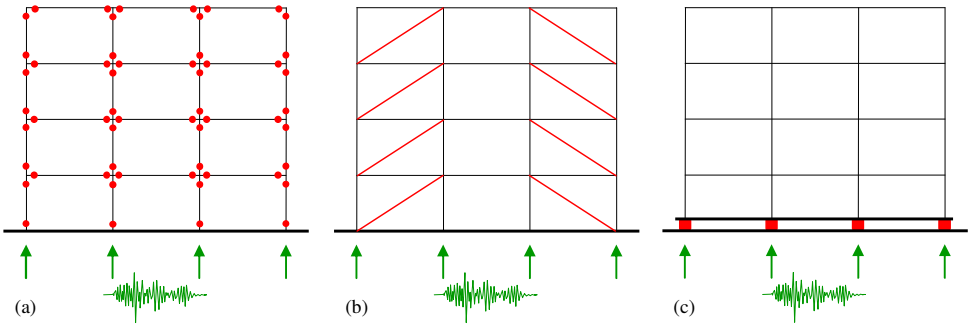

Figure 1-3 Seismic protection techniques: (a) Capacity Design, (b) Supplemental Dampers, (c) Seismic Isolation

Seismic actions effects on a structure can be seen through an energy balance formulation as the one reported in Eqn. (1-1):

$$E_I = E_k + E_s + E_v + E_h \qquad (1\text{-}1)$$

where E_I denotes earthquake input energy transmitted to a structure depending on its inherent properties, i.e. period of vibration; E_k is the kinetic energy produced by structural masses as a reaction to the seismic input energy; E_s is the strain energy related to elements elastic deformation; E_v is the viscous damping energy representative of the dissipated amount of energy, thanks to the inherent damping of the structure and or to supplemental viscous dampers action; E_h is the hysteretic energy related to structural deformation in the inelastic range (damages), hence symbolizes energy dissipated by means of plastic hinges in the frame members. Supplemental damping, therefore, can be seen as a way to prevent structural members from damaging, while seismic isolation has to be seen as a way to reduce the amount of input energy entering in the structure, through the lengthening of the fundamental period.

1.1 Seismic isolation

Seismic isolation concept consists of decoupling the motion, induced by a seismic excitation, between the structure and the ground. Isolators can be of different types, but all characterized by a high vertical stiffness to sustain vertical loads and low lateral one, with respect to that of the superstructure, which leads to the lengthening of the structural system fundamental period. As a consequence, a simultaneous reduction of the absolute accelerations and a major request in terms of displacements are evident, as shown in Figure 1-4. To enhance the performance of the isolation system it is possible to use a combination of isolators and dampers, which provides a supplemental control of the total amount of displacements.

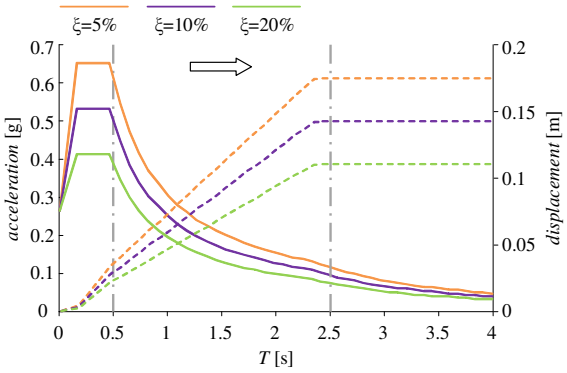

Figure 1-4 Lengthening of the fundamental period due to seismic isolation

The main advantage of an isolation system is the high reduction of damage to structural and non-structural elements and to contents, with related savings in case of strong earthquake hitting essential structures. Moreover isolators provides a response regularization, especially in the case of irregular structures as those which displays torsional coupling; the superstructure members do not require special design of detailing, thanks to the fact that no plastic hinges are expected.

Usually isolators are placed under a very thick slab and over the supports, so they can be readily checked or substituted and maintenance operations are greatly simplified with respect to bracings, that are installed within the frames. On the other hand bidirectional seismic gaps are needed due to the displacements required, furthermore isolation effectiveness is reduced in the case of tall buildings and there are some design problem related to light upper structures like wooden and/or steel structural systems.

There are two main types of isolators which are widely used: laminated-rubber bearings and friction pendulum system (FPS). Elastomeric isolators are self-centering devices, they display an high stiffness for ordinary conditions, which is the same in the two main horizontal directions. Their performance is less influenced by time-dependence and their dimension is governed by gravity loads (axial action), lateral stiffness and by the maximum relative displacements between bearings upper and lower base (geometrical relationship). To enhance damping properties of elastomeric bearings a cylindrical lead core can be inserted in the isolator centre, which can yields for shear actions. Figure 1-5 (a) depicts the components of a rubber isolator (without lead core), while Figure 1-5 (b) displays a typical force-shear deformation hysteretic loop.

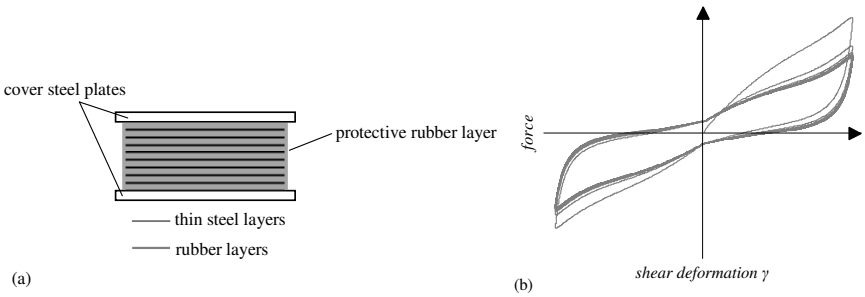

Figure 1-5 Elastomeric bearing: (a) scheme, (b) force-shear deformation hysteretic loop

Friction pendulum isolators (FPSs), differently from elastomeric bearings, can have diverse periods between the two main directions of analysis, moreover they use gravity as a restoring force. Their stiffness is proportional to masses and their period do not depend on the structure features. This type of isolator may have some drawbacks, because they are partially restoring and they can have some problems with static friction with the consequence of a different behaviour than the predicted one. Figure 1-6 (a) and (b) display a double surface FPS and a dissipative friction rigid plastic hardening loop, respectively; in Figure 1-6 (b) μ denotes friction coefficient and W is the weight acting on the isolator.

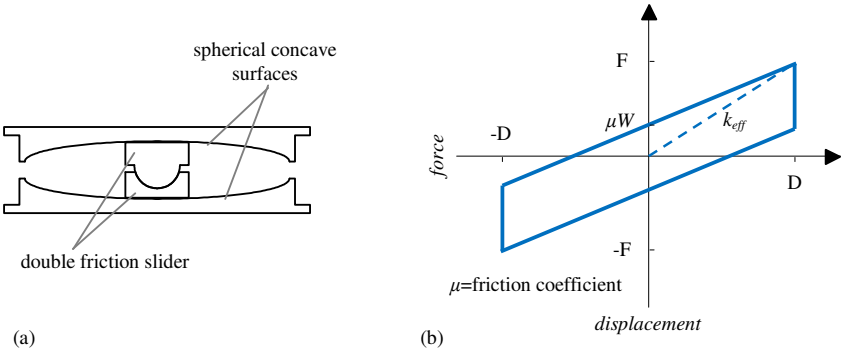

Figure 1-6 FPS: (a) double surface scheme, (b) force-displacement loop

1.2 Passive supplemental dampers

Supplemental dampers, whose efficiency in dissipating energy is expressed by the area included in one complete cycle of vibration, can be divided into three main categories:

1 Hysteretic Dampers;
2 Viscous and Visco-elastic Dampers;
3 Recentering systems.

The latter category is based on flag-shaped model for energy dissipation that can be achieved either by shape memories alloys and by post-tensioned rocking mechanisms.

1.2.1 *Hysteretic Dampers*

Hysteretic dampers are activated by relative displacements between connection points, among them there are friction devices, elasto-plastic and elasto-plastic hardening devices. Usually forces produced by these dampers are in phase with structural internal ones; their main positive features are a high dissipative capacity, a reduced economic cost and the fact that they are not velocity-, neither temperature-dependent. On the other hand, there are some uncertainties related to the time-dependent performance of friction devices, while the others need to be substituted after a certain number of cycles due to the low cyclic fatigue.

Figure 1-7 (a), (b) and (c) depicts hysteretic devices vibration cycles, where u denotes displacements and F_d dissipative forces.

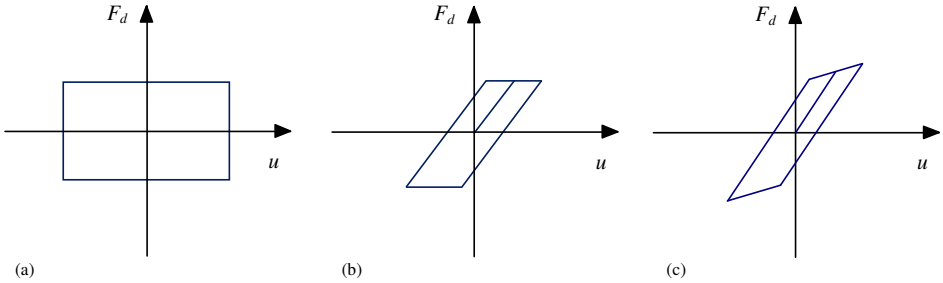

Figure 1-7 Hysteretic dampers cycles: (a) friction, (b) elasto-plastic, (c) elasto-plastic hardening

1.2.2 *Viscous and Visco-elastic Dampers*

The second category of passive supplemental damping devices is represented by either visco-elastic and viscous dampers. Visco-elastic dampers are able to provide not only a velocity-dependent force, which adds supplemental damping to the structure, but also an elastic displacement-dependent force which allows the restoring of the system. Therefore visco-elastic dampers provids not only an enhancement of damping, but also an increasing in the stiffness of the overall structure, which could lead to higher values of absolute accelerations for the frames to protect (Figure 1-8). Whereas viscous dampers provides only a velocity-dependent force (based on the relative value of velocity between the two ends of the device), so, in order to guarantee recentering they need to be coupled with a structure providing restoring force. Viscous dampers do not need of substitution after seismic events, because they are able to experience a very high number of cycles.

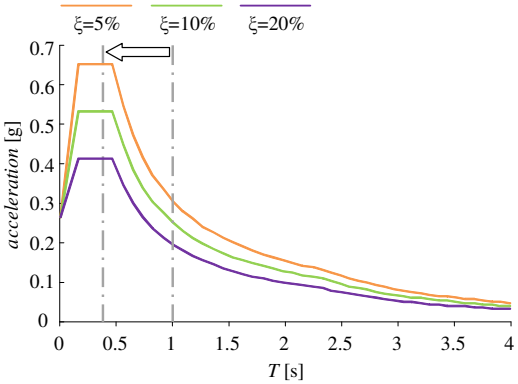

Figure 1-8 Effects of visco-elastic devices on the period of a structure

Figure 1-9 (a) depicts a visco-elastic device acting in shear, Figure 1-9 (b) shows a typical hysteretic cycle where it appears that maximum value of force is slightly out of phase with the maximum value of displacements.

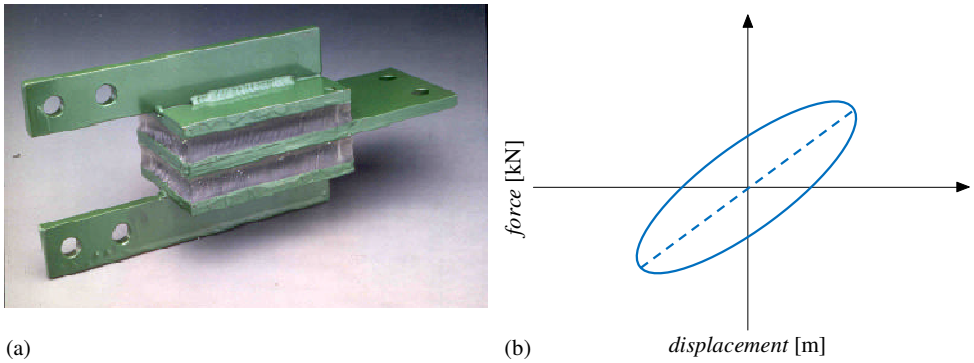

(a) (b)

Figure 1-9 Visco-elastic damper acting in shear (a), force-displacement cycle (b)

Fluid viscous dampers (FVDs) are particularly of interest not only for their features and their widely diffusion across Europe and North America, but also because they are an essential element of the dissipative rocking system, subject of this thesis. Forces produced by FVDs are related to velocities by the expression reported in Eqn. (1-2)

$$F_d = C_\alpha \left|\dot{u}^\alpha\right| \mathrm{sgn}\left(\dot{u}^\alpha\right) \qquad (1\text{-}2)$$

where F_d denotes damper dissipative axial force, C_α is the damping constant, $\dot{u}$ is the relative velocity between the two ends of the device and α is the exponent whose value determines the linear or non linear behaviour of the damper; when α is equal to unity there is a linear dependence between force and velocity. Usually for civil engineering applications α=1. Figure 1-10 (a) shows a FVD scheme and it is observable that this kind of device consists of a stainless steel piston with a bronze orifice head, filled with silicone oil. The piston head utilizes specially shaped orifices that alter the flow characteristics with fluid relative velocity; the force produced by the damper is generated by the pressure differential across the piston head, as well explained by Christopoulos and Filiatrault 2006. Figure 1-10 (b) displays force-velocity curves at various level of the exponent α and it is clear that non linear viscous dampers with α<1, display smaller forces for high values of velocity and higher displacements, with respect to linear FVD (α=1).

Figure 1-11 displays a comparison of the force-displacement loop for decreasing values of the exponent α, starting from unity, which means linear behaviour, until the value of α=0. It is evident that for α=1 the loop has an elliptical shape with the highest values of forces corresponding to the smallest values of displacements and vice versa. Generally for decreasing values of α forces generated by non-linear FVDs are still out of phase with those developed by the structure, but their cyclic response approaches the rectangular load-displacement shape of hysteretic dampers (limit case of α=0). Anyway, non-linear FVDs still exhibit forces that are linearly proportional to the damping constant C_α to the power of α and to the displacements amplitude.

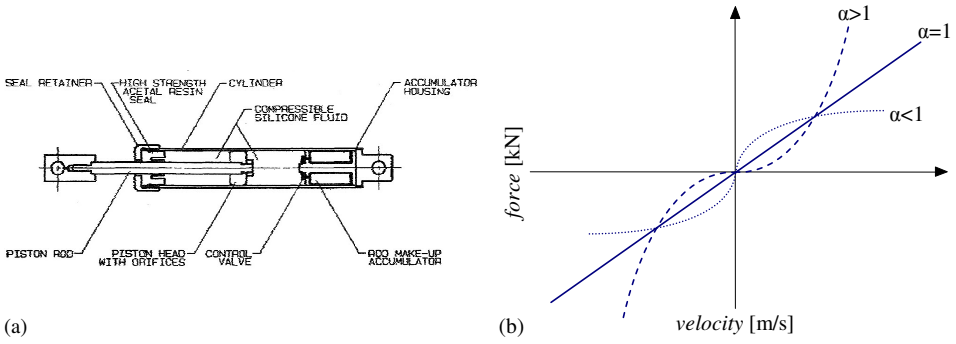

Figure 1-10 FVD scheme (a), force-velocity curves for linear and non-linear FVDs (b)

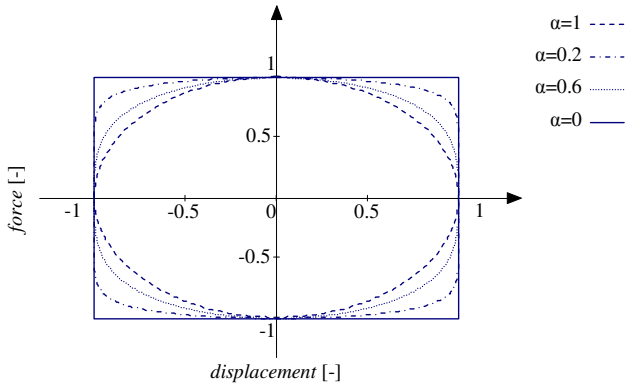

Figure 1-11 Force-displacement loops for linear and non-linear FVDs

1.2.3 *Recentering systems*

Recentering systems are characterized by a flag-shaped loop, as the one depicted in Figure 1-12; this behaviour can be achieved principally in two ways, that is through shape memory alloys or through devices based on articulated mechanisms that aim to provide both energy dissipation and recentering. By observing the flag-shaped loop of Figure 1-12, where u denotes displacements and F_d dissipative forces, it is noteworthy that the amount of dissipated energy is reduced, when compared with an elasto-plastic hysteretic device, but the self-centering system returns to zero-force, zero-displacement position, not only at every cycle, but also at the end the seismic action.

Shape memory alloys (SMA) are a class of materials able to develop the so-called super-elastic behaviour; they are principally made of different metals, like nickel, titanium, zinc, copper and aluminium. Super-elastic behaviour is a process that involves the changing in chemical phases when the temperature of the alloying is increased, resulting in an hysteretic effect with near zero residual strain, as shown in Figure 1-12.

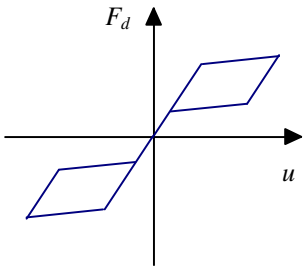

Figure 1-12 Flag-Shaped hysteresis loop

An example of self-centering device is the Energy Dissipating Restraint (EDR) (Nims et al. 1993), shown in Figure 1-13. EDR incorporates a sliding friction mechanism with an internal end stop, limiting the range of motion. The friction develops at the interface between the bronze wedges and the steel cylinder, while an additive stiffness is provided by a helical spring coaxial to the steel cylinder.

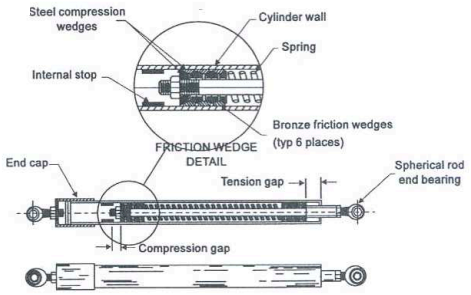

Figure 1-13 EDR device proposed by Nims et al. 1993

Recently, a new Self-Centering Energy Dissipative (SCED) steel brace (Christopoulos et al. 2008) was proposed; this system involves element of traditional steel bracings, a dissipative mechanism and a tensioning system, used to provide a prestress to the SCED. This system is developed to exhibit the flag-shaped loop, undergoing large axial deformations, providing energy dissipation capacity and a self-centering behaviour. A concept of SCED device is reported in Figure 1-14.

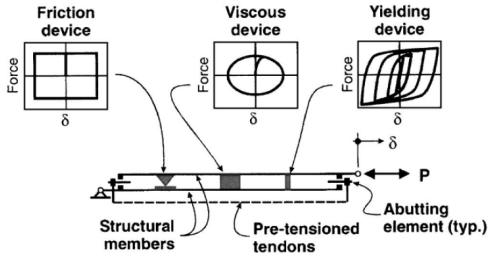

Figure 1-14 SCED system proposed by Christopoulos et al. (2008)

1.3 Supplemental damping: structural configurations

The seismic protection of new constructions and especially existing structures can be achieved thanks to the use of passive control systems, introduced in previous sections. The efficiency of these systems is proved in many studies, involving comprehension and theoretical analysis of their behaviour, developments in the state of the art and illustrations of some practical applications (Song and Constantinou 1994, Song and Dargush 1997, Song and Spencer 2002, Christopoulos and Filiatrault 2006, Ragni et al 2009). Moreover in the last three decades theoretical studies have been supported by experimental analysis, laboratory tests and, in some cases, by the observation of their performances during seismic events. All these efforts have been done to make the research community more and more confident with passive control systems and able to improve their wide diffusion and application to practical engineers too, especially in seismic regions prone, like North America, Europe and Japan over all.

This section aims to provide a state of the art of the possible structural configurations of passive supplemental damping systems, with a particular attention reserved to configurations exploiting FVDs and/or rocking motion, in order to contextualize the dissipative rocking system, subject of this dissertation. It is noteworthy that there is a high flexibility in the choice of the arrangement of the supplemental damping systems and various configurations can be characterized by different kinematic behaviours. In general, almost all of them permit to control the total amount of dissipated energy and the deformations at different storeys.

A first configuration is based on the use of Tuned-Mass Damper (TMD) system, which aims to limit the displacements of the structure to protect, through the movement of an auxiliary mass. The input energy is dissipated through a damper which connects the main structure with the auxiliary mass. Hence TMD can be seen as a secondary mass-spring-dashpot system connected to the main structure (Figure 1-15) so as to be in resonance with a specified period of the building to protect, usually the fundamental one, but out of phase with it. In such a way, when the structure is subjected to a seismic action, the TMD is able to divert input energy from the main structure to itself and dissipation is realized through inertia forces applied by TMD on the main frame. Usually these kind of devices are installed on the roof and are active also against wind actions, in the case of tall buildings. To exploit their function, TMDs need a large mass, even though it is just a portion of the total mass of the main structure and due to the fact that TMDs are in resonance with the frame, there is also the need of a sufficiently large smooth surface for displacements without friction phenomenon.

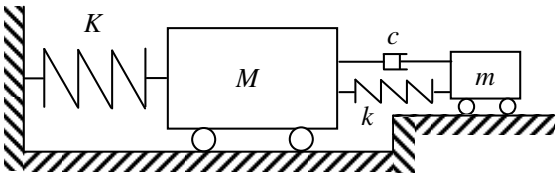

Figure 1-15 Scheme of an undamped SDOF (primary structure) connected to a TMD

FVDs have proven their efficiency in various configurations. In the late '80s in Japan a new solution, based on viscous damping walls (VD walls), was proposed, analyzed and tested (Arima et al. 1988, Symans and Constantinou 1988). Both the behaviour and the structure of the system are depicted in Figure 1-16; VD wall consists, essentially, of two main components: an external protective part and an internal damping one. The internal one is composed of an inner steel plate hanging from the upper floor, an external steel case fixed to the lower floor in which the inner plate is enclosed and where it can slide and finally an high viscous fluid which fills the external case. The external protective part is a cover, realized with fireproof materials or reinforced concrete, which aims to avoid damages due to fire or impacts. VD walls were applied in 1992 for the retrofit of the SUT Building in Shizuka, Japan, an r.c. frame of 78 m height; the retrofit system provides a supplemental damping nearly equal to 20%.

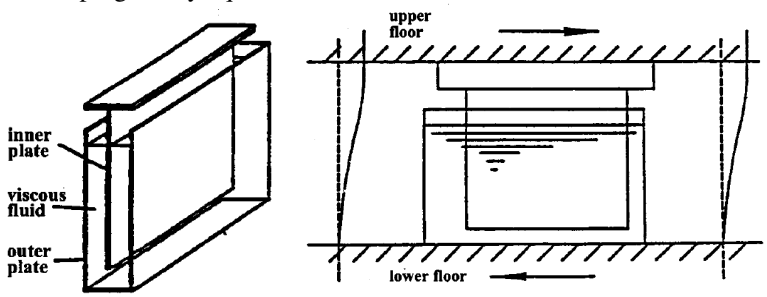

Figure 1-16 VD Walls proposed by Arima et al. 1988

FVDs have been traditionally used installed within a building frame, in either diagonal or chevron brace configurations connecting adjacent storeys, as shown in Figure 1-17 (a) and (b). A well detailed description of such practical applications is provided by Symans and Constantinou (1998). Specific studies, concerning the dynamic properties of the damped system, comparisons of distribution methods and criteria for the design, have been implemented and improved recently (e.g. Whittle et al. 2012, Di Cesare et al. 2012, Ponzo et al. 2012, Hwang et al. 2013, Lavan and Avishur 2013, Tubaldi et al. 2014, Passoni et al. 20014, Tubaldi et al. 2015, Dall'Asta et al. 2016). FVDs do not interfere with the period of an existing structure, nor with its stiffness, while elastic or visco-elastic braces provide an increment in terms of stiffness, which leads to a displacements reduction but, at the same time, also to major accelerations, which are dangerous for contents. Thanks to the addition of supplemental damping, FVDs provide a reduction of both displacements and accelerations, however they may present some disadvantages, particularly when employed for the retrofit of existing buildings. Usually, the addition of dissipative diagonals in existing frames provides an increment of axial forces in the columns and this may lead to premature local failures (Freddi et al. 2012). Furthermore, there may be some feasibility limits on the strengthening of the existing foundations at the base of the bracing system and finally, the indirect costs related to the interruption of the building utilization during the execution of the retrofit can be very demanding, in particular for strategic buildings, such as hospitals or schools.

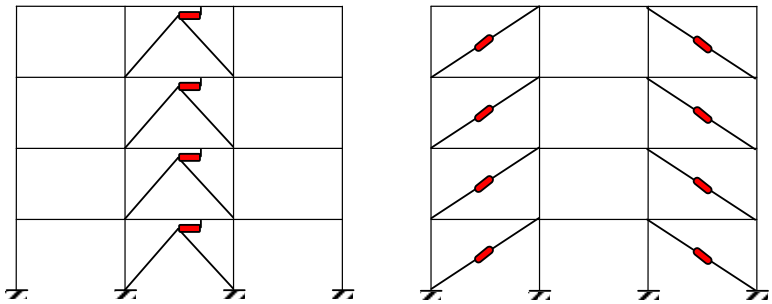

(a) (b)

Figure 1-17 FVD traditional installations within the frames (a) chevron braces, (b) diagonal braces

The use of external damper configurations, i.e. placing the dissipative bracings and the relevant foundations outside the building frame, provides some advantages. Among them, external structures could also host elevators or emergency stairs, thereby providing accessory benefits like the building upgrading to safety and accessibility standards and, at the same time, allowing an architectural redevelopment. The arrangement of the dampers in a new structure greatly simplifies the inspection, maintenance and replacement process. Finally, the external system is easily removable, and permits to restore the building to its original state. Anyway external solutions can be feasible only in the case of available spaces around the structure to protect, as for standalone buildings, and advantages in terms of seismic performance need to be proven.

External dampers and bracing components can be arranged in very different three-dimensional or planar configurations; a possible solution is provided by the insertion of FVDs into the frames of a ventilated facade (Figure 1-18 (a)), providing, thereby, the achievement of the seismic protection and the upgrading from an energetic point of view. Otherwise FVDs can be installed into external planar bracings, properly connected to the existing structure and specialized to work for just one of the two main directions (Figure 1-18 (b)).

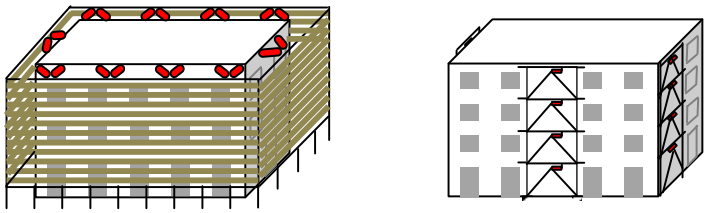

(a) (b)

Figure 1-18 External alternative FVDs configurations: (a) inserted into a ventilated facade, (b) installed within planar bracing connected to the building

FVDs can also be used for the coupling with external structures, as in the case shown in Figure 1-19, where dampers are placed horizontally at the storey level, between the frame and an external stiff structure (Trombetti and Silvestri 2007, Lavan and Abecassis 2015).

This way, the links are activated by the floor absolute displacements. A similar configuration can be obtained by placing the dampers between adjacent buildings, though this solution is efficient if the two buildings have strongly different dynamic properties (Gattulli et al. 2013, Tubaldi 2015).

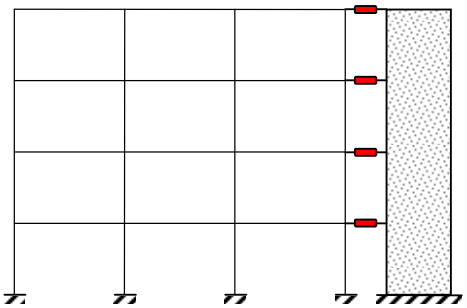

Figure 1-19 Coupling with an external stiff contrasting structure

An alternative solution can be obtained by coupling the frame with an external shear deformable bracing structure (Figure 1-20). The new and the existing structures are connected at the storey level and the dissipative devices are activated by the relative displacements between adjacent floors, as in the more traditional case of bracings placed within the existing structure (Christopoulos and Filiatrault 2006).

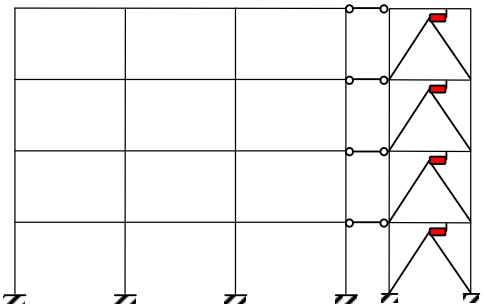

Figure 1-20 Coupling with an external shear deformable bracing structure

An interesting solution, dealing with coupling of shear walls through FVDs, was recently analyzed (Lavan 2012). The author proposed two different configurations of coupling, in the first one FVDs work as the coupling element in coupled shear walls (Figure 1-21 (a)), while in the second dissipative devices are mounted on frames between adjacent floors set in parallel to the wall (Figure 1-21 (b)). Both the two systems are investigated, through planar analysis, by assuming a linear elastic behaviour of all the components. Moreover both the two structural configurations analyzed are partitioned into two subsystems which work in parallel; the first one serves as stiffness system, while the second is the damping system. The efficiency of the proposed solutions is demonstrated for low-rise walls and the benefits are, as expected, the reduction of deformations and wall bending moments. In addition the reduction of absolute accelerations, total base shear and total overturning moments is provided by the proposed configurations.

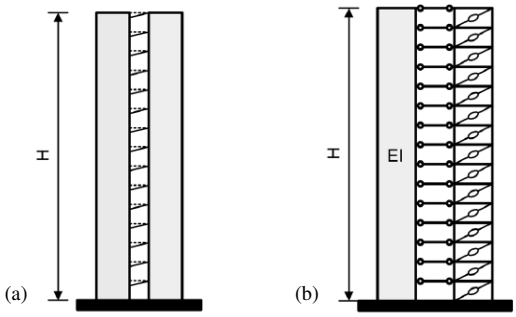

Figure 1-21 FVDs coupling adjacent shear walls (a) wall dissipative bracings set in parallel (b) as proposed by Lavan 2012

Due to the fact that a strong seismic event (mainshock) is often preceded by foreshocks or followed by aftershocks, it can happen that the repair cost associated with downtime, structural and non-structural damages, could be also increased by the fact that a structure can display residual deformations. For this reason in the recent past many studies (e.g. Christopoulos 2002, Christopoulos et al. 2002) have been addressed to exploit self-centering hysteretic systems, like rocking walls, post-tensioned concrete- or steel-moment-resisting frames and shape memory alloys devices, which are all characterized by flag-shaped hysteresis loops, for the seismic protection of new and existing structures. The rocking motion of structures is thought to be a way to prevent them from damages and from residual deformations, when subjected to inertia forces, therefore alternatives solutions based on the coupling of existing frames with rocking structures, even though not always equipped with viscous dampers, have been proposed and herein briefly recalled.

Alavi and Krawinkler (2004) analyzed the effects of adding elastic and inelastic shear walls to reduce maximum storey ductility and drift demand with the aim to protect existing moment-resisting frame against near-fault ground motion effects. The proposed strengthening schemes are based on the coupling with both fixed shear walls and hinged shear walls and results are compared. The performances of dual systems, i.e. existing frame linked at floor levels with shear wall, was evaluated by means of parametric analysis involving walls-to-frame stiffness ratios and the strengthening with hinged walls is proven to be an effective technique in reducing drift demands for both stiff and flexible frames, within the context of the assumption made. The two analyzed configurations are reported in Figure 1-22 (a) and (b).

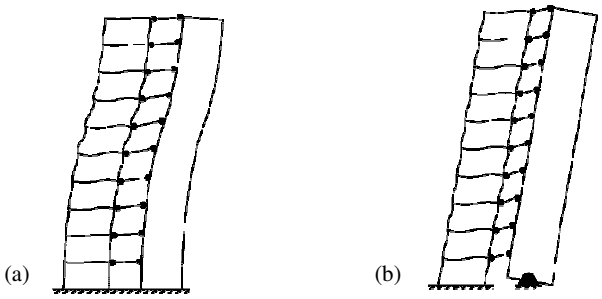

Figure 1-22 Systems analyzed by Alavi and Krawinkler: (a) fixed wall, (b) hinged wall

Ajrab et al. (2004) proposed a scheme for the improvement of the seismic response of rocking shear walls in frame structures. The solution was based on the placement of energy dissipative devices, exploiting for their activations the displacements associated to rocking motions. Figure 1-23 shows the configuration of the proposed rocking wall-frame structure enhanced with supplemental draped tendons equipped with non-linear dampers and fuse elements; it is observable that the tendons arrangement is similar to the overturning moment diagram shape.

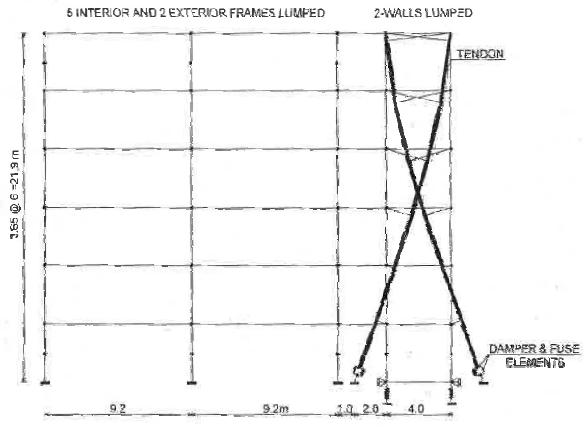

Figure 1-23 Rocking wall-frame structure with supplemental tendon systems proposed by Ajrab et al.

The rocking wall is expected to rock about its toes and it is supported on two bearing elements, which are activated under compression forces and unload elastically with the opening of a gap in tension, that is, under the uplift. The proposed solution performance was evaluated for a specific case study, through parametric analysis involving the level of pretension in the tendons and various base width of the wall. It is observable that the system could provide a significant equivalent viscous damping contribution, nearly 20% together with no damages to structural components, related to seismic actions. On the other hand, there could be some damages to non structural components if the rocking motion leads to large interstorey drifts, which are, anyway, almost uniform.

Marriott et al. (2008) have focused their attention to the performance evaluation of post-tensioned precast rocking wall systems, which could be used as a retrofit technique for existing frame buildings and also for the design of new structures. Figure 1-24 reports a scheme of the proposed configuration, which was evaluated by means of dynamic tests. The precast, post-tensioned rocking wall is equipped with external dissipative devices, which, alternatively, can be fluid viscous dampers, tension-compression yielding steel dampers or a combination of both of them. It is observed that the external devices are located in parallel to post-tensioned tendons which guarantee the system recentering The efficiency of the proposed arrangement was proved against the effects of far-field and velocity-pulse ground motion.

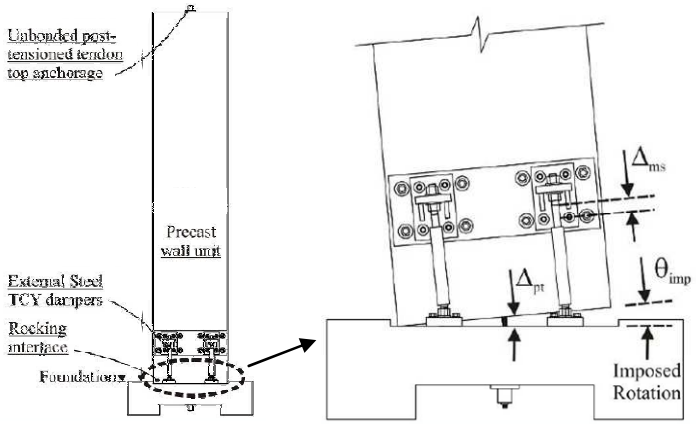

Figure 1-24 Scheme of the precast, post-tensioned rocking wall systems tested by Marriott et al.

Wiebe and Christopoulos (2009) proposed an upgrade to the base-rocking wall systems configuration, in order to reduce the increasing of structural forces throughout the height of a building due to the high order modes effect. Figure 1-25 (a) displays the base-rocking system and a first upgrade which consists in allowing the occurrence of rocking at multiple sections along the height. This improvement do not amplifies the peak displacements of the system, while reduces the bending moment envelope above the base of the wall. Figure 1-25 (b) displays an alternative configurations proposed by Wiebe et al. (2013) again for the mitigation of higher mode effects in base rocking systems. The proposed solution consists of a rocking steel frames equipped with Self-Centering Energy Dissipative (SCED) brace at one or more levels; besides, the rocking of multiple sections along the height is allowed.

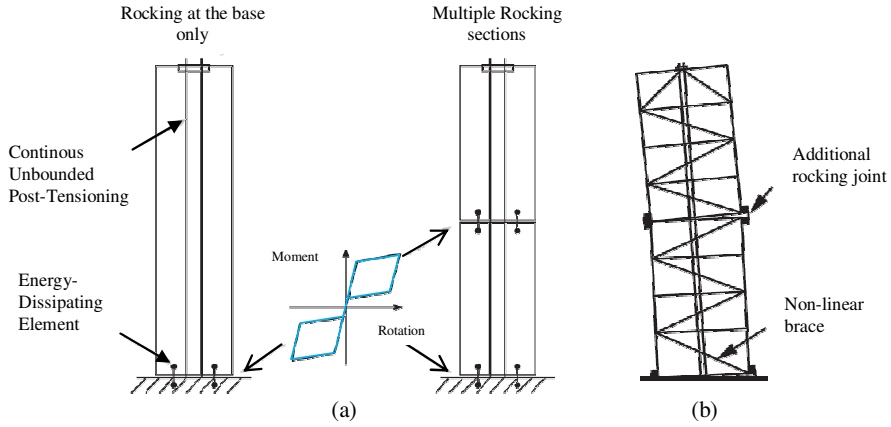

Figure 1-25 Upgrades of the base rocking systems proposed by Wiebe and Christopoulos (a) and by Wiebe et al. (b)

The last configuration dealing with rocking systems is proposed by Wu and Lu (2015) and is very similar to the dissipative rocking system subject of this thesis, presented and described in next chapter, together with the related formulation. Figure 1-26 describes the similar arrangement, which is based on the coupling of an existing r.c. frame structure with a light-weight energy-dissipation rocking frame (EDLRF) equipped with self-centering energy dissipative braces (SCED). As in the case of the dissipative rocking system, EDLRF is an external solution which exploits the rocking motion for the SCEDs activation, which are located in vertical position at the base of the system. Anyway SCED braces, differently from FVDs, provide energy dissipation only for moderate or severe seismic actions; for small actions the light-weight rocking frame provides only added stiffness to the existing structure, therefore this arrangement too provides a double contribution to the existing frame. It is also interesting to observe that a design method is proposed and based on storey stiffness demand.

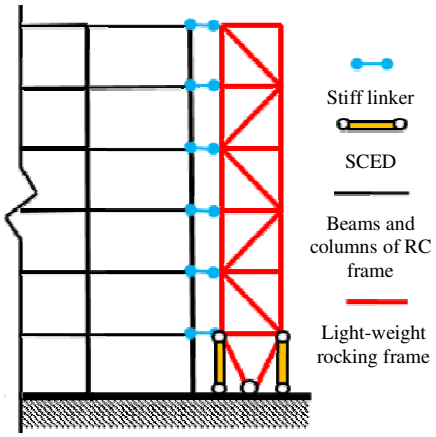

Figure 1-26 EDLRF system proposed by Wu and Lu

Chapter 2

Dissipative rocking system: problem formulation

The external dissipative rocking system, subject of this thesis, is a retrofit solution which exploits the rocking motion of a stiff brace pinned on a spherical hinge at the foundation level to provide a dissipative contribution to the existing frame. Fluid viscous dampers, in fact, are located at the base and are activated by the rotation of the base itself (Figure 2-1). The analyzed arrangement can be, therefore, thought as an articulated mechanism for the dampers activation.

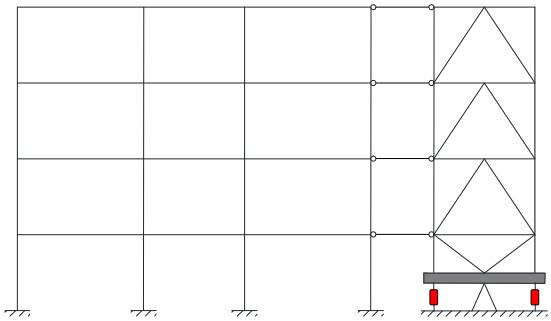

Figure 2-1 External dissipative rocking system

The proposed configuration provides two contributions to the dynamic behaviour of the coupled system, the first one is in terms of stiffness, while the second is in terms of added damping. Stiffness contribution is used for the linearization of displacements distribution along the height of the existing frame, that is why the investigated system is particularly appropriate for the seismic protection of r.c. moment resisting frames designed without seismic standards or with inadequate ductile detailing. Usually this type of structures is characterized by a deformed shape similar to an "S", which shows higher displacements at intermediate storeys. In the case of infinitely stiff external bracing, the dynamic behaviour of the overall system, external bracings-building to protect, would be governed and

completely determined by the knowledge of a single parameter, which is the base rotation φ. Both the motion of the storeys and those of the dampers, in fact, are a function of the base rotation φ, through the heights of the building and through the base dimension of the bracing (Figure 2-2).

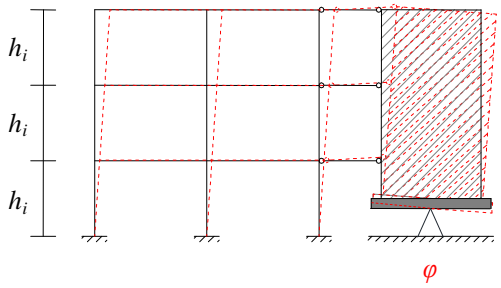

Figure 2-2 Deformed shape of the overall system in the case of infinitely stiff bracing

To better understand the displacements linearization produced by the stiffness of the external bracing, the analysis of the dynamic behaviour of two limit configurations is carried out. In the first case a three elevation shear-type frame is connected with an infinitely stiff undamped bracing. Figure 2-3 (a) depicts the displacements distribution before and after the coupling, while Figure 2-3 (b) depicts the exchange actions due to the mutual interaction between the frame and the rocking system. As expected the bare frame has bigger displacements at lower-intermediate storeys (red line), therefore, to reach the target deformed shape (green line) the external structure acts on the frame with forces that have different signs and that are higher in the middle.

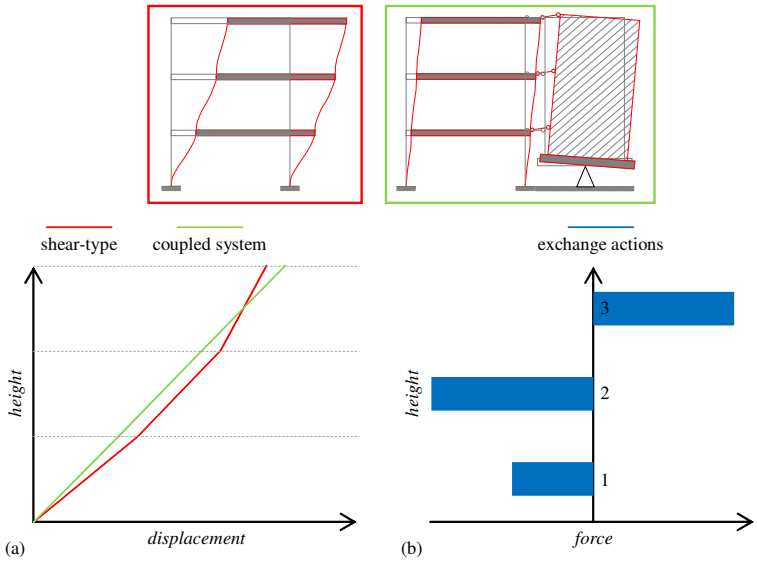

Figure 2-3 Shear-type structure coupled with an infinitely stiff system: (a) modal displacements, (b) exchange actions

Figure 2-4 (a) and (b) shows the results related to the second configuration, which is the coupling between the same infinitely stiff system and a three levels cantilever frame. It can be observed that the bare frame (violet line) shows higher displacement on top. In this latter case the highest value of exchange force is located at the first elevation and the interaction forces have different signs, as shown by Figure 2-4 (b).

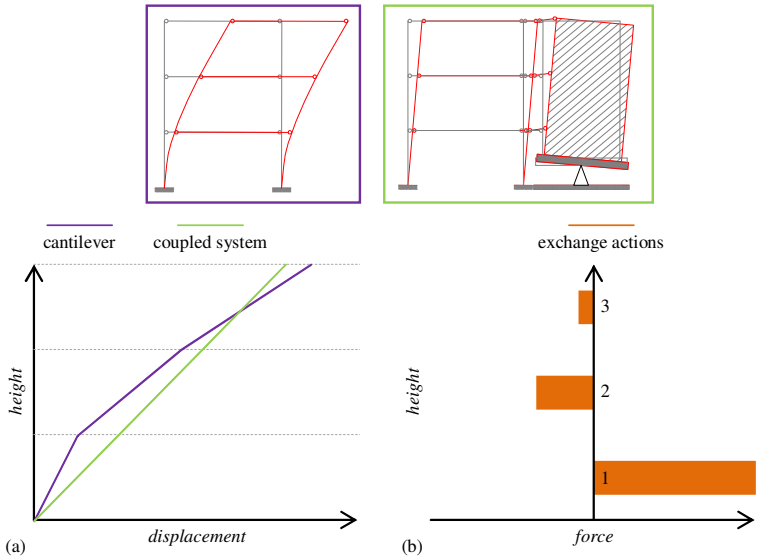

Figure 2-4 Cantilever structure coupled with an infinitely stiff system: (a) modal displacements, (b) exchange actions

Differently from others rocking systems (characterized by a flag-shaped hysteresis loop) which could exploit pre-tensioned cables for the system recentering, the analyzed solution aims to achieve a very high level of seismic protection avoiding any structural damage, therefore only the elastic strain energy of the existing r.c. frame can be exploited for the return at rest condition, at the end of a seismic excitation. Moreover the rocking motion of the investigated system is activated in the middle of the bracing base, where the spherical hinge is located, while in traditional rocking system configurations the motion is activated at the edges of the structures with an uplift.

Dissipative rocking system can be used either in three dimensional configurations and in planar arrangements, as shown by Figure 2-5 (a) and (b). In the case of planar structures the behaviour is specialized for just one of the two horizontal directions; in the case of three dimensional arrangements, the upgrading is achieved with the insertion of, at least, two dissipative bracings for a single structure to protect. Generally, the aim is to pursue the regularization of the dynamic behaviour, reducing or minimizing thereby torsional coupling. The ideal position of the dissipative structures should be the one that provides a double symmetry to the existing frame, with respect to the longitudinal and transverse direction. Anyway the external structures can be installed in the same side or in the opposite ones of the building, depending on both the target behaviour and the available space, necessary condition for every kind of external passive control configurations.

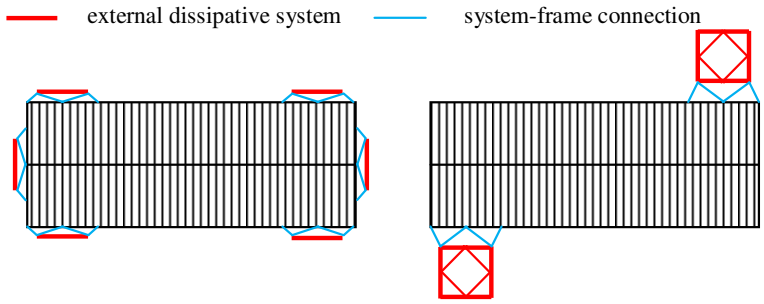

Figure 2-5 Dissipative rocking system alternative configurations: (a) planar solution, (b) three-dimensional arrangement

A similar configuration, known as "Dissipative Tower", which is a patented solution (Balducci 2005), have been recently applied in Italy for the seismic retrofit of existing r.c. frame buildings, especially schools and hospitals. In such practical applications, the coupling between the tower and the existing frame is realized at storey levels by means of braces bolted to thick steel plates, connected to the main structure using steel threaded rods inserted in holes fulfilled of epoxy resins. The connection is usually done in correspondence of beam-column joints and lateral beams. To avoid the concentration of exchange actions in few elements it is possible to use, if necessary, horizontal steel rods to transfer a certain amount of the interaction forces to the beams of the internal frames. Figure 2-6 displays some details and a picture of the tower-building connections, realized for the retrofit of the "Varano" High School, which is located in Camerino, a small town sited in central Italy not far from the epicentre of Umbria-Marche 1997 and central Italy earthquakes. Figure 2-7 shows an image of the retrofit configuration of the "Varano" High School, which is a r.c. frame building built in the '60s. In this case the seismic protection has been achieved with the insertion of two dissipative towers, equipped with a total number of 12 non-linear FVDs (α=0.15).

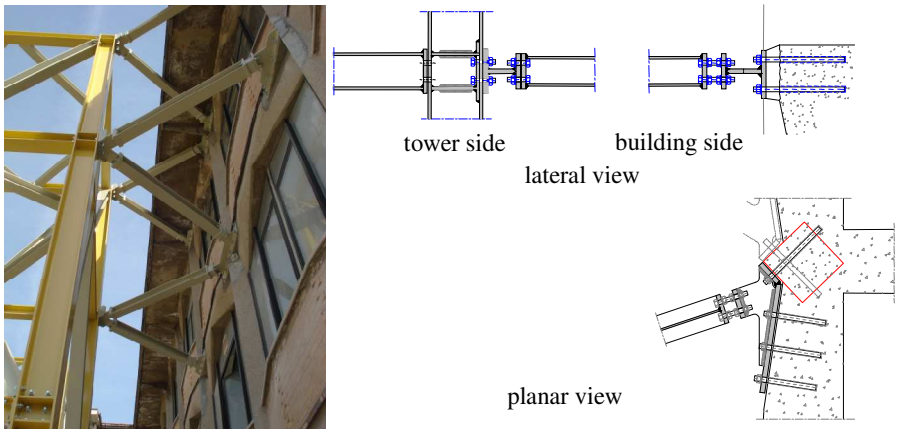

Figure 2-6 Details of the building-tower connection

Figure 2-7 Dissipative towers configuration for the retrofit of the "Varano" High School

In practical applications the FVDs are radially located at the vertices of the tower base in vertical position; moreover, to enhance FVDs displacements and velocities, they are inserted into an articulated quadrangle mechanism that amplifies their motions, with respect to the vertical displacements of the tower base. On the other hand, high precision metallic carpentry and bolted joints, as well as mechanical leverage with very low tolerances (more typical of mechanical engineering than civil engineering) are required to guarantee the activation of damping devices. Figure 2-8 reports an image and a detail scheme for the explanation of the mechanical leverage which amplifies the FVDs motion.

Figure 2-8 Details of the tower base and explanation of the leverage system

Figure 2-9 depicts the simplest mechanical scheme resulting from the connection of an existing SDOF frame with an external dissipative system. The rocking bracing (whose elements will be denoted by the subscript *"D"* in the sequel), can be seen as a spring and a dashpot in series (K_D and C_D, respectively), set in parallel to a spring, representative of the stiffness of the main structure (whose elements will be denoted in the sequel by the subscript *"F"*), (K_F). It is observable that the external damping system notably influences stiffness and dissipative capacity, while its contribution on the masses could be considered

less important. The dynamic properties of the mechanical scheme will be shown later in this chapter.

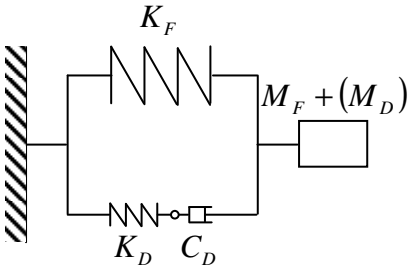

Figure 2-9 Mechanical scheme of the coupled system

In the next section the equation of motion of the dynamic behaviour of the coupled system is presented in the form of second order differential equations, as usually happens for civil engineering systems. The proposed problem formulation is presented in general terms to allow the comparison of the performance of different retrofit external techniques and to provide the opportunity to perform analysis either in time and frequency domain.

2.1 Equation of motion

The equations of motion for the system can be expressed as follows:

$$\mathbf{M}\ddot{\mathbf{u}}(t) + \mathbf{C}\dot{\mathbf{u}}(t) + \mathbf{K}\mathbf{u}(t) = \mathbf{M}\mathbf{p}a_g(t) \qquad (2\text{-}1)$$

where $\mathbf{u}(t) \in R^l$, is the vector of nodal displacements, the dot (·) denotes time-derivative; $\mathbf{p} \in R^l$ is the load distribution vector, l denotes the total number of degrees-of-freedom, and $a_g(t)$ is the external scalar loading function describing the seismic base acceleration. The time invariant matrices $\mathbf{M}$, $\mathbf{K}$, $\mathbf{C}$ describe the mass, stiffness and damping operators $R^l \rightarrow R^l$; they result from the sum of the contribution due to the existing frame and the one coming from the external dissipative bracing system. The damping contribution of the frame and of the dissipative system are denoted respectively as $\mathbf{C}_F$ and $\mathbf{C}_D$.

The frame contribution $\mathbf{C}_F$ to the overall damping matrix $\mathbf{C}$ is determined in accordance to the Rayleigh proportional damping model, which provides the damping matrix as a linear contribution of the existing frame mass matrix $\mathbf{M}_F$ and of the existing frame stiffness matrix $\mathbf{K}_F$

$$\mathbf{C}_F = \alpha\mathbf{M}_F + \beta\mathbf{K}_F \qquad (2\text{-}2)$$

where α and β denote Rayleigh constants. For the damping matrix the orthogonality holds and the relation between the two constants and the damping ratio ξ_i, provided for each *i*-vibration mode, is expressed by Eqn. (2-3)

$$\xi_i = \frac{1}{2}\left(\frac{\alpha}{\omega_i} + \beta\omega_i\right) \qquad (2\text{-}3)$$

α and β values can be found from the knowledge of the couple of values $(\xi_i\ \omega_i)$, usually related to the first two vibration modes, as

$$\alpha = 2\frac{\omega_1\omega_2(\omega_2\xi_1 - \omega_1\xi_2)}{\omega_2^2 - \omega_1^2}$$
$$\beta = 2\frac{\omega_2\xi_2 - \omega_1\xi_1}{\omega_2^2 - \omega_1^2} \qquad (2\text{-}4)$$

Figure 2-10 displays the proportional damping trend (violet line), for increasing values of frequency, together with the trends related to mass-proportional damping (green line) and stiffness-proportional damping (orange line). Mass-proportional damping is characterized by an hyperbolic shape, while the stiffness-proportional one is a straight line.

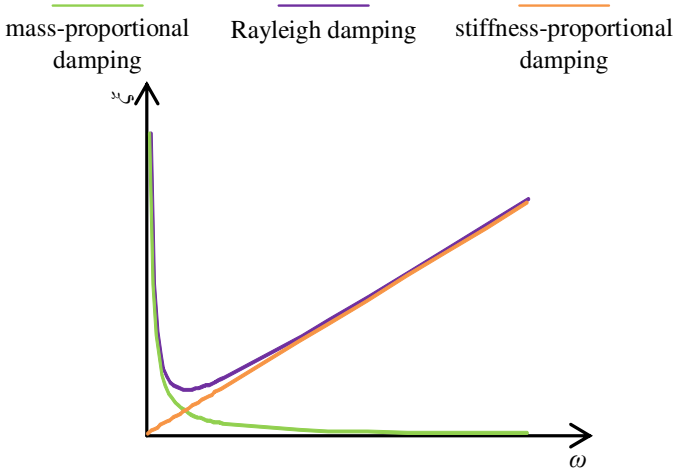

Figure 2-10 Proportional damping trend compared with those related to mass-proportional and stiffness-proportional damping

Generally, the external bracing system notably influences the stiffness and damping operators while it contributes only marginally to the mass operator. The displacement vector $\mathbf{u}(t)$ collects both the displacements required for the description of the frame response and the displacements involved in the bracing deformations.

In order to study the dynamic response of the system it is useful to separate the displacements associated with the masses, and thus involving inertial forces, from the displacements describing the internal degrees of freedom as the nodal rotations, the axial actions on the columns and in general all the quantities related to stiffness and damping

forces only. Accordingly, the total displacement vector $\mathbf{u}(t)$ can be split into the active components collected in the vector $\mathbf{x}(t) \in R^m$ and the other components $\mathbf{y}(t) \in R^n$ $(l = m+n)$. Figure 2-11 (a) and (b) depicts the contribution of the active components of displacements $\mathbf{x}(t)$ and those involved in the deformation and damping of bracing $\mathbf{y}(t)$, both in the mechanical scheme of the coupled system and in one possible external passive configuration.

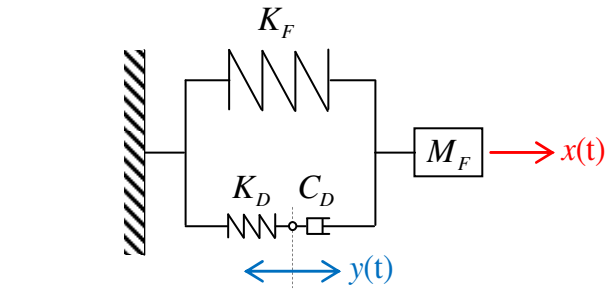

(a)

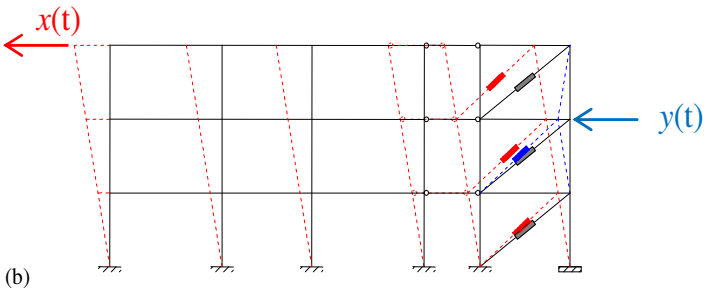

(b)

Figure 2-11 Displacements of the active degrees of freedom and displacements related to bracing deformation: (a) mechanical scheme, (b) external solution

The matrices describing the linear operators and the distribution vector can be consequently partitioned as follows:

$$\begin{vmatrix} \mathbf{M}_{xx} & 0 \\ 0 & 0 \end{vmatrix} \begin{vmatrix} \ddot{\mathbf{x}} \\ \ddot{\mathbf{y}} \end{vmatrix} + \begin{vmatrix} \mathbf{C}_{xx} & \mathbf{C}_{xy} \\ \mathbf{C}_{yx} & \mathbf{C}_{yy} \end{vmatrix} \begin{vmatrix} \dot{\mathbf{x}} \\ \dot{\mathbf{y}} \end{vmatrix} + \begin{vmatrix} \mathbf{K}_{xx} & \mathbf{K}_{xy} \\ \mathbf{K}_{yx} & \mathbf{K}_{yy} \end{vmatrix} \begin{vmatrix} \mathbf{x} \\ \mathbf{y} \end{vmatrix} = \begin{vmatrix} \mathbf{M}_{xx} & 0 \\ 0 & 0 \end{vmatrix} \begin{vmatrix} \mathbf{p}_x \\ 0 \end{vmatrix} a_g \qquad (2\text{-}5)$$

As usual, only the masses related to the horizontal floor displacements are considered in order to reduce the dimension of the dynamic problem and to simplify the interpretation of the results.

The presented equation of motion and the related partitioned system provide the core of the dynamic problem for the external dissipative configurations, that can be solved either through time-domain analyses, by means of a state-space formulation of the problem, either through frequency-domain analysis.

2.2 Generalized SDOF system approximation

Due to the fact that one of the results of the coupling with the dissipative rocking system analyzed is the achievement of a nearly linear distribution of displacements along the building height, which is perfectly obtained in the case of infinitely stiff rocking system, it is useful to provide a specific theoretical approach and the balance equations for this configuration. In this case the dynamic problem is reduced from a multiple-degrees-of-freedom (MDOF) to a single-degree-of-freedom (SDOF) system, obtained by introducing a constraint in the structure motion, as shown by Figure 2-12.

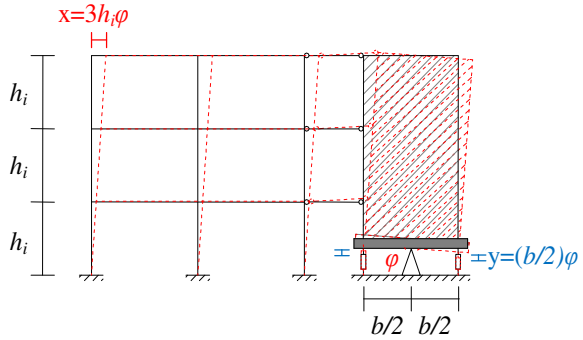

Figure 2-12 Deformed shape due to the coupling with an infinitely stiff system

All the degrees of freedom of the system (active displacements of the frame and displacements involved in the bracing deformations) are governed by the base rotation φ and the displacement vector $\mathbf{u}(t)$, shown in Eqn. (2-1), is a constrained displacements field that can be expressed as

$$\mathbf{u}(t) = \mathbf{l}\varphi \qquad (2\text{-}6)$$

in which $\mathbf{l}$ is a vector collecting both the heights of the frame and the base dimension, which are related to the dampers displacements. The D'Alembert Principle for the problem at hand can be expressed by introducing a virtual velocity field $\hat{\eta} = \mathbf{l}\hat{\varphi}$, in which $\hat{\varphi}$ is an arbitrary base rotation. Eqn. (2-1) can be rewritten for any time instant t as

$$\mathbf{M}\ddot{\mathbf{u}} \cdot \hat{\eta} + \mathbf{C}_F\dot{\mathbf{u}} \cdot \hat{\eta} + \mathbf{C}_D\dot{\mathbf{u}} \cdot \hat{\eta} + \mathbf{K} \cdot \hat{\eta} = \mathbf{M}\mathbf{p} \cdot \hat{\eta}a_g \quad \forall t \qquad (2\text{-}7)$$

where the matrix $\mathbf{M}$ collects masses of rigid floors, $\mathbf{K}$ is the stiffness matrix of the existing frame, $\mathbf{C}_F$ describes the damping of the frame and where $\mathbf{C}_D$ is the dissipative contribution of the dampers located at the tower base. This way, the tower influences only the damping operator and the shape of the virtual displacement field. Eqn. (2-7) can be rewritten as

$$\tilde{m}\ddot{\varphi} + (\tilde{c}_F + \tilde{c}_D)\dot{\varphi} + \tilde{k}\varphi = m^* a_g \qquad (2\text{-}8)$$

where $\tilde{m} = \mathbf{M}\mathbf{l} \cdot \mathbf{l}$, $\tilde{c}_F = \mathbf{C}_F\mathbf{l} \cdot \mathbf{l}$, $\tilde{c}_D = \mathbf{C}_D\mathbf{l} \cdot \mathbf{l}$, $\tilde{k} = \mathbf{K}\mathbf{l} \cdot \mathbf{l}$, $m^* = \mathbf{M}\mathbf{p} \cdot \mathbf{l}$ are the scalar parameters describing the properties of the system reduced to a SDOF, and $\cdot$ denotes

the scalar product. By solving Eqn. (2-8), the time-history of the base rotation is known, and the vector of nodal displacements of the MDOF system is determined by considering Eqn. (2-6).

2.3 Time domain analysis

This section is related to the dynamic problem resolution through time-domain, where the governing differential equations can be conveniently converted into a set of first order equations by following a state-space formulation. The state-space vector collects, per each time instant *t*, the functions necessaries to characterize the state of the system. Moreover a state-space formulation is a suitable way to handling systems with general viscous damping, as in the case of external passive control system, where concentrated location of dampers leads to a non-classically damped nature of the problem. This approach allows the use of complex modal analysis (CMA) to quantify the effective damping contribution per each vibration modes and its effectiveness is proved in some studies (Craig and Kurdila 2006, Chu et al. 2009, Occhiuzzi 2009).

2.3.1 *State space formulation*

The distribution of the damping in the structure and, in particular, the location of the concentrated dampers of the external bracings, leads to a non-classically damped system. For its solution it is convenient to formulate the problem by introducing the vector $\mathbf{v}(t)=\dot{\mathbf{x}}(t)$ and the state vector $\mathbf{z}(t)$ collecting the displacements and the velocities of the active displacements and the displacements of the internal nodes:

$$\mathbf{z}(t)=\begin{vmatrix}\mathbf{x}(t)\\ \mathbf{v}(t)\\ \mathbf{y}(t)\end{vmatrix} \qquad (2\text{-}9)$$

The kinetic energy (E_k) and the strain energy (E_s) of the coupled system can be expressed as reported in Eqn. (2-10)

$$\begin{aligned} E_k &= \frac{1}{2}\mathbf{M}_{xx}\mathbf{v}\cdot\mathbf{v} \\ E_s &= \frac{1}{2}\begin{vmatrix}\mathbf{K}_{xx} & \mathbf{K}_{xy}\\ \mathbf{K}_{yx} & \mathbf{K}_{yy}\end{vmatrix}\begin{vmatrix}\mathbf{x}\\ \mathbf{y}\end{vmatrix}\cdot\begin{vmatrix}\mathbf{x}\\ \mathbf{y}\end{vmatrix} \end{aligned} \qquad (2\text{-}10)$$

Eqn. (2-1) can be reduced to a first-order state space form:

$$\dot{\mathbf{z}}(t)=\mathbf{A}\mathbf{z}(t)+\tilde{\mathbf{p}}a_g(t) \qquad (2\text{-}11)$$

where:

$$\begin{cases} \dot{\mathbf{x}} = \mathbf{v} \\ \mathbf{M}_{xx}\dot{\mathbf{v}} + \mathbf{C}_{xx}\mathbf{v} + \mathbf{C}_{xy}\dot{\mathbf{y}} + \mathbf{K}_{xx}\mathbf{x} + \mathbf{K}_{xy}\mathbf{y} = 0 \\ \mathbf{C}_{yy}\dot{\mathbf{y}} + \mathbf{C}_{yx}\mathbf{v} + \mathbf{K}_{yx}\mathbf{x} + \mathbf{K}_{yy}\mathbf{y} = 0 \end{cases} \quad (2\text{-}12)$$

By assuming that the inverse of both mass $\left(\mathbf{M}_{xx}^{-1}\right)$ and damping $\left(\mathbf{C}_{yy}^{-1}\right)$ matrices exist Eqn. (2-12) can be rewritten as

$$\begin{cases} \dot{\mathbf{x}} = \mathbf{v} \\ \dot{\mathbf{v}} = -\mathbf{M}_{xx}^{-1}\left(\mathbf{K}_{xx} - \mathbf{C}_{xy}\mathbf{C}_{yy}^{-1}\mathbf{K}_{yx}\right) - \mathbf{M}_{xx}^{-1}\left(\mathbf{C}_{xx} - \mathbf{C}_{xy}\mathbf{C}_{yy}^{-1}\mathbf{C}_{yx}\right) - \mathbf{M}_{xx}^{-1}\left(\mathbf{K}_{xy} - \mathbf{C}_{xy}\mathbf{C}_{yy}^{-1}\mathbf{K}_{yy}\right) \\ \dot{\mathbf{y}} = -\mathbf{C}_{yy}^{-1}\mathbf{K}_{yx}\mathbf{x} - \mathbf{C}_{yy}^{-1}\mathbf{K}_{yy}\mathbf{y} - \mathbf{C}_{yy}^{-1}\mathbf{C}_{yx}\mathbf{v} \end{cases} \quad (2\text{-}13)$$

therefore the state-space operator $\mathbf{A}$ can be written as:

$$\mathbf{A} = \begin{vmatrix} \mathbf{0} & \mathbf{I} & \mathbf{0} \\ -\mathbf{M}_{xx}^{-1}\left(\mathbf{K}_{xx} - \mathbf{C}_{xy}\mathbf{C}_{yy}^{-1}\mathbf{K}_{yx}\right) & -\mathbf{M}_{xx}^{-1}\left(\mathbf{C}_{xx} - \mathbf{C}_{xy}\mathbf{C}_{yy}^{-1}\mathbf{C}_{yx}\right) & -\mathbf{M}_{xx}^{-1}\left(\mathbf{K}_{xy} - \mathbf{C}_{xy}\mathbf{C}_{yy}^{-1}\mathbf{K}_{yy}\right) \\ -\mathbf{C}_{yy}^{-1}\mathbf{K}_{yx} & -\mathbf{C}_{yy}^{-1}\mathbf{C}_{yx} & -\mathbf{C}_{yy}^{-1}\mathbf{K}_{yy} \end{vmatrix} \quad (2\text{-}14)$$

Vector $\tilde{\mathbf{p}}$ is defined as:

$$\tilde{\mathbf{p}} = \begin{vmatrix} 0 \\ \mathbf{M}_{xx}^{-1}\mathbf{p} \\ 0 \end{vmatrix} \quad (2\text{-}15)$$

2.3.2 *Free vibrations and modal properties*

The free vibration problem can be solved by assuming a solution of the form $\mathbf{z}(t) = \boldsymbol{\varphi} e^{\lambda t}$, where $\lambda, \boldsymbol{\varphi}$ are a eigenvalue-eigenvector pair of $\mathbf{A}$, such that:

$$\mathbf{A}\boldsymbol{\varphi} = \lambda\boldsymbol{\varphi} \quad (2\text{-}16)$$

Because the state-space operator $\mathbf{A}$ is real, the $2m+n$ eigenvalues must be either real or they must occur in complex conjugate pairs. Real *n* eigenvalues indicate over damped modes and correspond to the motion of the degrees of freedom with no mass, while the 2*m* complex pairs of eigenvalues and corresponding eigenvectors are related to under damped modes. The eigenvector $\boldsymbol{\varphi}$ corresponding to a complex eigenvalue λ, is also complex and similarly, the eigenvector corresponding to the complex conjugate of λ is the complex conjugate of its eigenvector $\boldsymbol{\varphi}$.

Complex eigenvalue has the following form:

$$\lambda_i = -\xi_i\omega_{0i} + i\omega_{0i}\sqrt{1-\xi_i^2} \quad (2\text{-}17)$$

and contains information regarding the damping ratio ξ_i, the corresponding natural circular frequency ω_{0i} and the damped circular frequency ω_{di} of the *i*-th mode. These information can be extrapolated as follows:

$$\begin{aligned} \omega_{0i} &= |\lambda_i| \\ \xi_i &= -\mathrm{Re}(\lambda_i)/|\lambda_i| \\ \omega_{di} &= \mathrm{Im}(\lambda_i) \end{aligned} \qquad (2\text{-}18)$$

It should be noted that, in the case of viscous-damped systems, the natural circular frequency ω_{0i} is equal to the undamped circular frequency only in the case of proportional damping.

For what concern complex eigenvectors they can be expressed in polar form, which means magnitude and phase angles in degrees. The magnitude of a complex eigenvectors can be expressed as

$$|\varphi_i| = \sqrt{\mathrm{Re}(\varphi_i)^2 + \mathrm{Im}(\varphi_i)^2} \qquad (2\text{-}19)$$

while the phase angle θ_i related to same complex eigenvectors can be found as shown in Eqn. (2-20)

$$\theta_i = \tan^{-1}\frac{\mathrm{Im}(\varphi_i)}{\mathrm{Re}(\varphi_i)} \qquad (2\text{-}20)$$

It is observable that when the damping is proportional all masses of a system will be either in phase or 180° out of phase, otherwise when the system is non-classically damped the masses won't be neither in phase or 180° out of phase and the difference will be higher in function of the extent of non-classical damping of the system. Moreover it is important to note that the modes arising from systems with zero or classical damping have nodes, which are stationary points at which the structure has zero displacement. In contrast, for a non-classically damped system, mode-shapes have no stationary point on the structure.

Known the modal properties, the problem solution can be obtained as a linear combination of the single mode contributions. Let $\mathbf{\Lambda}$ be the diagonal matrix containing the complex eigenvalues and $\mathbf{\Phi} = |\boldsymbol{\varphi}_1, \boldsymbol{\varphi}_2, ..., \boldsymbol{\varphi}_{2m+n}|$ the complex eigenmatrix containing the eigenvectors, such that the orthogonality property $\mathbf{\Lambda} = \mathbf{\Phi}^{-1}\mathbf{A}\mathbf{\Phi}$ holds.

2.3.3 *Seismic response via modal decomposition method*

Modal decomposition method is already been use in other studies (Peng and Conte 1998) to characterize the seismic response of a system.

The motion can be obtained as a linear combination of modes:

$$\mathbf{z}(t) = \mathbf{\Phi}\mathbf{q}(t) \qquad (2\text{-}21)$$

where $\mathbf{q}(t)$ is a vector collecting the modal coordinates. The orthogonality property leads to the diagonal problem:

$$\dot{\mathbf{q}}(t) = \mathbf{\Lambda q}(t) + \boldsymbol{\gamma} a_g(t) \qquad (2\text{-}22)$$

where $\gamma_i = \left[\mathbf{\Phi}^{-1}\tilde{\mathbf{p}}\right]_i$ is the *i*-th (complex-valued) modal participation factor.

Introducing the normalized complex modal response vector $\mathbf{s}(t)$ such that: $q_i(t) = \Gamma_i s_i(t)$, the problem can be written in a normalized form:

$$\dot{\mathbf{s}}(t) = \mathbf{\Lambda s}(t) + \mathbf{I} a_g(t) \qquad (2\text{-}23)$$

Assuming that the system is initially at rest, the solution can be obtained by the Duhamel integral:

$$\mathbf{s}(t) = \int_0^t \mathbf{h}(t-\tau) a_g(\tau) d\tau \qquad (2\text{-}24)$$

where the components $h_i(t) = e^{\lambda_i t}$ are the solutions related to an impulsive unitary input.

2.3.4 *Modal properties of a SDOF system*

It is interesting to analyze the free vibration problem for the mechanical scheme introduced previously (and here recalled in Figure 2-13), through a state-space formulation of the problem. Let's define m and k_0 as the mass and the stiffness of the SDOF structure to protect; k_1 and c as the contributions provided by the external dissipative system in terms of stiffness and damping, respectively; ε as the displacement of the active degree of freedom; ε_e and ε_v as the degrees of freedom related to bracing deformations.

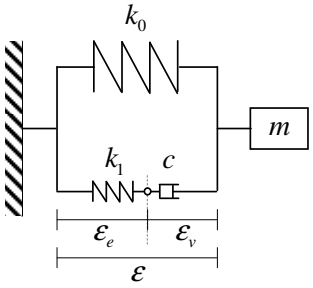

Figure 2-13 Displacements relof the active DOFs and displacement related to bracing deformation in the case of the simplest mechanical system

In the case of $\varepsilon_e = \varepsilon - \varepsilon_v$ it is possible to rewrite the equation of motion of the system through the state-variables approach, that is $\dot{\mathbf{z}}(t) = \mathbf{A}\mathbf{z}(t)$ where the state-vector is $\mathbf{z}(t) = \left|\varepsilon(t) \quad v(t) \quad \varepsilon_v(t)\right|^T$

$$\begin{cases} \dot{\varepsilon} = v \\ m\dot{v} + k_0\varepsilon + k_1(\varepsilon - \varepsilon_v) = 0 \\ k_1(\varepsilon - \varepsilon_v) = c\dot{\varepsilon}_v \end{cases} \quad (2\text{-}25)$$

and the state-operator **A** is expressed as shown in Eqn. (2-26)

$$\mathbf{A} = \begin{vmatrix} 0 & 1 & 0 \\ -\left(\frac{k_0}{m} + \frac{k_1}{m}\right) & 0 & \frac{k_1}{m} \\ \frac{k_1}{c} & 0 & -\frac{k_1}{c} \end{vmatrix} \quad (2\text{-}26)$$

The free vibration problem can be solved and leads to the subsequent third-order equation

$$\lambda^3 + \lambda^2 \frac{k_1}{c} + \lambda\left(\frac{k_0}{m} + \frac{k_1}{m}\right) + \frac{k_0 k_1}{mc} = 0 \quad (2\text{-}27)$$

The eigenvalue eigenvector problem is solved by assuming that m=1 [kNs^2/m], k_0=200 [kN/m], k_1=200 [kN/m] and c=5 [kNs/m]. The fundamental period of the undamped system is equal to $T = 0.444s$ and the damping coefficient related to the fundamental mode is equal to $\xi_1 = 0.16$. Successively the values of added damping and added stiffness due to the external system (k_1 and c), are varied in a range of 25-1200 [kN/m] for k_1 and of 0-50 [kNs/m] for c.

Figure 2-14 displays the trends of the period and of the damping associated to the fundamental mode by varying only the stiffness of the dissipative system, i.e. k_0=200 kN/m and c=5 kNs/m. It is observable that for values of added stiffness smaller than k_1<200 kN/m the period initially decreases, reach a minimum when k_1=75 kN/m and then increases. For values of stiffness higher than 425 kN/m the period do not change sensibly anymore. The damping is affected by the stiffness values only in the range k_1=25-425 kN/m, showing always an increasing trend, while for higher values ξ_1 do not change anymore. A stiffness ratio between the frame and the bracing equal to 0.75-1 provides very similar results in terms of added damping, while higher values do not provide benefits.

Figure 2-15 displays the period and modal damping trend for different values of added damping c, i.e. k_0=k_1=200 kN/m. It is observable that the damping coefficient of the first mode increases in the range c=0-7.5 kNs/m where it reaches its maximum ($\xi_1 = 0.20$), successively remains almost constant until c=10 kNs/m. For higher values of added damping ξ_1 continues to decrease until the value of 0.05. The period T_1 shows an evident decreasing trend in the range c=0-12.5 kNs/m, while for higher values of c, it remains almost equal to 0.31 s.

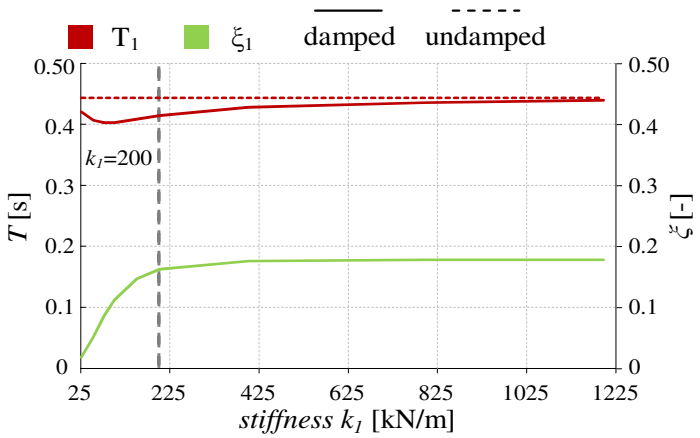

Figure 2-14 Period and modal damping trend for different values of stiffness k_1

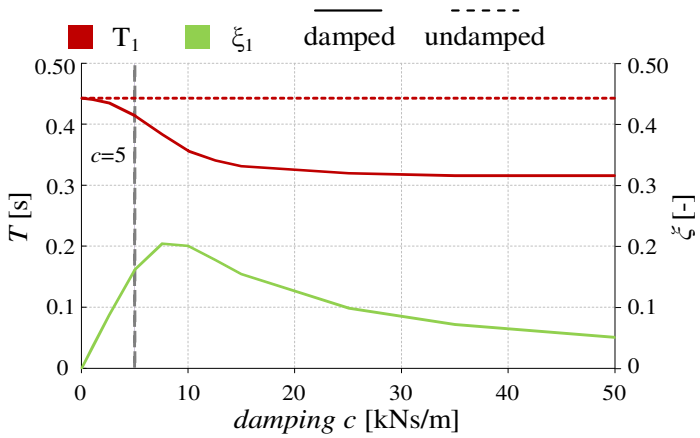

Figure 2-15 Period and modal damping trend for increasing values of damping c

2.4 Frequency domain analysis

Moving from analysis performed in time domain to analysis performed in frequency domain provides some benefits, in fact the differential system shown in Eqn. (2-11) becomes an algebraic system; moreover, a frequency-domain solving procedure allows using the condensation technique and to work, therefore, with a reduced problem.

Usually condensation technique is an operation applied with the objective of reducing the number of degrees of freedom, without losing information regarding the features of the structure; usually static condensation is an operation which involves the stiffness matrix. Let's consider an undamped system having a mass matrix with non-zero elements in correspondence of actives degrees of freedom (**x**) and zero elements in correspondence of dependent degrees of freedom (**y**), the static condensation of the stiffness matrix on the active degrees of freedom can be achieved as follows:

$$\left|\begin{array}{c:c} \mathbf{M}_{xx} & \mathbf{0}_{xy} \\ \hdashline \mathbf{0}_{yx} & \mathbf{0}_{yy} \end{array}\right| \left\|\begin{array}{c} \ddot{\mathbf{x}} \\ \hdashline \ddot{\mathbf{y}} \end{array}\right\| + \left|\begin{array}{c:c} \mathbf{K}_{xx} & \mathbf{K}_{xy} \\ \hdashline \mathbf{K}_{yx} & \mathbf{K}_{yy} \end{array}\right| \left\|\begin{array}{c} \mathbf{x} \\ \hdashline \mathbf{y} \end{array}\right\| = \left|\begin{array}{c} -\mathbf{M}_{xx}\mathbf{p}_x \\ \hdashline \mathbf{0}_y \end{array}\right| a_g \qquad (2\text{-}28)$$

The lower partition of the system provides a static constraint equation from which the dependent displacements vector **y** can be written as

$$\mathbf{y} = -\mathbf{K}_{yy}^{-1}\mathbf{K}_{yx}\mathbf{x} \qquad (2\text{-}29)$$

and substituted into the upper partition of the system, providing

$$\mathbf{M}_{xx}\ddot{\mathbf{x}} + \left(\mathbf{K}_{xx} - \mathbf{K}_{xy}\mathbf{K}_{yy}^{-1}\mathbf{K}_{yx}\right)\mathbf{x} = -\mathbf{M}_{xx}\mathbf{p}_x \qquad (2\text{-}30)$$

therefore the stiffness condensed matrix $\widehat{\mathbf{K}}_{xx}$ is reported into Eqn. (2-31)

$$\widehat{\mathbf{K}}_{xx} = \mathbf{K}_{xx} - \mathbf{K}_{xy}\mathbf{K}_{yy}^{-1}\mathbf{K}_{yx} \qquad (2\text{-}31)$$

Nevertheless, the system is still governed by differential equations. Thus, in order to have the chance to work with a reduced problem, it is convenient to change the analysis domain.

The way to operate the change of analysis domain is represented by the use of the Fourier transform function, which is widely diffuse in the dynamic of structures and here briefly recalled.

Starting from a signal, denoted as $s(t)$ and defined into the time domain, it is often useful to take into account its own equivalent representation. A suitable signal representation in frequency domain is intended to provide a one-to-one correspondence, such that it is possible to going back to its corresponding time trend. The circular frequency ω could be the appropriate parameter able to provide the one-to-one correspondence between time domain and frequency domain; therefore a signal $s(t)$, which satisfies the condition of existence of the integral $\left(\int_{-\infty}^{+\infty}|s(t)|dt < \infty\right)$, condition met by most physically realizable functions representing forces, displacements and so on, can be represented by means of the Fourier transform F, which is defined as:

$$\bar{s}(\omega) = F[s(t)] = \int_{-\infty}^{+\infty} s(t) e^{-i\omega t} dt \qquad (2\text{-}32)$$

Similarly, starting from the representation in the frequency domain, $S(\omega)$, it is possible to return back to time domain through the inverse Fourier transform defined as

$$s(t) = F^{-1}[\bar{s}(\omega)] = \frac{1}{2\pi} \int_{-\infty}^{+\infty} \bar{s}(\omega) e^{i\omega t} d\omega \qquad (2\text{-}33)$$

Eqn. (2-32) and (2-33) are known as Fourier transform pair and they realize the one-to-one correspondence $s(t) \leftrightarrow \bar{s}(\omega)$. It is also useful to recall the derivative property of the Fourier transform through Eqn. (2-34), where ˆ denotes time derivative:

$$\hat{s}(t) = \frac{d^m s(t)}{dt^m} \rightarrow \hat{\bar{s}}(\omega) = (i\omega)^m \bar{s}(\omega) \qquad (2\text{-}34)$$

Therefore the time derivatives of displacement, that is velocity and acceleration, can be expressed, respectively, as $F[\dot{u}(t)] = i\omega\bar{u}(\omega)$ and $F[\ddot{u}(t)] = -\omega^2\bar{u}(\omega)$.

The combination of amplitude versus frequency and phase versus frequency information is called the frequency response of the system.

2.4.1 *Fourier transform of the problem*

By defining $\bar{\mathbf{x}}$ and $\bar{\mathbf{y}}$ as the transformed vectors of active degrees of freedom and dependent degrees of freedom and $\bar{a}_g$ as the transformed external scalar loading function, representative of the seismic base acceleration, the differential system of Eqn. (2-5) can be rewritten as an algebraic system:

$$\left|\begin{array}{c:c} -\omega^2\mathbf{M}_{xx} + \mathbf{H}_{xx} & \mathbf{H}_{xy} \\ \hdashline \mathbf{H}_{yx} & \mathbf{H}_{yy} \end{array}\right| \left|\begin{array}{c} \bar{\mathbf{x}} \\ \hdashline \bar{\mathbf{y}} \end{array}\right| = \left|\begin{array}{c} -\mathbf{M}_{xx}\mathbf{p}_x \\ \hdashline 0 \end{array}\right| \bar{a}_g \qquad (2\text{-}35)$$

where $\mathbf{H}_{\alpha\beta} = \mathbf{K}_{\alpha\beta} - i\omega\mathbf{C}_{\alpha\beta}$. In this case, the active displacements can be derived from the condensed problem:

$$\bar{\mathbf{x}} = \left[-\omega^2\mathbf{M}_{xx} + \mathbf{H}_{xx} - \mathbf{H}_{xy}\mathbf{H}_{yy}^{-1}\mathbf{H}_{yx}\right]^{-1} \mathbf{M}_{xx}\mathbf{p}_x\bar{a}_g \qquad (2\text{-}36)$$

where $\left[-\omega^2\mathbf{M}_{xx} + \mathbf{H}_{xx} - \mathbf{H}_{xy}\mathbf{H}_{yy}^{-1}\mathbf{H}_{yx}\right]^{-1}$ is the transfer function $\bar{\mathbf{H}}(\omega)$ of the problem, while the dependent displacements can be deduced successively from $\bar{\mathbf{x}}$:

$$\bar{\mathbf{y}} = -\mathbf{H}_{yy}^{-1}\mathbf{H}_{yx}\bar{\mathbf{x}} \qquad (2\text{-}37)$$

The solution provides the basis to evaluate the motion in the frequency domain. It is clear that to obtain the time-history of the response parameters, like displacements or internal

actions, it is necessary to return back to time domain, by means of the inverse Fourier transform. The frequency content of the response is expressed as

$$\left|\bar{\mathbf{x}}\right| = \left|\left[-\omega^2\mathbf{M}_{xx} + \mathbf{H}_{xx} - \mathbf{H}_{xy}\mathbf{H}_{yy}^{-1}\mathbf{H}_{yx}\right]^{-1}\right|\left|\mathbf{M}_{xx}\mathbf{p}_x\bar{a}_g\right| \qquad (2\text{-}38)$$

2.5 The Chu et al. formulation

In this section the Chu et al. formulation (Technical Report MCEER-09-0001), which focuses on the modal analysis of arbitrarily damped three-dimensional linear structures subjected to seismic excitations, is reported. With respect to the proposed formulation the Chu et al. formulation can be used only when all the degrees of freedom have associated masses, therefore it is more traditional. This formulation provides a state-space formulation of the problem and provides the chance to perform analysis either through time domain and frequency domain, but, differently from the proposed one, is based on two symmetric real-valued state-space operators. According to Chu et al. the equation of motion of the dynamic problem shown in Eqn. (2-1) can be written in the state-space form as shown in Eqn. (2-39)

$$\mathbf{A}\dot{\mathbf{v}}(t) + \mathbf{B}\mathbf{v}(t) = \mathbf{f}_s(t) \qquad (2\text{-}39)$$

where

$$\begin{gathered}\mathbf{A} = \begin{vmatrix}\mathbf{0} & \mathbf{M}\\ \mathbf{M} & \mathbf{C}\end{vmatrix} \in R^{2Nx2N}, \mathbf{B} = \begin{vmatrix}-\mathbf{M} & \mathbf{0}\\ \mathbf{0} & \mathbf{K}\end{vmatrix} \in R^{2Nx2N}\\ \mathbf{v}(t) = \begin{vmatrix}\dot{\mathbf{u}}(t)\\ \mathbf{u}(t)\end{vmatrix} \in R^{2N}, \mathbf{f}_s(t) = \begin{vmatrix}0\\ f(t)\end{vmatrix} \in R^{2N}\end{gathered} \qquad (2\text{-}40)$$

$\mathbf{u}$ is the displacements vector $\in R^N$, N is the number of degrees of freedom of the system, $(\cdot)$ denotes time-derivative, f(t) is the dynamic loading vector, while $\mathbf{A}$ and $\mathbf{B}$ are non-singular matrices, which means that both $\mathbf{A}^{-1}$ and $\mathbf{B}^{-1}$ exist.

The eigenvalue problem associated to Eqn. (2-39) is given by Eqn. (2-41) where λ, $\boldsymbol{\varphi}$ are a eigenvalue-eigenvector pair:

$$(\lambda\mathbf{A} + \mathbf{B})\boldsymbol{\psi} = \mathbf{0} \qquad (2\text{-}41)$$

the solution of the problem leads to $2N$ eigenvalues λ_i and $2N$ eigenvectors $\boldsymbol{\psi}_i$, which can be either complex-valued $(2N_C)$ or real valued $[N_P = 2(N - N_C)]$, therefore related to over damped modes. Assuming that there are N_C pairs of complex eigenvalues, the corresponding eigenvalues and eigenvectors can be expressed as

$$\lambda_j, \lambda_j^* = -\xi_j\omega_j \pm i\omega_{dj} \quad (j = 1,2,...,N_C) \qquad (2\text{-}42)$$

$$\boldsymbol{\psi}_j = \begin{Bmatrix} \lambda_j \boldsymbol{\varphi}_j \\ \boldsymbol{\varphi}_j \end{Bmatrix}, \boldsymbol{\psi}^*_j = \begin{Bmatrix} \lambda^*_j \boldsymbol{\varphi}^*_j \\ \boldsymbol{\varphi}^*_j \end{Bmatrix}$$

where the superscript * denotes conjugate operation.

In the case of over damped modes, instead, the eigenvalues and eigenvectors can be expressed as

$$\lambda^P_j = -\omega^P_j \quad (j = 1,2,...,N_P)$$
$$\boldsymbol{\psi}^P_j == \begin{Bmatrix} \lambda^P_j \boldsymbol{\varphi}^P_j \\ \boldsymbol{\varphi}^P_j \end{Bmatrix} \qquad (2\text{-}43)$$

It is noteworthy that the use of two symmetric matrices, as state operators, leads to the fact that all the degrees of freedom of the system have to be associated to a value of mass, otherwise the two matrices $\mathbf{A}$ and $\mathbf{B}$ would be singular. This is the substantial difference, together with the use of just one state-operator, with the proposed formulation, where the displacements vector **u**(t) is partitioned into active degrees of freedom **x**(t) related to masses and displacements of internal nodes **y**(t). Anyway the Chu et al. formulation is used in this work as a term of comparison for the proposed formulation in order to understand the weight, on the total response, of masses associated to degrees of freedom involved into the deformation and damping of the bracing (i.e. **y**(t)).

Analysis with increasing values of masses associated to dependent degrees of freedom were performed with the Chu et al. formulation and the results were compared with those obtained with the proposed formulation for one of the two case studies successively presented (i.e. Camerino building). It is observable that the two formulation have provided equal results for a wide range of mass values associated to the deformation of the bracings (0.01-300 kNs^2/m, the latter value of mass is comparable to the mass associated to floor type).

Figure 2-16 (a) and (b) report and compare the fifth floor responses in terms of displacements and absolute accelerations, for ten seconds of time history, obtained with the proposed formulation (green lines) and with the Chu et al. formulation with a value of mass associated to the dependent degrees of freedom equal to 0.01 kNs^2/m (violet lines) and of 300 kNs^2/m (orange lines). It is observable that the responses are very close one to each other, for both the two monitored engineering demand parameters (EDPs).

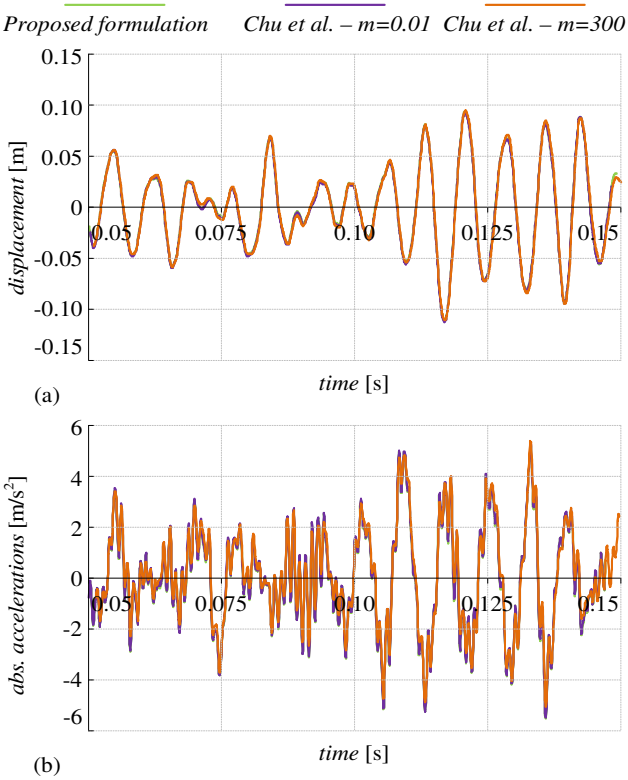

Figure 2-16 Comparison of the fifth floor displacement responses (a) and of the fifth floor absolute accelerations

Moreover the alternative formulation gives a way to evaluate the effective modal mass. Usually, for classically damped or undamped systems, the *i*-th modal participation factor Γ_i is defined as shown in Eqn. (2-44)

$$\Gamma_i = \frac{\boldsymbol{\psi}_i^T \mathbf{M} \mathbf{J}}{\boldsymbol{\psi}_i^T \mathbf{M} \boldsymbol{\psi}_i} \qquad (2\text{-}44)$$

where **J** is the load distribution vector, **M** is the mass matrix, $\boldsymbol{\psi}_i \in R^N$ is the *i*-th mode of the classically damped or undamped system and *N* is the number of degrees of freedom of the system. The participant mass ratios M_i^* can be, therefore, defined as $M_i^* = \left(\mathbf{M}\mathbf{p} \cdot \boldsymbol{\psi}_i\right)^2 / \mathbf{M}\boldsymbol{\psi}_i \cdot \boldsymbol{\psi}_i \geq 0 \in R$.

For an arbitrarily damped structure, which can be characterized by either complex and conjugates modes and over damped modes, the participant mass ratios can be determined as

$$\sum_{i=1}^{N_C} \frac{\hat{m}_i^{eff}}{M_\Sigma} + \sum_{i=1}^{N_P} \frac{\hat{m}_i^{Peff}}{M_\Sigma} = 1 \qquad (2\text{-}45)$$

where M_Σ is total mass of the structure, $\hat{m}_i^{eff}$ is the effective modal mass associated with the *i*-th complex mode, including its conjugate counterpart, $\hat{m}_i^{Peff}$ is the effective modal mass associated with the *i*-th over damped mode; N_c and N_P are representative of total number of the complex modes and over damped ones, respectively. Eqn. (2-46) displays how $\hat{m}_i^{eff}$ and $\hat{m}_i^{Peff}$ can be found

$$\begin{aligned} \hat{m}_i^{eff} &= 2\,\mathrm{Re}\left(\frac{\lambda_i \left(\boldsymbol{\varphi}_i^T \mathbf{M} \mathbf{J} \right)^2}{a_i} \right) \\ \hat{m}_i^{Peff} &= \frac{\lambda_i^P \left[\left(\boldsymbol{\varphi}_i^P \right)^T \mathbf{M} \mathbf{J} \right]^2}{a_i^P} \end{aligned} \qquad \text{(2-46)}$$

where $a_i = \boldsymbol{\psi}_i^T \mathbf{A} \boldsymbol{\psi}_i$ and $a_i^P = \left(\boldsymbol{\psi}_i^P \right)^T \mathbf{A} \boldsymbol{\psi}_i^P$, respectively.

It is noteworthy that effective modal masses, reported in Eqn. (2-46), associated to both complex and over damped modes, may be positive or negative and are independent of how modal shapes are normalized, although the summation of contributions from all modes converges to the total mass of the system. As in the case of classically damped systems, modes participant mass ratios can be considered as indicators to determine the number of modes required in the superposition.

Chapter 3

Case studies

In this thesis the proposed formulation is used to analyze the dynamic behaviour of two case studies, the first one is a well known benchmark structure, the Van Nuys building, already investigated through several studies (Blume & Associates 1973, Islam 1996, Doulatabadi 1997, Trifunac et al. 1999, Trifunac et al. 2001, Beck et al. 2002, Porter et al. 2002, Krawinkler et al. 2005, Bazzurro et al.) and used as testbed by the Pacific Earthquake Engineering Research Center (PEER). The second one is a 5-storey r.c. moment resisting frame built in Italy during the '80s without seismic standards and without any ductile detailing, therefore representative of the Italian building heritage of the '60s-'80s.

The two case studies are investigated through their coupling with the external dissipative rocking system and the results will be shown in terms of modal properties and seismic response via modal decomposition method, in the successive chapters.

3.1 Van Nuys building

The Van Nuys building is an Hotel located at 8244 Orion Avenue, Van Nuys, California in the San Fernando Valley of Los Angeles County. The building was lightly damaged by the M6.6 1971 San Fernando event, approximately 20 km to the northeast, and severely damaged by the M6.7 1994 Northridge Earthquake, whose epicenter was approximately 4.5 km to the southwest. After the Northridge earthquake the building was declared out of service, due to the severe structural damages suffered by perimeter columns of the two longitudinal facades, better described successively. Successively the building was repaired and upgraded with the insertion of shear walls, but specific details of the intervention are not available. The original state of the building before the upgrading works is considered.

3.1.1 *Description*

The building is a 7-storey 3 bay-by-8 bay cast-in-place r.c. moment-resisting frame building, with non ductile column detailing, designed in 1965 in compliance to the lateral force requirements of 1964 Los Angeles City Building Code. The structural system consists of perimeter moment frames and interior slab-column frames, as shown by the planar view and the transverse section of Figure 3-1.

The design was done by Rissman and Rissman Associates, the planar configuration has a rectangular shape of about 6200 m^2, by considering all the floors, with the principal direction, the longitudinal one, oriented east-west. The main dimensions are nearly 46 m x 19 m; the first elevation is about 4.12 m, while the storey 2 through 6 are 2.65 m and the last floor is 2.60 m, for a total height of about 20 m.

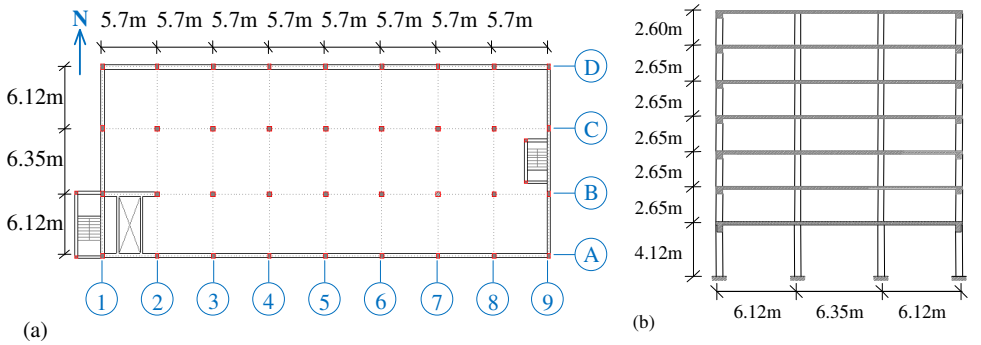

Figure 3-1 Van Nuys Building: (a) planar view and (b) transverse section

Lateral force resistance is provided by the perimeter moment frames, although the interior columns and slabs also contribute to lateral stiffness. The gravity system comprises 2-way reinforced-concrete flat slabs supported by square columns at the interior and by the rectangular columns of the perimeter frame. Slabs are 25.4 cm deep at the 2nd floor, 22 cm at the 3rd through 7th floors, and 20.3 cm at the roof. The roof also has lightweight concrete topping varying in thickness between 8.2 cm and 20.3 cm.

The connections between different elevations are provided by two stairwells, located at both opposite transverse facades, moreover lifts are located in correspondence of alignments A1-2, B1-2. The stairs structure seems to do not interfere with the frames, but no details were available. The building is approximately symmetric, with the exception of the beams for the elevators openings and for the 4 bays of infill walls located at the east end of the north side, at the first elevation only.

More details dealing with beams and columns sections and material properties are reported in Appendix A, section dedicated to the FEM model features.

The foundation system (Figure 3-2) consists of drilled piles, diameter 61 cm depth roughly 12 m, grouped in caps, with an height of about 97 cm, from two to four piles. Single piles are used for the stairwells. The three piles caps are used for the perimeter columns, while the four pile caps is used for interior columns; in both cases the column are located in the centre of the caps. All the pile caps are connected by a grid of beams. Each pile has a design capacity of over 450 kN vertical load and up to 90 kN lateral load.

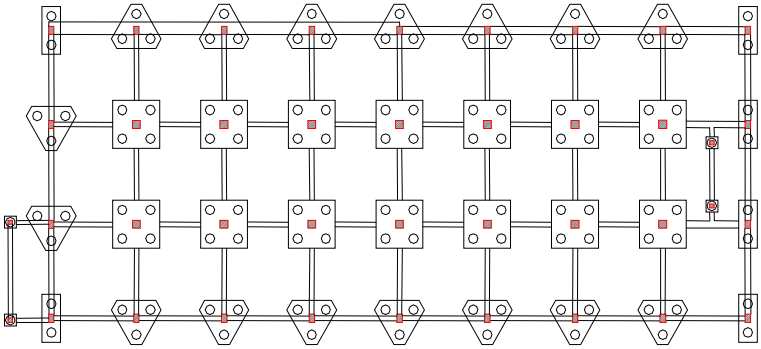

Figure 3-2 Van Nuys building foundation plan

From an architectonical point of view, the ground floor contains the reception area, hotel office, kitchen, dining room and other hotel services (Figure 3-3). Floors 2 through 6 (Figure 3-4) have 22 hotel suites each, for a total of 132 rooms. The building is clad on the North and South facades with aluminium window wall, comprising 5 mm heavy sheet glass in sliding frames, and 6 mm cement asbestos board panels with an ornamental site-obscuring mashed of baked enamel or coloured vinyl. Interior partitions are constructed of gypsum wallboard on metal studs. Ceilings at the 2nd through 7th floors are textured coating applied to the soffit of the concrete slab above; while at the first floor, ceilings are suspended wallboard or lath and plaster. The East and West end-walls are finished on the inside with gypsum wallboard and on the outside with stucco. Room air conditioning is provided by through-wall air-conditioning units mounted in the waist panels below the windows (Beck et al. 2002).

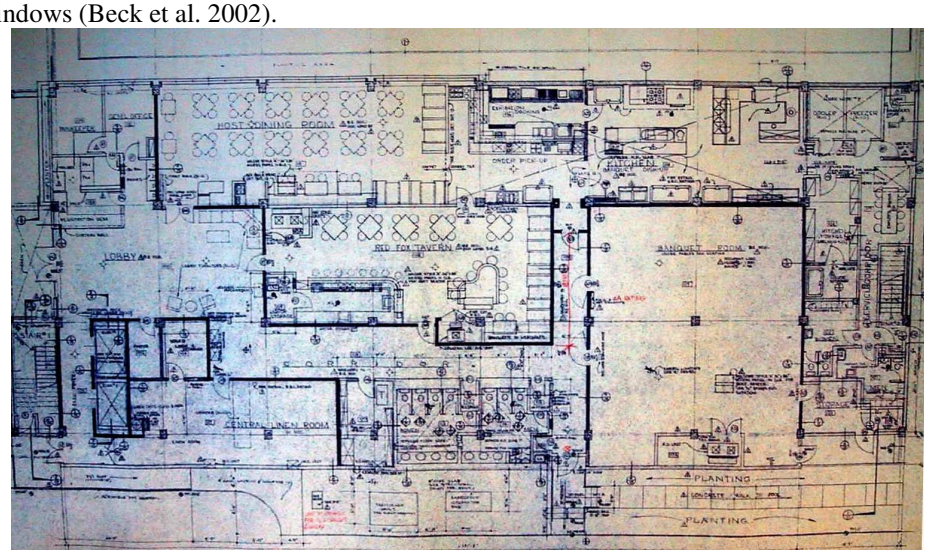

Figure 3-3 First floor architectural plan (Rissman and Rissman Associates)

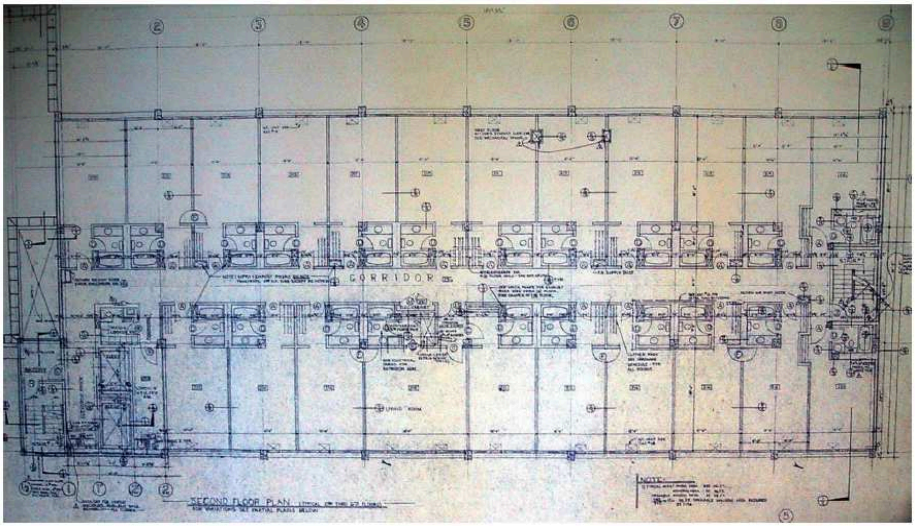

Figure 3-4 Second floor architectural plan (Rissman and Rissman Associates)

The geological data indicate that the site lies on recent alluvium and the results of boring logs executed in 1965 and 1994 (Blume & Associates 1973, Krawinkler 2005), indicate that the underlying soil consists primarily of fine sandy silts and silty fine sands, with a shear-wave velocity average of 300 m/s in the top 30 m (Trifunac et al. 2001).

3.1.2 *Recorded earthquakes and related damages*

Van Nuys building was widely investigated thanks to the fact that was instrumented since 1971 and many earthquake records, listed in Table 3-1, are available. That could give the opportunity to make correlations between data records and results provided by FEM models, moreover between observed damages and related behaviour predictions.

The building response to the 1971 San Fernando earthquakes was recorded by three self contained triaxial accelerometers located at first, fourth and at the last elevations, respectively. All the other earthquakes were recorded by an enhanced recording system provided by the California Division of Mines and Geology (CDMG) within the Strong Motion Instrumentation Program.

Table 3-1 Earthquake recorded through the Van Nuys Building instruments

Earthquake	*Data*	*Magnitude*	*Epicentral distance* [km]
San Fernando	09/02/1971	6.6	22
Whittier Narrows	01/10/1987	5.9	41
Whittier Narrows aftershock	04/10/1987	5.3	38
Pasadena	03/10/1988	4.9	32
Montebello	12/06/1989	4.1	34
Malibu	19/01/1989	5.0	36
Sierra Madre	28/06/1991	5.8	44
Landers	28/06/1992	7.5	186

Earthquake	*Data*	*Magnitude*	*Epicentral distance* [km]
Big Bear	28/06/1992	6.5	149
Northridge	17/01/1994	6.5	1.5
Northridge aftershock	20/03/1994	5.2	1.2
Northridge aftershock	06/12/1994	4.5	10.8

Even though Van Nuys building was hit by several earthquakes, it was damaged only by San Fernando and Northridge earthquakes; related damages are very well described by Blume and Associates 1973 and Trifunac et al. 1999. A brief report is herein recall.

Structural damages caused by 1971 San Fernando earthquake consisted in cracks in the spandrel beam-to-column connection at the north-east corner of the building; those damages were repaired by means of epoxy. Damages to the partitions and exterior plaster were considerable, moreover those to bathrooms tiles and plumbing fixtures were severe on the second and third floors, while they were minimal at the sixth and seventh floors. The damage level detected, substantial non-structural damages, with columns remained into the elastic limit with high stresses, is related to an interstorey drift value larger than 2.54 cm – 3.05 cm.

An overview of damages produced by Northridge earthquakes can be seen in Figure 3-5 and Figure 3-6; where Trifunac et al. clearly report a description of typology and dimension of structural damages. Significant structural damages occurred in the external longitudinal facades; in frame A (South facade Figure 3-5) wide shear cracks appeared in the column just below the 5th floor spandrel beams, while in frame D (North facade Figure 3-6) shear cracks were smaller and located in correspondence of lower floors, especially 2nd and 3rd. Cracks were also evident on the infill bricks walls of the first elevation. The non-structural damage was extensive and almost every guest room suffered some damages.

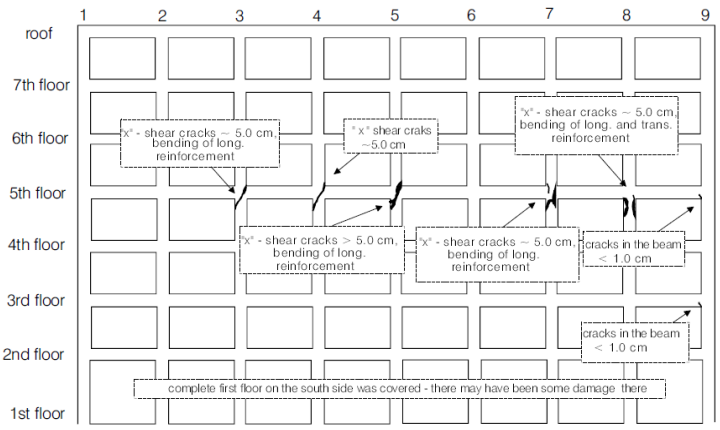

Figure 3-5 Structural damages on the South A facade of the Van Nuys Building, after Northridge earthquake, detected by Trifunac et al. in the survey of 04/02/1994

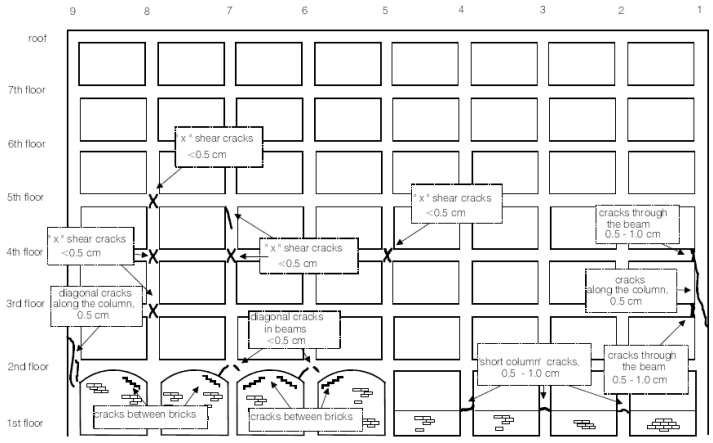

Figure 3-6 Structural damages on the North D facade of the Van Nuys Building, after Northridge earthquake, detected by Trifunac et al. in the survey of 04/02/1994

3.1.3 *Seismic hazard*

The seismic hazard has been described by employing a design value of PGA, related to a given Limit State (Life Safety) having a probability of exceedance of 10% in 50 years, therefore a return period of 475 years. The ground motions variability, instead, is represented by a set of 60 records provided by Somerville et al. used in the SAC project, whose characteristics are reported in literature (Somerville et al. 1997). Among these records two suite of ten time-history, for the site of Los Angeles, area in which the benchmark structure is located, have been choose. Selected ground motions are characterized by different seismic intensities, frequency content and duration. The relation between the seismic input and the dynamic properties of the case studies is illustrated in Figure 3-7, where the pseudo-acceleration response spectra of the 20 records are reported together with the mean response spectrum. In the same figure, the spectral values at the first vibration period in the transverse and longitudinal direction of the Van Nuys building are also reported by red and white circles, respectively.

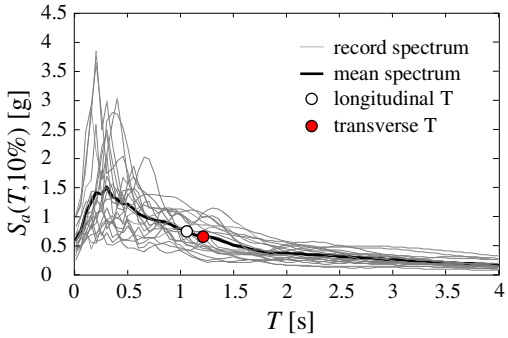

Figure 3-7 Pseudo-acceleration response spectra describing the seismic scenario

The 20 records are related to subsequent earthquakes: Imperial Valley (19/05/1940), Landers (28/06/1992), Loma Prieta (17/10/1989), Northridge (17/01/1994) and North Palm Springs (08/07/1986).

3.1.4 *Modelling criteria*

The dynamic problem, existing building to protect plus external dissipative rocking system, is a general system described by a vector of displacements $\mathbf{u}(t) \in R^l$ which is split into two components, one related to the active degrees of freedom (DOFs) $\mathbf{x}(t) \in R^m$ and the other to the internal DOFs $\mathbf{y}(t) \in R^n$. A convenient way to describe the overall system is to choose a reduced number of degrees of freedom; therefore the active ones express the horizontal displacements of the masses, concentrated at the storey levels which are assumed to be rigid. The internal degrees of freedom, instead, aim to describe the damping capacity of the system, hence they are representative of the dampers displacements only. For the Van Nuys case study the vector **x***(t)* collects the motions of the seven storeys, while the vector of dependent degrees of freedom **y***(t)* the motions of the two FVDs. Therefore all the matrices have size $l \times l$, where $l = m + n$.

For the mass matrix $\mathbf{M}$ construction, a lumped-mass model is used, which provides a mass matrix with non-zero terms only in the principle diagonal and in correspondence of active degrees of freedom of the coupled system. The non-zero terms are equal to the sum of masses of the existing frame and of the retrofitting external structure, read at every floor level and accounting for structural masses, dead loads and a percentage of accidental loads. Figure 3-8 portrays a scheme of the procedure for the mass matrix construction of the bare frame.

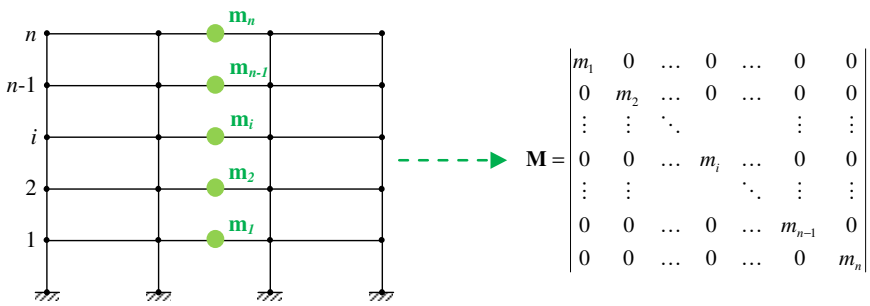

Figure 3-8 Steps for the mass matrix construction

For the problem at hand also the stiffness matrix of the system, $\mathbf{K}$, results from the sum of the contributions of the existing frame and of the external dissipative structure. It is possible to determine manually all the components of the matrix, that is $\mathbf{K}_{xx}$, $\mathbf{K}_{xy}$ and $\mathbf{K}_{yy}$, but it is advisable to use a FEM model of the structures involved, which accounts for all the aspects that need a description. A three dimensional finite element model is

developed in SAP2000 and used to better describe the local stiffness distribution; this way all the matrices found are condensed.

The FEM model describes both the bare Van Nuys building and the overall system by using three-dimensional linear elastic elements for the frame as well as for the interior slabs, which are modelled as equivalent beams by adopting the general criteria used in ASCE Standard (ASCE/SEI 41-13). In a practical way for the stiffness matrix construction the translation of all the joints, related to both active and dependent degrees of freedom, is restrained. No diaphragm constraint is defined and a unitary displacement is assigned to all the joints, in the direction in which the translation is restrained, i.e. vertical displacement for the FVDs and horizontal displacements for each joint of all the floor levels. Successively the sum of the reactions, read at every joint of each floor level and on the FVDs to the given displacement, provides the related terms on the stiffness matrix, that is $\mathbf{K}_{xx}$, $\mathbf{K}_{xy}$ and $\mathbf{K}_{yy}$. Figure 3-9 provides a schematic view of the procedures involved in the stiffness matrix construction of the bare building.

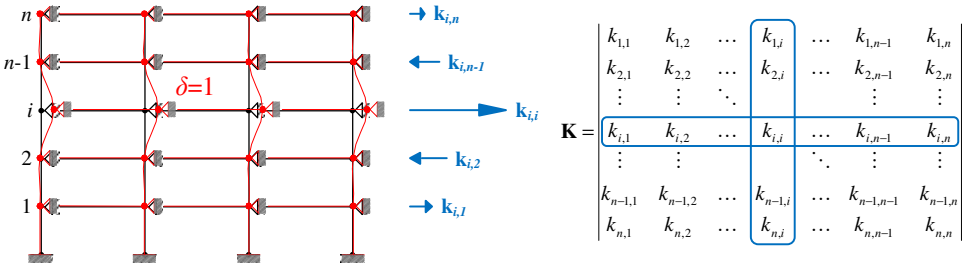

Figure 3-9 Steps for the stiffness matrix construction

Once known the mass and stiffness matrices the damping contribution of the bare frame $\mathbf{C}_F$ is determined through a Rayleigh approach, while the contribution related to the external structure $\mathbf{C}_D$ is obtained through the knowledge of the damping features of the FVDs. Hence the damping matrix of the coupled system $\mathbf{C}$ is obtained as sum of the two contributions.

Successively all the analysis are performed with MATLAB, according to the proposed formulation.

3.1.5 *Retrofit configurations*

The Van Nuys building retrofit is achieved with the insertion of the external dissipative rocking system investigated. In order to understand how the added stiffness (displacements linearization) and added damping provided by the rocking structure, influence the seismic performance of the coupled system, a parametric study is carried out. The study is based on the variation of both the external structure stiffness and the dampers viscous constant and by evaluating, successively, the corresponding changes in the dynamic of the system and in its seismic response.

Two non-dimensional parameters are used to synthetically describe the contribution of the external structure (tower) to the stiffness and damping. The first one is $\kappa = K_D / K_F$, denoting the tower-to-frame stiffness ratio, where the stiffness measures for the frame and the tower, K_F and K_D respectively, are evaluated by imposing a unit horizontal displacement at their top and by evaluating the corresponding base reaction. In the case of the external structure, a fixed base condition is considered, i.e., the rocking motion is restrained. The measure of damping ξ_{add}, is an estimate of the damping added to the first mode of vibration of the coupled system.

In the analyses, different configurations are considered, corresponding to values of κ in the range between 0 and 1, and of ξ_{add} in the range between 0 and 0.30. The case of the bare existing frame (denoted to as *As is* configuration), correspond to κ=0, ξ_{add}=0. In addition to this case, also the one corresponding to an infinitely stiff external structure (denoted as *Stiff*), with ξ_{add}=0.30, is considered for comparison purposes. The external dissipative rocking system is dimensioned with a seismic action having a probability of exceedance of 10% in 50 years, with the aim to reach a limited damaging on the non-structural components of the existing frame; Table 3-2 reports the geometrical properties of the profiles employed for the bracing systems forming the external structure for all the different retrofit configurations considered. In fact only the number of towers inserted is varied among the different retrofit cases, while the geometrical properties and the FVDs constant remain the same. It is noteworthy that each tower is equipped with four FVDs, located at the base. The profiles properties satisfy all the EC3 code requirements concerning the safety checks. Figure 3-10 depicts the reference retrofit configuration characterized by κ=1, which is achieved with the insertion of four external dissipative towers. The number of external dissipative rocking structures is determined for feasibility question, in order to avoid high stresses on the dissipative system and related foundations, usually realized through drilled piles.

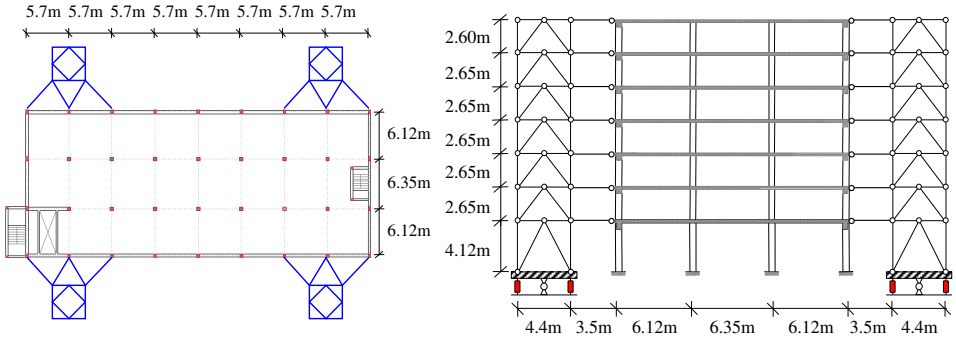

Figure 3-10 Van Nuys building retrofit configuration

Table 3-2 Geometrical properties of the external dissipative rocking system for all the retrofit configurations considered

Floor	*Retrofit*	
	column	Brace
1	HEB300	HEB300
2	HEB200	HEB200
3	HEB180	HEB180
4	HEB160	HEB160
5	HEB160	HEB160
6	HEB160	HEB160
Roof	HEB160	HEB160

For what concern the analyses performed with MATLAB, the external bracing system is always represented as single matrix of mass, stiffness and damping, even if the number of rocking structures is higher than one. Similarly, the FVDs are always represented by the two degrees-of-freedom involved in the bracings deformation.

3.2 Camerino building

The second case study deals with an existing r.c. frame building designed in Italy during the '80s without seismic standards or any ductile detailing therefore representative of the Italian building heritage of the period 60's-80's. The building is assumed to be located in Camerino, a small town in central Italy very close to the epicentre of the Marche-Umbria 1997 and central Italy 2016 earthquakes, therefore representative of an area characterized by an high level of seismic hazard.

3.2.1 *Description*

The building has a rectangular shape, with a planar dimension of 25.30 m x 10.85 m, and is characterized by 5 storeys plus the roof, for a total height of 18.20 m. The first elevation has an height of 2.8 m, floors 2 through 5 are 3 m, while the roof has a variable dimension (1.7-3.4 m). Along the longitudinal direction, the structure consists of two external frames with 6 spans and a central one with 7 spans (Figure 3-11 (a) and (b)). The connection between floors is realized through a central stairwell and a lift, located in central position with respect to the transverse direction of the building.

The floors are one way r.c. and have a thickness of 20 cm (16+4 cm), while the balconies are r.c. slabs of same thickness. The frame has a shallow foundation, which is realized through a grid of beams.

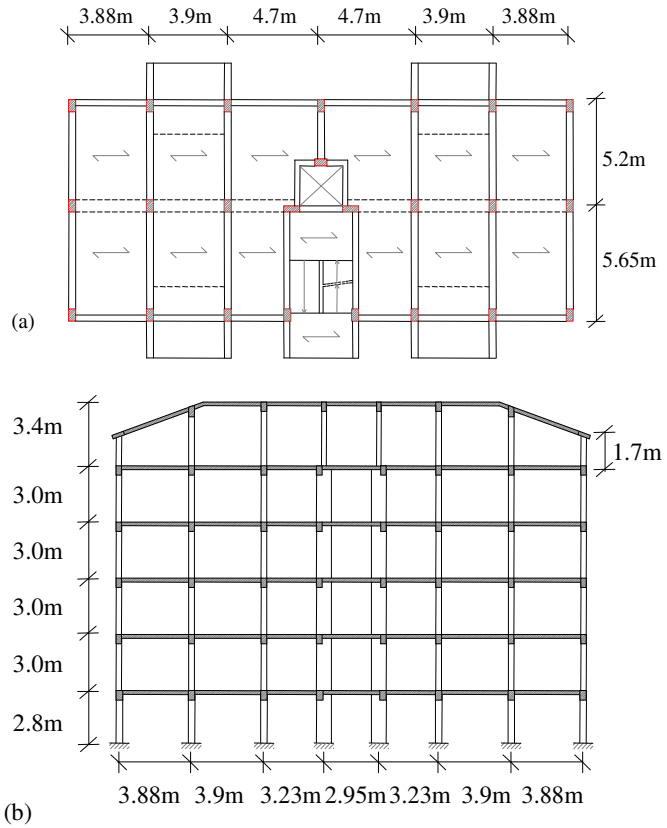

Figure 3-11 Planar view (a) and longitudinal section (b) of the bare building

More details, regarding structural dimensions, material properties, loads and everything concerning the FEM model are reported in Appendix A.

3.2.2 *Seismic hazard*

The seismic hazard has been described by employing a design value of PGA, related to the Ultimate Limit State (SLV), as defined by the Italian Standards (NTC 2008), having a probability of exceedance of 10% in 50 years.. The ground motions variability is represented by seven groups of artificial earthquakes generated in accordance with NTC 2008 (total duration 25 s and stationary part duration at least equal to 10 s) for a reference period V_R of 50 years with soil category C and topographical one T1, for the over mentioned Limit State.

3.2.3 *Modelling criteria*

As already seen for the Van Nuys building, also for Camerino building case study the active degrees of freedom, $\mathbf{x}(t) \in R^m$, are related only to the horizontal displacements of the masses concentrated at the storey levels, which are assumed to be rigid. Hence the vector collects the motions of the five storeys, while the contribution of the roof in terms of mass is considered together with the lower level. For what concern the stiffness contribution of the roof a static condensation is operated, so that the dimension of the related matrix is 5x5. Also in this case the dependent degrees of freedom, involved in the bracing system deformation, $\mathbf{y}(t) \in R^n$, are represented by the FVDs motions only.

A three dimensional finite element model is developed in SAP2000 for the Camerino building too and used to better describe the mass, stiffness and damping matrices of the overall system. The analysis are successively performed in MATLAB, in accordance with the proposed formulation.

3.2.4 *Retrofit configurations*

The Camerino building retrofit configuration is achieved with the insertion of two external rocking structures, located as shown in Figure 3-12. The bracings have a square plan of dimension 4.1 m x 4.1 m and the same interstorey heights of the building. The chosen criterion for their stiffness design is the reduction and regularization of the interstorey drifts (Θ_i), with respect to the bare frame at the Ultimate Limit State (SLV). The damping contribution provided by the towers in all the analyzed configuration is ξ_{add}=0.20.

The results shown in successive chapters concern not only the retrofit configuration shown in Figure 3-12, but also other three solutions. All the four cases analyzed are herein described:

1. the bare existing frame (*As is*);
2. the r.c. frame coupled with two dissipative structures connected with the frame at every elevation, except the roof (*Retrofit*);
3. the same features of the previous case, connected to the existing building only at the fifth floor (*Retrofit 1F*);
4. the case of two infinitely stiff rocking structures (*Stiff*).

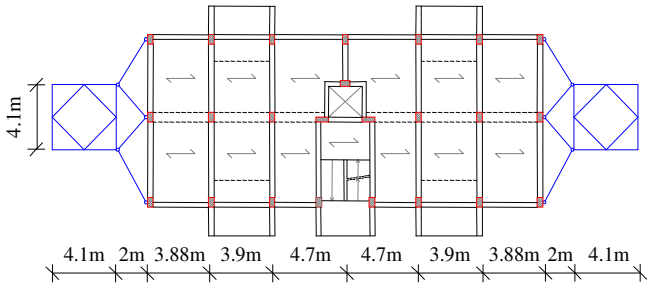

Figure 3-12 Camerino building retrofit configuration

Chapter 4

Modal Properties

This chapter deals with modal properties of the coupled system existing building plus external dissipative rocking system. As said in previous sections the bracing system influences both the stiffness and the damping properties of the coupled system, while its contribution to the masses is negligible. Hence it is useful to separately analyze the variations on damping and stiffness, intended as linearization of displacements distribution. For this purpose, the case of the added bracing without dampers is considered separately from the case of the bracing with dampers.

In general the effect of the retrofit in terms of added stiffness is observed through the monitoring of vibration periods and related mass participant factors before and after the coupling. Moreover the distribution of interstorey drifts and shear action resisted by the frame in the principle vibration modes is compared for all the analyzed configurations.

For what concern the added damping the term ξ_{add} is introduced as an estimate of the damping added to the first mode of vibration of the coupled system according to the expression reported in ASCE/SEI 41-13:

$$\xi_{add} = \frac{\sum_{j=1}^{N} E_j}{4\pi E_k} \qquad (4\text{-}1)$$

where E_j is the work done by j-th device in one complete vibration cycle at the fundamental frequency of the coupled system, N is the total number of FVDs and E_k is the maximum strain energy in the system. In evaluating ξ_{add}, the coupled system is assumed to deform according to its first undamped vibration mode and E_j can be directly related to the displacements of the dampers induced by the rocking motion.

In addition, the effects of added damping can be seen and evaluated through the monitoring of some parameters herein briefly introduced.

Due to the fact that all the dampers are concentrated at the base of the bracing, the system is non-classical damped and the extent of non-classical damping can be synthetically quantified by the coupling index ρ (Claret e Venancio-Filho 1991), expressed as:

$$\rho = \max \left| \frac{\Xi_{ij}^2}{\Xi_{ii}\Xi_{jj}} \right| (i, j=1,2,\ldots,m)\ i \neq j \qquad (4\text{-}2)$$

where $\Xi_{ij} = \boldsymbol{\psi}_i^T \mathbf{C} \boldsymbol{\psi}_j$ represents the coupling between the responses of mode *i* and *j*, and $\boldsymbol{\psi}_i$ are the eigenvectors of the undamped system. The index ρ assumes the value 0 for classical damped systems and it spans the range [0,1] in the case of non-classical damping.

Information about the effects of added damping can be obtained also through the monitoring of the complex eigenvectors $\boldsymbol{\varphi}_i$, for increasing values of ξ_{add}. The real and imaginary components of the complex eigenvectors $\boldsymbol{\varphi}_i$ are plotted separately and normalized in such a way that the first component of the real part of the eigenvector $\boldsymbol{\varphi}_i$ is equal to one, while the imaginary one is equal to zero.

Finally another way to investigate the effects of added damping is to report complex eigenvectors $\boldsymbol{\varphi}_i$ in polar form (magnitude $\left| \ \right|$, phase angle ϑ). When the system is classically-damped all the masses are either in phase or 180° out of phase, while, if the system is non-classically damped the masses are no more in phase neither 180° out of phase and it can be useful to observe their variation with increasing values of added damping.

The results shown successively will concern both the Van Nuys building and the Camerino building.

4.1 Van Nuys building

The dynamic system is described by considering only the motion along the transverse direction.

4.1.1 *Modal properties of the undamped system*

As said previously, the bracing system influences both the stiffness and the damping properties of the coupled system, while its contribution to the masses is negligible; this section analyzes the changes in the dynamic behaviour of the coupled system due to the external rocking system in the undamped case (ξ_{add}=0).

Table 4-1 reports, for the seven modes of the bare building (*As is*), the vibration periods, the undamped natural frequencies and the participant mass ratios M_i^*, defined as $M_i^* = (\mathbf{Mp} \cdot \boldsymbol{\psi}_i)^2 / \mathbf{M}\boldsymbol{\psi}_i \cdot \boldsymbol{\psi}_i$, where $\boldsymbol{\psi}_i$ are the eigenvectors of the undamped system. The

same results are reported for the two retrofit configurations corresponding to κ=0.5 and κ=1, in Table 4-2 and Table 4-3, respectively.

In general, it can be observed that the coupling with the external system does not affect significantly the first vibration period. In fact, its reduction is of about 2.2% in the case of the bracings with stiffness ratio κ=1 and of about 1.9% in the case of the bracings with stiffness ratio κ=0.5. The variation of the second vibration period is higher, in fact in the case of κ=1 the reduction, with respect to the bare frame, is nearly 34.3%, while in the case of κ=0.5 the reduction is nearly 22.7%.In all the cases, the first two vibration modes involve more than 95% of the total participating mass, with small variations due to the addition of the rocking systems. It is noteworthy that the case of the existing frame coupled with an infinitely stiff system is characterized by one vibration mode only, with vibration period T=1.149 s as it behaves as a SDOF system governed by the bracing rocking motion.

Table 4-1 Van Nuys building: modal analysis results of the bare building

T_i [s]	ω_0	M_i^*	ΣM_i^*
1.204	5.22	0.831	0.831
0.391	16.06	0.118	0.949
0.218	28.86	0.035	0.984
0.138	45.61	0.011	0.995
0.093	67.34	0.003	0.998
0.068	91.94	0.001	1
0.056	112.42	0.000	1

Table 4-2 Van Nuys building: modal analysis results of the retrofit case κ=0.5

T_i [s]	ω_0	M_i^*	ΣM_i^*
1.182	5.32	0.833	0.833
0.302	20.77	0.120	0.953
0.151	41.62	0.032	0.985
0.097	64.85	0.010	0.995
0.070	89.48	0.003	0.998
0.054	115.39	0.001	1
0.046	135.25	0.000	1

Table 4-3 Van Nuys building: modal analysis results of the retrofit case κ=1

T_i [s]	ω_0	M_i^*	ΣM_i^*
1.177	5.34	0.832	0.832
0.257	24.46	0.122	0.954
0.123	51.11	0.031	0.985
0.079	79.31	0.010	0.995
0.059	106.80	0.003	0.999
0.047	134.32	0.001	1
0.041	154.55	0.000	1

Figure 4-1 reports and compares the values of the interstorey drifts along the building height corresponding to the first three vibration modes of the bare building and of the coupled system with κ=1 and κ=0.5. The interstorey drift values are obtained from the displacements distribution along the height, with the maximum top displacement normalized to unity. It can be observed that the addition of the bracings yields a regularization of the drift demands along the building height, this implies higher and lower values of the drift required at different levels.

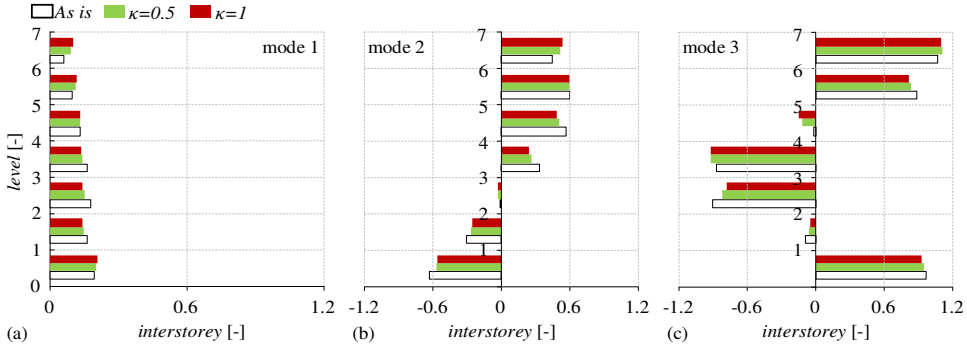

Figure 4-1 Van Nuys building: interstorey drifts along the building height for mode 1 (a), mode 2 (b) and 3 (c)

Figure 4-2 reports the distribution of the shear force resisted by the frame in the *As is* and in the retrofit cases, for the first three vibration modes. Again, it is possible to observe the effects of the coupling, resulting in a more uniform distribution of the storey shear of the first mode.

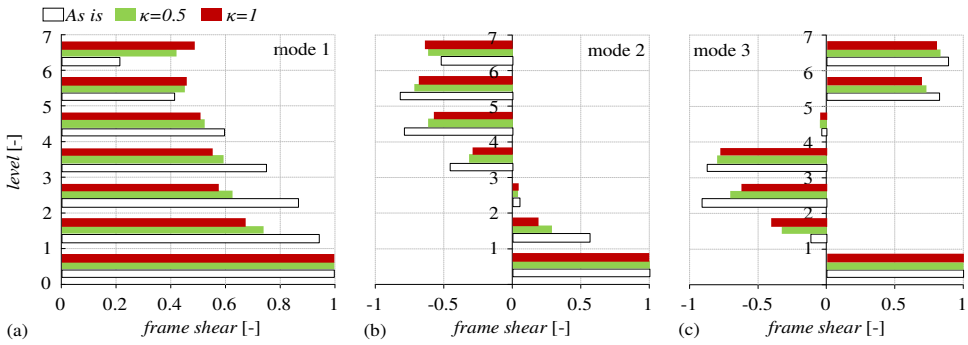

Figure 4-2 Van Nuys building: comparison of the shear force resisted by the frame for mode 1 (a), mode 2 (b) and 3 (c)

Figure 4-3 shows, for the retrofit case with κ=1, the total storey shear distribution, and the separate contributions of the frame and of the bracing, normalized to a unity value, with respect of the total base shear. It is worth to note that the shear contribution of the existing frame and of the bracing have different signs at some levels and, for the considered case, at the first and the last two levels the first mode shear force acting on the existing frame is higher than both the total shear force and the force resisted by the bare frame. This evidence is representative of a possible drawback of the interstorey drifts regularization.

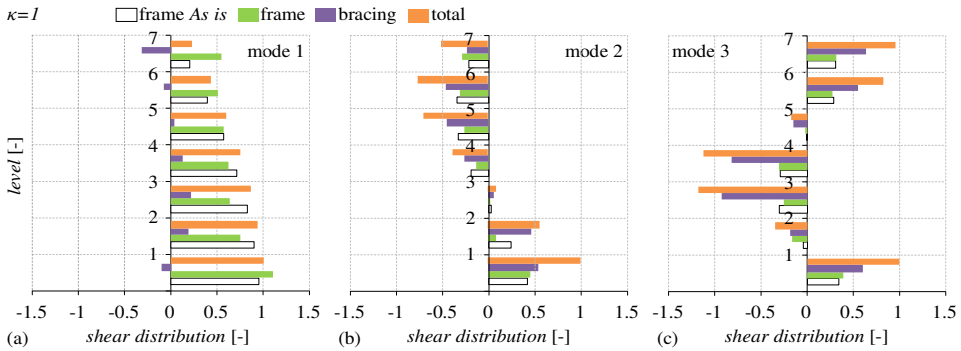

Figure 4-3 Van Nuys building: shear force distribution for mode 1 (a), mode 2 (b) and 3 (c) in the $\kappa = 1$ retrofit case

4.1.2 *Modal properties of the damped system*

This section analyzes the influence of the damping due to the added bracings on the dynamic behaviour of the system. It is useful to remember that the damping of the coupled system is the sum of the contribution of the existing frame $\mathbf{C}_F$, providing a inherent damping ξ=0.05 at the first two vibration modes and the contribution of the external rocking system $\mathbf{C}_D$, directly related to the FVDs displacements produced by the rocking motion of the bracings.

The variation of the modal properties at different damping levels is evaluated via complex modal analysis by considering values of the added damping factor ξ_{add} in the range between 0 and 0.9.

Figure 4-4 shows the influence of ξ_{add} on the vibration periods of the first three modes for the retrofit configuration with κ=1. In general, the vibration periods of the coupled system decrease for increasing damping level but only the first vibration period of the system is significantly affected by ξ_{add}. For ξ_{add}=0.9, the first period attains the value 0.731 s (62% of the value observed for undamped case), the second 0.222 s (86% of the related undamped period) and the third 0.118 s (96% of the related undamped period).

Figure 4-5 reports the variation with ξ_{add} of the damping ratio of the first, second and third vibration modes of two retrofit configurations corresponding, respectively, to κ=1 and to κ=0.5. The trends of the damping ratios are very similar for two retrofit configurations, with higher variations observed for the first mode and negligible variation for the second and third ones. In both cases, the first modal damping ratio (ξ_1) is well approximated by the design formula of Eqn. (4-1) up to the design values of ξ_{add}, that is values up to 0.3 in the retrofit case κ=1 and up to 0.15 in the κ=0.5, configuration. For increasing values beyond these limits, the amount of the effective damping decreases. As already observed for the periods, the influence of the damper dimensions on the second and

third mode is less notable; for the κ=1 configuration the damping ratio varies in the range 0.050-0.089 with a maximum 0.135 when ξ_{add} reaches the design value for the second mode, while for the third mode the range is 0.090-0.099 with a maximum value of 0.110 when ξ_{add}=0.15. For the κ=0.5 case the trend is very similar, in fact also in this configuration the second mode has its maximum, 0.111, for the design value of ξ_{add}=0.15, while the damping ratio varies in the range 0.050-0.085. Finally for the third mode the range is 0.085-0.092 with a maximum value of 0.100 when ξ_{add}=0.1.

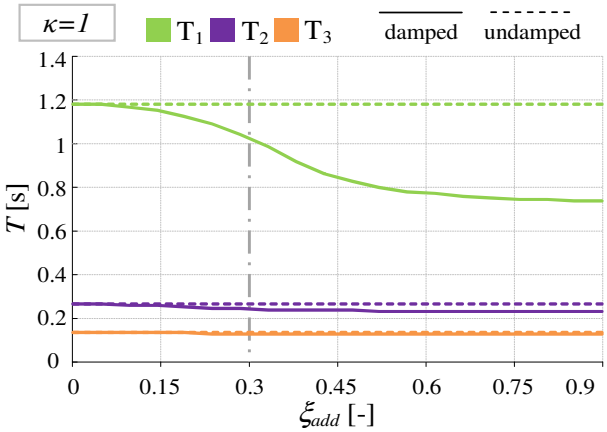

Figure 4-4 Van Nuys building: first three period trends in the retrofit case κ=1

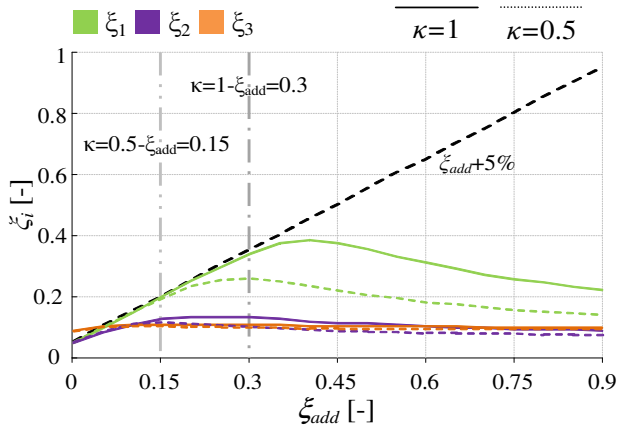

Figure 4-5 Van Nuys building: comparison of the first three modes damping trends for both κ=1 and κ=0.5 configurations

The particular location of viscous dampers, concentrated at bracings base, significantly simplifies the inspection and maintenance operation, while on the other side leads the system to become non-classically damped. A measure of non-classically damping can be given through the coupling index ρ, introduced in Eqn. (4-2).

Figure 4-6 reports the values assumed by the coupling index for the two different retrofit configurations for increasing damping levels. It can be seen that ρ increases less than linearly for increasing values of ξ_{add} and that the two retrofit cases provide nearly the same values of the index. Figure 4-7, instead, shows the values of Ξ_{ij} obtained for the case $\kappa = 1 - \xi_{add} = 0.3$. In particular, for $-\xi_{add} = 0.3$ $\Xi_{12} = 0.68$ and it coincides with the coupling index ρ, i.e., the coupling is highest between the first and the second mode of vibration with respect to the other modes.

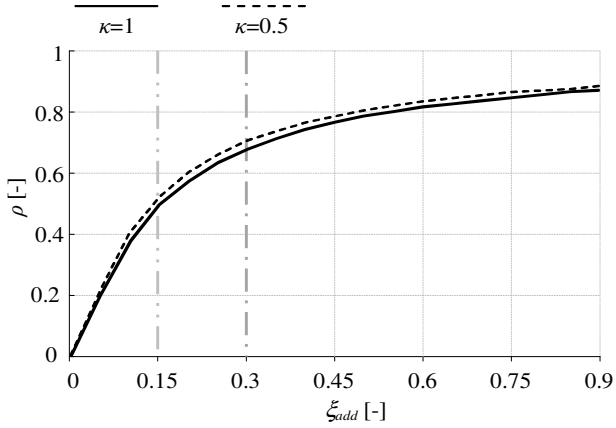

Figure 4-6 Van Nuys building: ρ-index trend comparison for increasing damping levels for both $\kappa = 1$ and $\kappa = 0.5$ configurations

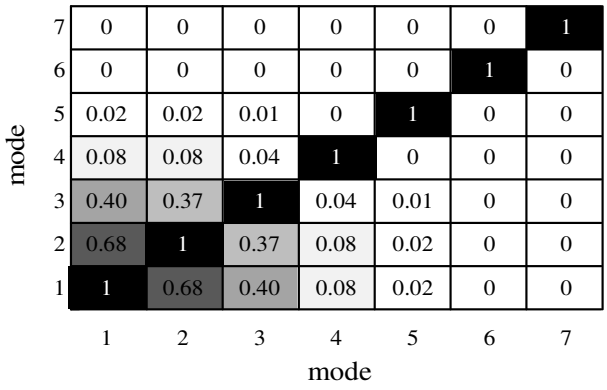

Figure 4-7 Van Nuys building: ρ-index values for the seven modes of the system in the retrofit case $\kappa = 1$ and $\xi_{add} = 0.3$

Figure 4-8 shows the first three modal shapes of the coupled system with $\kappa = 1$ and for different levels of ξ_{add}. The real and imaginary components of the complex eigenvectors $\boldsymbol{\varphi}_i$ are plotted separately and normalized in such a way that the first component of the real

part, r_{1i}, of the eigenvector $\boldsymbol{\varphi}_i$ is equal to one, while the imaginary one, i_{1i}, is equal to zero. In the case of ξ_{add} =0, the system is classically damped, and the eigenvectors are real. Increasing the damping level affects significantly the first mode, while the higher modes are less influenced by ξ_{add}.

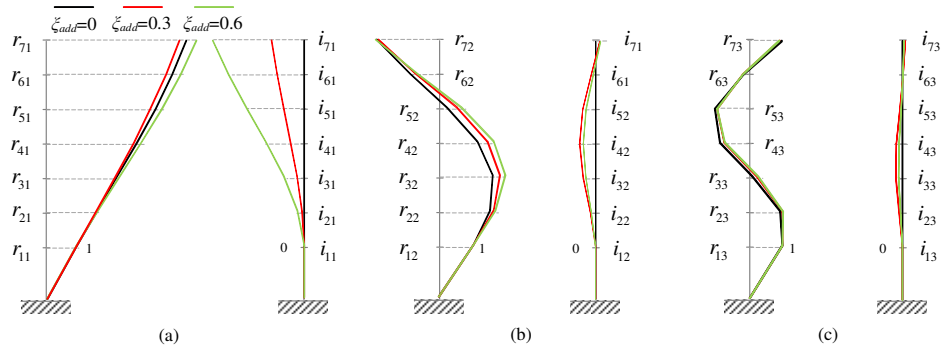

Figure 4-8 Van Nuys building retrofit κ =1 configuration: real and imaginary part of the complex eigenvectors for increasing values of damping (a) first mode (b) second mode (c) third mode

Another way to understand the effects of increasing added damping into a system is to observe the complex eigenvectors $\boldsymbol{\varphi}_i$, in polar form. It is observable that when the system is non-classically damped the masses are no more in phase neither 180° out of phase; the changing in the values of the phase gives an extent of how the system becomes non classically damped, for increasing values of ξ_{add}, and it is also possible to understand in which vibration modes the effects are higher. Table 4-4 lists the first three complex eigenvectors $\boldsymbol{\varphi}_i$ in polar form, with reference to the retrofit configuration κ =1- ξ_{add} =0.3. For each mode, just one of the two complex eigenvector of the pair is reported; the first seven components are related to displacements of the active degrees of freedom, the successive seven represent their velocities and last two are the displacements of the dissipative devices, denoting internal degrees of freedom. In the case in which the external bracings do not provide any damping contribution (ξ_{add}=0, classically damped system) it is clear that all the masses of the modes are in phase or 180° out of phase, as expected. For what concern the first mode at the design value of damping (ξ_{add}=0.3), it is useful to underline the difference of phase among the first and the last mass, that is the maximum value and which is equal to 15.71°. For ξ_{add}=0.6 the difference becomes higher and equal to 34.61°.

Table 4-4 Van Nuys building κ=1-ξ_{add}=0.3 configuration: polar form of the first three eigenvectors pairs for increasing values of damping

First mode						Second mode						Third mode					
c=0		*c*=1		*c*=2		*c*=0		*c*=1		*c*=2		*c*=0		*c*=1		*c*=2	
0,02	92,9	0,02	125,7	0,01	142,8	0,01	-87,1	0,01	105,0	0,01	101,3	0,01	-84,8	0,01	94,7	0,01	96,9
0,04	92,9	0,03	122,3	0,02	134,0	0,02	-87,1	0,02	101,4	0,02	98,6	0,01	-84,8	0,01	92,9	0,01	95,8
0,05	92,9	0,05	118,7	0,03	125,2	0,02	-87,1	0,02	97,5	0,02	95,9	0,00	-84,8	0	79,5	0,00	88,7
0,07	92,9	0,06	115,4	0,04	118,2	0,01	-87,1	0,01	92,9	0,02	93,1	0,01	95,2	0,01	-81,2	0,01	-80,7
0,08	92,9	0,07	112,9	0,05	113,3	0,00	-87,1	0,01	79,5	0,01	85,9	0,01	95,2	0,01	-83,9	0,01	-82,3
0,09	92,9	0,08	111,1	0,06	110,1	0,01	92,9	0,01	-67,3	0,01	-74,3	0,00	95,2	0	-86,8	0	-84,0
0,10	92,9	0,09	110,0	0,07	108,2	0,02	92,9	0,02	-77,4	0,02	-81,5	0,01	-84,8	0,01	96,4	0,01	97,8
0,11	0	0,12	15,7	0,09	34,6	0,31	180	0,29	7,51	0,27	5,41	0,45	-180	0,47	-1,40	0,47	1,07
0,19	0	0,20	12,4	0,16	25,8	0,45	-180	0,44	3,88	0,43	2,69	0,42	-180	0,47	-3,24	0,48	0
0,27	0	0,28	8,67	0,24	17,0	0,47	-180	0,50	0	0,51	0	0,04	180	0,11	-16,6	0,12	-7,18
0,35	0	0,35	5,42	0,33	10,0	0,34	180	0,41	-4,58	0,43	-2,88	0,41	0	0,37	-177,3	0,36	-176,5
0,42	0	0,42	2,92	0,42	5,14	0,07	180	0,16	-18,0	0,18	-10,0	0,49	0	0,47	-180	0,47	-178,2
0,49	0	0,49	1,13	0,51	1,92	0,25	0	0,19	-164,8	0,17	-170,3	0,09	0	0,10	177,1	0,10	-179,9
0,55	0	0,55	0	0,58	0	0,54	0	0,49	-174,9	0,49	-177,4	0,44	-180	0,43	0,24	0,42	1,98
0,01	92,9	0,01	135,0	0,01	168,1	0	-87,1	0	151,3	0,00	166,1	0	-84,8	0	155,6	0	169,2
0,01	-87,1	0,01	-45,0	0,01	-11,9	0	92,9	0	-28,7	0,00	-13,9	0	95,2	0	-24,4	0	-10,8

4.2 Camerino building

The dynamic system is described by considering only the motion along the longitudinal direction.

4.2.1 *Modal properties of the undamped system*

Table 4-5 reports, for the five modes of the bare building (*As is*), the vibration periods, the undamped natural frequencies and the participant mass ratios, defined as $M_i^* = (\mathbf{Mp} \cdot \boldsymbol{\psi}_i)^2 / \mathbf{M}\boldsymbol{\psi}_i \cdot \boldsymbol{\psi}_i$ where $\boldsymbol{\psi}_i$ are the eigenvectors of the undamped system.

Table 4-5 Camerino building: modal analysis results of the *As is* configuration

T_i [s]	ω_0	M_i^*	ΣM_i^*
1.021	6.18	0.787	0.787
0.300	21.03	0.117	0.904
0.153	41.26	0.052	0.956
0.097	65.51	0.03	0.985
0.074	86.05	0.015	1

The modal analysis results of the coupled system in the *Retrofit 1F* configuration are summarized in Table 4-6; it is important to remember that this configuration is based on the coupling with the same two external dissipative rocking bracings of the *Retrofit* configuration, but connected with the existing frame only at the last elevation. From the analysis of the results it is observable that there is an increment of nearly 1.5% on the value

of the period of the first three vibration modes with respect to the bare frame, whereas the percentage of the total mass involved is almost the same (90%). Hence the connection with this arrangement seems to do not modify sensibly the modal properties of the bare frame.

Table 4-6 Camerino building: modal analysis results of the *Retrofit 1F* configuration

T_i [s]	ω_0	M_i^*	ΣM_i^*
1.034	6.07	0.787	0.787
0.304	20.64	0.117	0.903
0.156	40.40	0.052	0.956
0.098	63.96	0.030	0.985
0.075	83.47	0.015	1

The results of the coupling with the *Retrofit* configuration are summarized in Table 4-7, where it can be observed that the first two vibration modes involve the 95% of the total mass and the second period reduces to about half the value obtained with the *As is* configuration. The last analyzed case, i.e. the existing frame coupled with an infinitely stiff tower (*Stiff*), is characterized by one vibration mode only (T=0.925 s) as it behaves like a SDOF system governed by the tower rocking motion.

Table 4-7 Camerino building: modal analysis results of the *Retrofit* configuration

T_i [s]	ω_0	M_i^*	ΣM_i^*
0.964	6.52	0.806	0.806
0.147	42.84	0.138	0.945
0.073	86.24	0.035	0.980
0.051	124.17	0.015	0.995
0.041	151.63	0.005	1

Figure 4-9 reports and compares the values of the interstorey drifts along the building height corresponding to the first three modes of vibration for the *As is*, *Retrofit 1F* and *Retrofit* configurations. It can be observed that the addition of the bracings yields a regularization of the drift demands along the building height only for the *Retrofit* case, even though a higher value of the drift is required at the first level.

Figure 4-10 reports, for the first three modes, the distributions of shear action resisted by the frame in the *As is*, *Retrofit 1F* and *Retrofit* cases, normalized to a unitary value at the base. Figure 4-11 shows, for the *Retrofit* configuration only, the storey shear demand for the building and the bracing, compared with the total one, moreover, for the first vibration mode only (Figure 4-11 (a)), there is also the shear action in the *As is* configuration. It is worth to note that the shear contributions of the existing frame and the bracings could have different signs at some levels and, for the considered case, the first mode shear forces acting on the existing frame are higher at the first level than both the total shear force and the shear action on the bare frame.

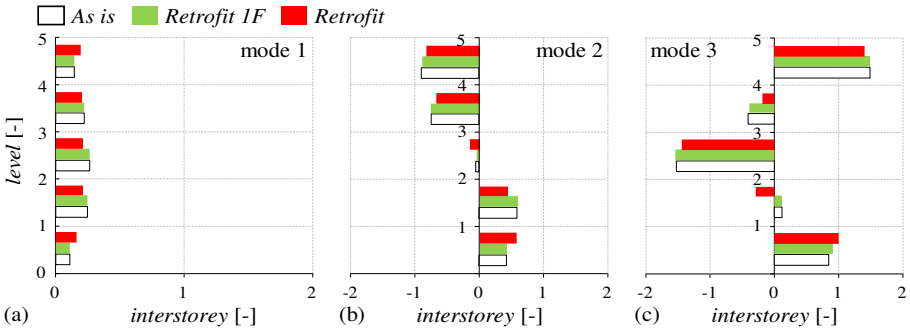

Figure 4-9 Camerino building: interstorey drifts distributions for mode 1 (a), mode 2 (b) and 3 (c)

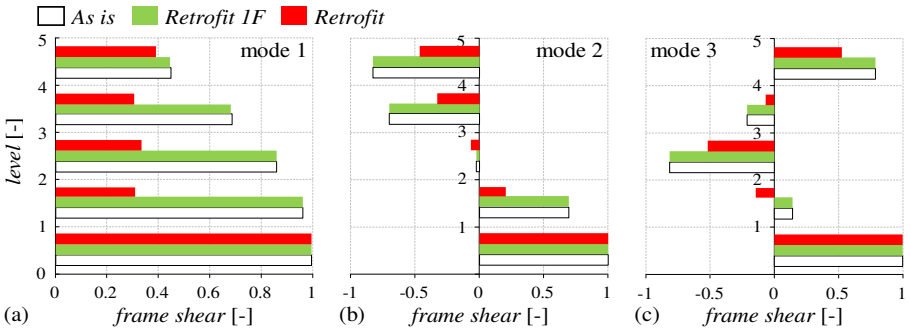

Figure 4-10 Camerino building: shear action resisted by the frame for mode 1 (a), mode 2 (b) and 3 (c)

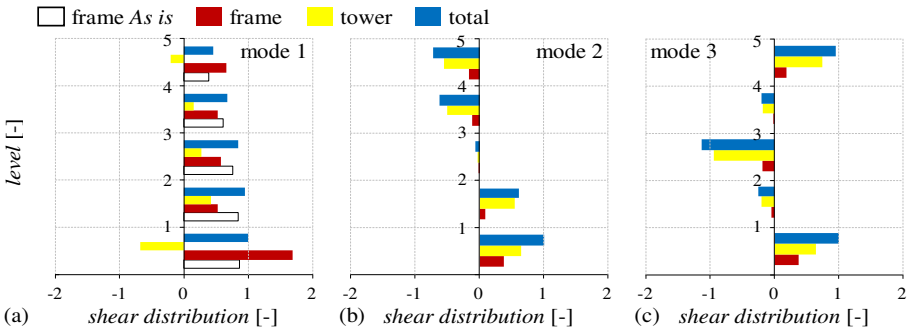

Figure 4-11 Camerino building: shear force distribution for mode 1 (a), mode 2 (b) and 3 (c) in the *Retrofit* configuration

4.2.2 *Modal properties of the damped system*

The damping of the coupled system is the sum of the contribution of the existing frame $\mathbf{C}_F$, providing a inherent damping ξ=0.05 at the first two vibration modes and the contribution of the external dissipative rocking system $\mathbf{C}_D$, directly related to the FVDs displacements produced by the rocking motion of the bracings.

The results shown in this section are related only to the *Retrofit* configuration, which consists of eight dampers, four per external structure, whose viscous constant values are designed by employing Eqn. (4-1) assuming that the coupled system deforms according to its first undamped vibration mode. The total amount of added damping is measured by C_0=135020 kNs/m, which is the sum of the viscous damping constant of the eight devices, dimensioned to provide an added damping of $\xi_{add} = 0.20$.

By means of the complex modal analysis it is possible to identify the damping ratio ξ_i corresponding to each one of the vibration modes, as shown in Eqn. (2-18); moreover, by introducing a damper multiplier c for the total added damping C_0, it is possible to evaluate the variation of the modal properties at different damping levels, defined by the parameter c.

Figure 4-12 (a) shows the influence of c on the vibration periods of the first three modes. The first three natural periods of the undamped system (dashed line in Figure 4-12) are 0.964 s the first period (red line), 0.147 s the second (yellow line), and 0.073 s the third period (blue line). The vibration periods of the coupled system decreases for increasing damping. For c=3.0, which corresponds to an added damping of $\xi_{add} = 0.60$, the first period attains the value 0.595 s (62% of the related undamped period), the second 0.141 s and the third 0.072 s, (96% and 99% of the related undamped periods, respectively). Thus, the amount of damping introduced influences significantly only the first vibration period of the system. Figure 4-12 (b) shows the variation, with the total added damping c, of the damping ratio of the first, second and third vibration modes, ξ_1, ξ_2 and ξ_3. It also reports the variation of the estimate of the damping ratio, plus the inherent damping of the existing frame ($\xi_{add} + 0.05$), obtained by employing the approximate formula of Eqn. (4-1), for increasing values of c. It is observed that the first modal damping trend is well approximated by the design formula up to high values of added damping (c=2.25), that is $\xi_{add} = 0.45$. For increasing values beyond this limit the amount of the effective damping decreases. As already observed for the periods, the influence of the damper dimensions on the second and third mode is negligible; the damping ratio varies in the range 0.050-0.067 with a maximum 0.074 when c=1.25 $(\xi_{add} = 0.25)$ for the second mode, while for the third mode the range is 0.091-0.094 with a maximum value of 0.097 when c=0.75 $(\xi_{add} = 0.15)$.

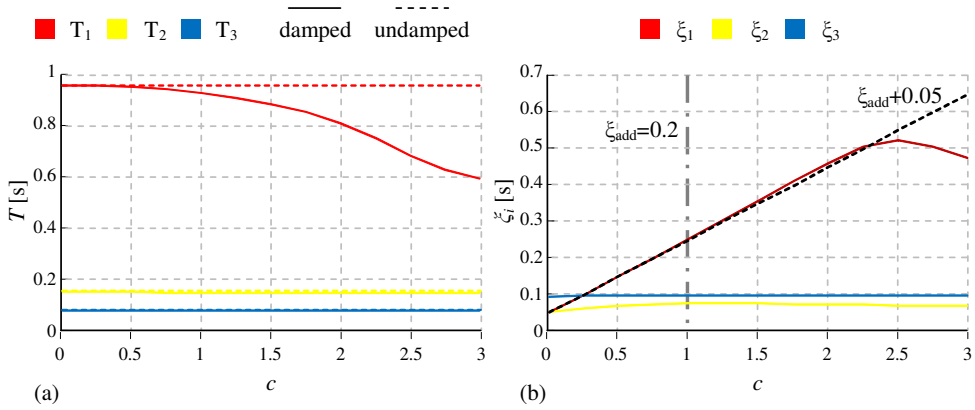

Figure 4-12 Camerino building: first three periods trends (a) and comparison of the first three damping ratio trends (b)

To provide an extent that synthetically quantified the non-classical damping nature of the coupled system the index ρ is expressed, as shown by Eqn. (4-2). Figure 4-13 (a) shows the coupling index trend for increasing damping levels, while Figure 4-13 (b) shows the values of ρ obtained for the damping target value c=1. In the latter case the maximum value of ρ is equal to 0.35 and corresponds to the coupling among the first and the second mode.

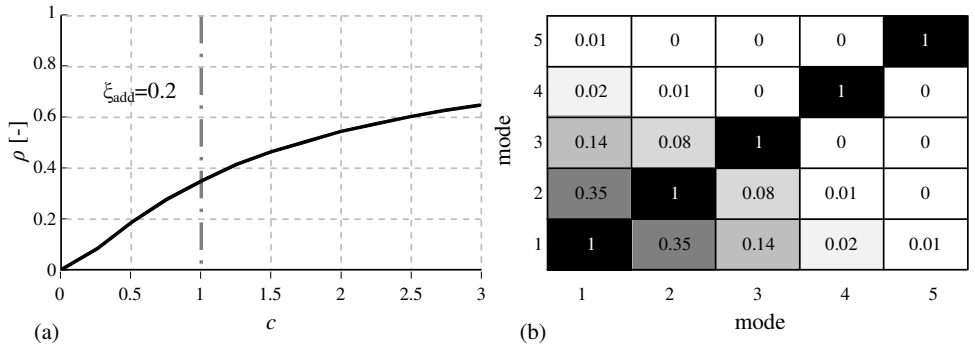

Figure 4-13 Camerino building ρ-index: trend for increasing damping level (a) and values of the five modes of the system for an added damping of 0.20 (b)

Figure 4-14 shows the first three modal shapes of the coupled system in the *Retrofit* configuration for different levels of the damper multiplier c, therefore for various ξ_{add} defined in the range 0-0.4. The real and imaginary components of the complex eigenvectors $\boldsymbol{\varphi}_i$ are plotted separately and normalized in such a way that the first component of the real part, r_{1i}, of the eigenvector $\boldsymbol{\varphi}_i$ is equal to one, while the imaginary one, i_{1i}, is equal to zero. In the case of ξ_{add} =0, the system is classically damped, and the eigenvectors are real. Increasing the damping level affects significantly the first mode only, while the higher modes are less influenced by ξ_{add}.

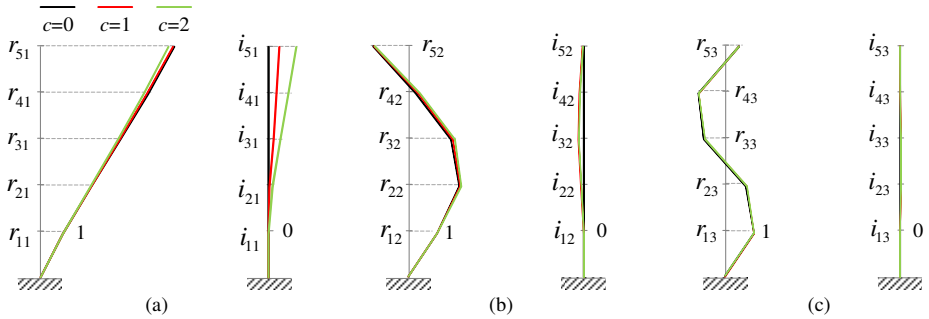

Figure 4-14 Camerino building *Retrofit* configuration: real and imaginary part of the complex eigenvectors for increasing values of damping (a) first mode (b) second mode (c) third mode

Table 4-8 lists the first three complex eigenvectors $\boldsymbol{\varphi}_i$ of the *Retrofit* configuration in polar form, magnitude-phase angle in degrees. For each vibration mode, just one of the two complex eigenvector of the pair is reported; the first five components are related to displacements of the active degrees of freedom, the successive five represent their velocities and last two are the displacements of the dissipative devices.

In the case in which the external bracings do not provide any damping contribution ($c=\xi_{add}=0$, classically damped system) all the masses of the modes are in phase or 180° out of phase, as expected. While for increasing damping values (system non-classically damped) the changing of the values of the phase gives an extent of how the system becomes non classically damped. It is noticeable that the increasing damping values are appreciable on the first mode only. The maximum value of difference of phase is obtained between the first and the last mass, for the design value of damping (c=1, $\xi_{add}=0.2$) is equal to 3.9°, while for c=2 $(\xi_{add}=0.4)$ the difference is bigger and equal to 9.3°. The second and third mode, instead, seem to be not influenced by the higher values of damping introduced.

Table 4-8 Camerino building *Retrofit* configuration: polar form of the first three eigenvectors pairs for increasing values of damping

First mode						Second mode						Third mode					
c=0		c=1		c=2		c=0		c=1		c=2		c=0		c=1		c=2	
| |	ϑ	| |	ϑ	| |	ϑ	| |	ϑ	| |	ϑ	| |	ϑ	| |	ϑ	| |	ϑ	| |	ϑ
0.02	92.9	0.02	108.5	0.01	126.8	0.01	-87.1	0.01	95.9	0.01	95.6	0.01	-84.8	0.01	95.5	0.01	95.4
0.04	92.9	0.04	106.9	0.03	123.0	0.01	-87.1	0.01	94.2	0.01	94.1	0.00	-84.8	0.00	94.0	0.00	94.5
0.06	92.9	0.06	105.7	0.05	120.2	0.01	-87.1	0.01	92.3	0.01	92.5	0.00	95.2	0.00	-82.8	0.00	-83.5
0.08	92.9	0.08	105.0	0.07	118.5	0.00	-87.1	0.00	81.8	0.00	84.7	0.01	95.2	0.01	-84.0	0.01	-84.3
0.10	92.9	0.10	104.6	0.09	117.5	0.01	92.9	0.01	-82.5	0.01	-83.1	0.00	-84.8	0.00	95.5	0.00	95.4
0.11	0	0.11	3.82	0.11	9.3	0.36	-180	0.35	1.7	0.34	1.6	0.56	-180	0.57	0	0.57	0
0.25	0	0.26	2.24	0.26	5.5	0.63	-180	0.63	0	0.63	0	0.40	-180	0.42	-1.6	0.43	-1.0
0.40	0	0.40	1.10	0.40	2.7	0.53	180	0.54	-1.9	0.55	-1.6	0.42	0	0.40	-178.4	0.40	-179.0
0.54	0	0.54	0.37	0.54	0.9	0.09	-180	0.12	-12.4	0.14	-9.3	0.52	0	0.52	-179.5	0.52	-179.7
0.67	0	0.67	0	0.67	0	0.44	0	0.41	-176.7	0.40	-177.2	0.27	-180	0.27	0.01	0.27	0.0
0.01	92.9	0.01	113.5	0.01	138.2	0.00	-87.1	0.00	133.8	0.00	152.9	0.00	-84.8	0.00	150.8	0.00	164.2
0.01	-87.1	0.01	-66.5	0.01	-41.8	0.00	92.9	0.00	-46.2	0.00	-27.1	0.00	95.2	0.00	-29.2	0.00	-15.8

Chapter 5

Seismic response

This section analyzes the response of the two analyzed case studies in terms seismic response of the bare frame and of the alternative retrofit configurations to the set of time-histories representative of the seismic hazard (PGA having a probability of exceedance of 10% in 50 years). The higher order modes contributions on the response of both displacements and internal actions is investigated.

The results successively presented, concern the engineering demand parameters (EDPs) of major interest for the performance assessment of the frame and the external bracing, that is:

- displacements,
- interstorey drifts (IDR);
- shear actions, total distribution and contributions of both the frame and the bracing;
- velocities;
- absolute accelerations;
- exchange actions resulting of towers-existing frame interaction.

The IDR is a useful index for the monitoring of structural and non-structural damages; the base shear provides the chance to control the stresses on both new and existing foundations; the exchange actions are necessary for the design of the connection between frame and external structure. Finally the absolute accelerations provide the performance evaluation of acceleration-sensitive non structural components.

For what concern the viscous dampers, the monitored EDPs are:

- displacements;
- velocities;
- axial actions;
- viscous bending moments.

Strokes and forces of the FVDs are the parameters which provide the control of the cost, moreover the viscous bending moments is representative of the actions necessary for the design of the bracing system foundation.

5.1 Van Nuys building

The values of EDPs reported below are the mean of the maximum values obtained for each of the twenty time-histories considered. The configurations analyzed are in number of five and include the subsequent cases:

1 the bare frame (*As is*);
2 retrofit configuration with a tower-to-frame stiffness ratio (see section 3.1.5) equal to 0.5 and a added damping contribution equal to 15% (κ=0.5-ξ_{add} =0.15);
3 retrofit configuration with a unitary tower-to-frame stiffness ratio and a added damping contribution equal to 15% (κ=1-ξ_{add} =0.15)
4 retrofit configuration with a unitary tower-to-frame stiffness ratio and a added damping contribution equal to 30% (κ=1-ξ_{add} =0.3);
5 the case of coupling with infinitely stiff towers and ξ_{add} =0.3 (*Stiff*).

It is useful to remember that the external dissipative rocking system is dimensioned with a seismic action having a probability of exceedance of 10% in 50 years, with the aim to reach a limited damaging on the non-structural components of the existing frame. The reference retrofit configuration (κ=1-ξ_{add} =0.3), is achieved with the insertion of four external dissipative rocking structures. The number of external bracings is determined for feasibility question, in order to avoid high stresses on the dissipative system and related foundations, usually realized through drilled piles.

Table 5-1 reports the floor displacements and the interstorey drifts for the five configurations analyzed. It is observed that the displacement demand of the bare frame (*As is* configuration) is maximum at the top of the frame and assumes a value of 30.6 cm. The frame undergoes significant inelastic displacements with a maximum interstorey drift ratio (IDR) of 0.0207 attained at the third storey. In the retrofit configuration corresponding to κ=1 and ξ_{add} =0.3, a maximum displacements demand of 20.1 cm is attained, with a maximum IDR of 0.0089. The *Stiff* configuration yields a maximum IDR of 0.0072. It is noteworthy that these IDR values are slightly larger than the value 0.5% allowed for the Operational Limit State by seismic codes such as FEMA. However, it should be noted that analysis of the frame done by Blume and Associates in 1973, revealed that IDR values inferior than 1% result in damage of the non-structural building components only, whit the columns remaining into the elastic limit, even though they showed high stresses. It is important to point out that the aim of this study is to understand the linear elastic behaviour of the coupled system with respect to that of the bare frame, and the contribution of higher order modes to the seismic response, via complex modal analysis. For this reason, it is interesting to highlight the percentage of reduction of monitored EDP's due to the coupling, rather than numerical values themselves. This justifies the use of a linear elastic model for the frame.

Figure 5-1 (a) reports distribution of the displacements (x_i) along the height of the building, for i=1, 2, .., 7, normalized with respect to the value observed at the top of the bare frame. The coupling with dissipative tower (dissipative rocking system) induced a reduction of 53% for the *Stiff* case, of 48% for the case corresponding to κ=1-ξ_{add}=0.3, of 35% for κ=0.5-ξ_{add}=0.15 and of 36% for κ=1-ξ_{add}=0.15. Figure 5-1 (b) reports the distribution of the IDRs (θ_i). The *Stiff* configuration provides a constant interstorey at every level, with a reduction of 65% with respect to the bare frame, the case corresponding to κ=1-ξ_{add}=0.3 yields a reduction of 57%. The cases corresponding to κ=0.5-ξ_{add}=0.15 and κ=1-ξ_{add}=0.15 yield similar results, with a reduction of respectively 43% and 47% with respect to the bare frame case.

Table 5-1 Van Nuys building: floor displacements and drifts results

level	*As is*		κ=0.5-ξ_{add}=0.15		κ=1-ξ_{add}=0.15		κ=1-ξ_{add}=0.3		*Stiff*	
	x_i [m]	θ_i [%]	x_i [m]	θ_i [%]	x_i [m]	θ_i [%]	x_i [m]	θ_i [%]	x_i [m]	θ_i [%]
1	0.063	1.52	0.040	0.96	0.040	0.97	0.031	0.75	0.030	0.72
2	0.113	1.90	0.069	1.11	0.068	1.06	0.053	0.84	0.049	0.72
3	0.165	2.07	0.099	1.17	0.096	1.09	0.076	0.88	0.068	0.72
4	0.213	1.98	0.129	1.16	0.124	1.07	0.098	0.89	0.087	0.72
5	0.253	1.72	0.156	1.10	0.150	1.03	0.120	0.88	0.106	0.72
6	0.285	1.35	0.180	0.99	0.174	0.96	0.141	0.84	0.125	0.72
7	0.306	0.91	0.201	0.83	0.195	0.85	0.158	0.74	0.144	0.72

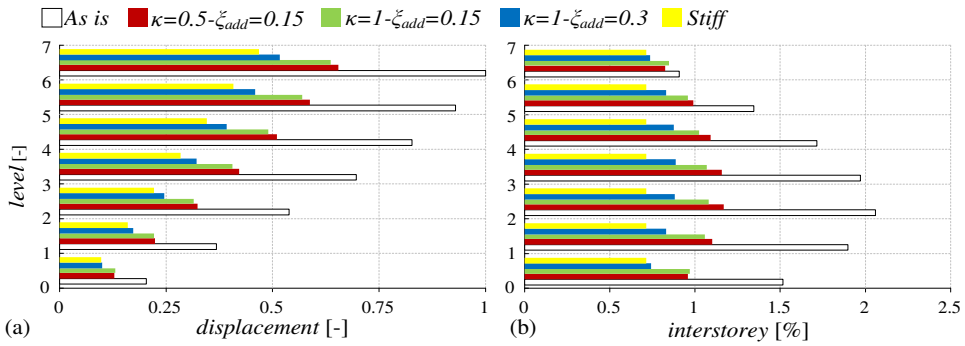

Figure 5-1 Van Nuys building: displacements (a) and interstorey drifts (b) distributions for the five configurations analyzed

Having employed the complex mode superposition approach to solve the seismic problem, the contribution of the higher vibration modes to the response can be estimated by comparing the full response accounting for all the modes to the response obtained by considering the contribution of the first mode only. Table 5-2 reports the displacement response for the *As is* case and different retrofit configurations. It can be seen that in all the cases considered the displacement demand is controlled mainly by the first mode, while the contribution of higher order modes is negligible. Figure 5-2 (a), (b), (c) and (d) provides a deeper insight on the first mode contribution comparing it, graphically, to the full response

in terms of displacements for the bare frame (a) and the retrofit configurations κ=0.5-ξ_{add}=0.15 (b), κ=1-ξ_{add}=0.15 (c) and κ=1-ξ_{add}=0.3 (d).

Table 5-2 Van Nuys building: higher order modes contribution on floor displacements and drifts results

level	*As is*		κ=0.5-ξ_{add}=0.15		κ=1-ξ_{add}=0.15		κ=1-ξ_{add}=0.3	
	x_{full} [m]	x_1 [m]	x_{full} [m]	x_1 [m]	x_{full} [m]	x_1 [m]	x_{full} [m]	x_1 [m]
1	0.063	0.059	0.040	0.040	0.040	0.040	0.031	0.032
2	0.113	0.109	0.069	0.069	0.068	0.068	0.053	0.053
3	0.165	0.163	0.099	0.100	0.096	0.097	0.076	0.076
4	0.213	0.213	0.129	0.129	0.124	0.124	0.098	0.098
5	0.253	0.253	0.156	0.156	0.150	0.150	0.120	0.120
6	0.285	0.283	0.180	0.180	0.174	0.174	0.141	0.140
7	0.306	0.301	0.201	0.199	0.195	0.195	0.158	0.157

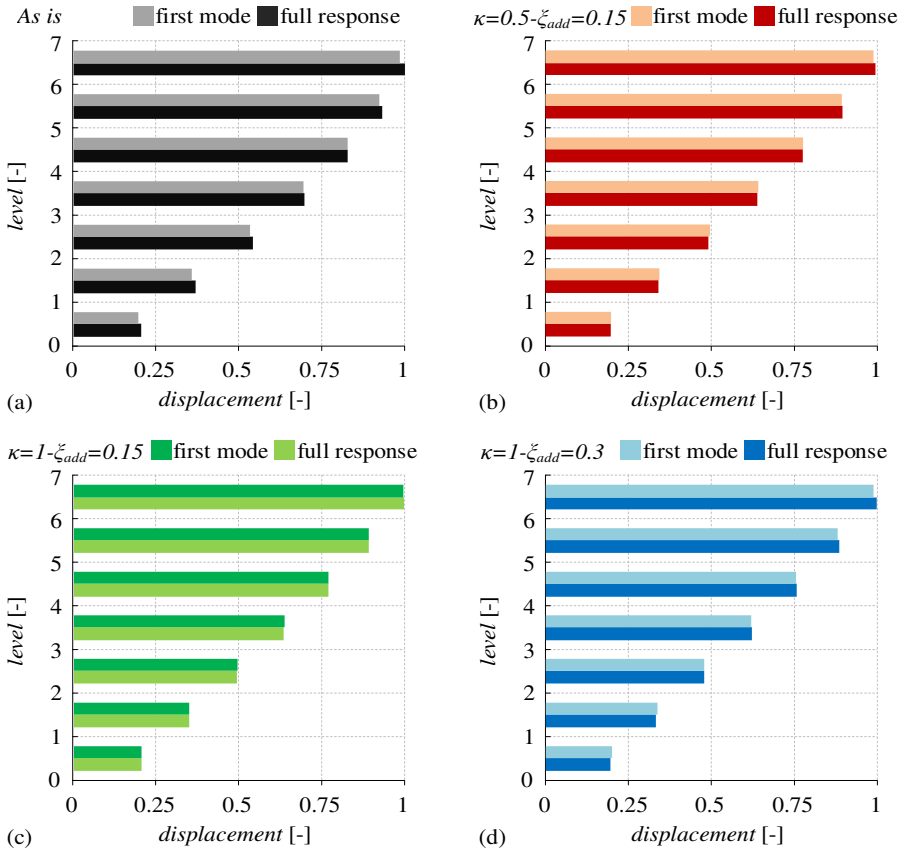

Figure 5-2 Van Nuys building: contribution of the first mode to the full response in terms of displacements for different analyzed configurations

Table 5-3 reports the shear actions resisted by the frame and by the tower, together with the total shear, for the five different configurations. It is noteworthy that the maximum shear for the tower and the frame may not occur at the same instant of time for all the records considered. This can be explained as a drawback due to the regularization of the displacements distribution along the building height, provided by dissipative towers. Moreover, the different sign on the shear contributions leads to a concentration of higher exchange actions between the frame and the towers at the base and on top as shown in Figure 5-7, successively. As already discussed for the displacements, the addition of the towers results in a reduction of the global shear demand. Moreover, the performance of the case corresponding to $\kappa = 1 - \xi_{add} = 0.3$ is very close to that of the stiff tower with $\xi_{add} = 0.3$. In particular, the infinitely stiff bracing provides better results in terms of shear reduction along the height of the building, with the exception of the last storey. The relative reduction of the maximum base shear acting on the frame, with respect to the bare building, is nearly 48% for the cases corresponding to $\kappa = 1$ and to the stiff tower, 34% and 32% for $\kappa = 0.5 - \xi_{add} = 0.15$ and for $\kappa = 1 - \xi_{add} = 0.15$, respectively.

Table 5-3 Van Nuys building: shear actions results

level	*As is*	$\kappa = 0.5 - \xi_{add} = 0.15$			$\kappa = 1 - \xi_{add} = 0.15$			$\kappa = 1 - \xi_{add} = 0.3$			*Stiff*		
	$V_{b,\text{frame}}$ [kN]	$V_{b,\text{frame}}$ [kN]	$V_{b,\text{tower}}$ [kN]	$V_{b,\text{total}}$ [kN]	$V_{b,\text{frame}}$ [kN]	$V_{b,\text{tower}}$ [kN]	$V_{b,\text{total}}$ [kN]	$V_{b,\text{frame}}$ [kN]	$V_{b,\text{tower}}$ [kN]	$V_{b,\text{total}}$ [kN]	$V_{b,\text{frame}}$ [kN]	$V_{b,\text{tower}}$ [kN]	$V_{b,\text{total}}$ [kN]
1	25498	16796	8900	19970	17214	9379	19417	13129	12972	19547	13126	11008	15511
2	22910	12523	6598	17750	11590	7156	16950	9237	9575	16882	7197	8846	13350
3	20925	11206	5338	15907	10145	5994	15360	8292	7769	14944	6575	7505	11965
4	19136	10954	3649	14012	9954	4284	13496	8346	5667	12866	6425	6261	10586
5	16472	10165	2876	12219	9408	3556	11953	8105	4475	11700	6514	4703	8828
6	12621	9154	2483	9960	8636	3406	9730	7614	3702	9688	6018	3513	6481
7	7145	8177	3570	5948	8843	5096	5826	7707	4109	5898	8234	5869	3486

Figure 5-3 (a) reports distribution of the shear actions along the height of the frame, normalized after dividing them by the value of the base shear in the *As is* configuration. As observed for the displacements, similar performances are achieved for $\kappa = 0.5 - \xi_{add} = 0.15$ and for $\kappa = 1 - \xi_{add} = 0.15$. Figure 5-3 (b) reports the distribution of the shear action in the tower along its height; the values are normalized by dividing them by the values of the base shear in the frame for the case of infinitely stiff tower. It is also observable, from the analysis of Figure 5-3, that a unitary tower-to-frame stiffness ratio ($\kappa = 1$) is a good approximation of the infinitely stiff tower, for the same given value of added damping ($\xi_{add} = 0.3$).

Figure 5-4 (a), (b), (c) and (d) provides a graphic insight on the shear actions distribution between tower and frame, compared to the total one, for all the retrofit cases, that is $\kappa = 0.5 - \xi_{add} = 0.15$ (a), $\kappa = 1 - \xi_{add} = 0.15$ (b), $\kappa = 1 - \xi_{add} = 0.3$ (c) and *Stiff* (d).

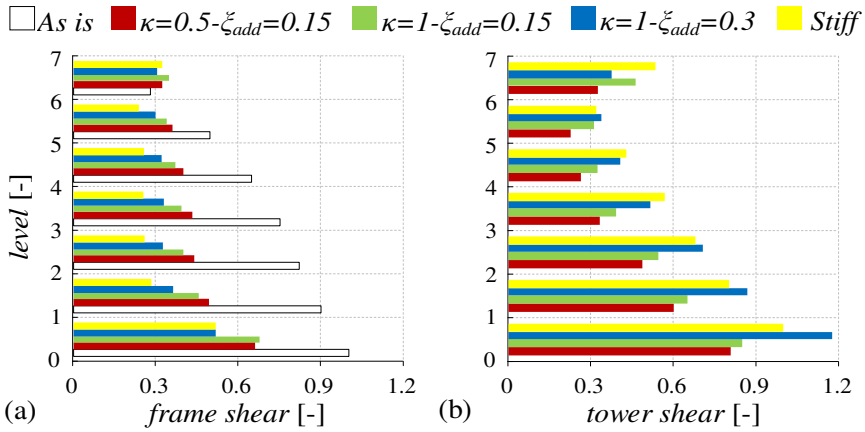

Figure 5-3 Van Nuys building: shear actions resisted by the frame (a) and by the tower (b)

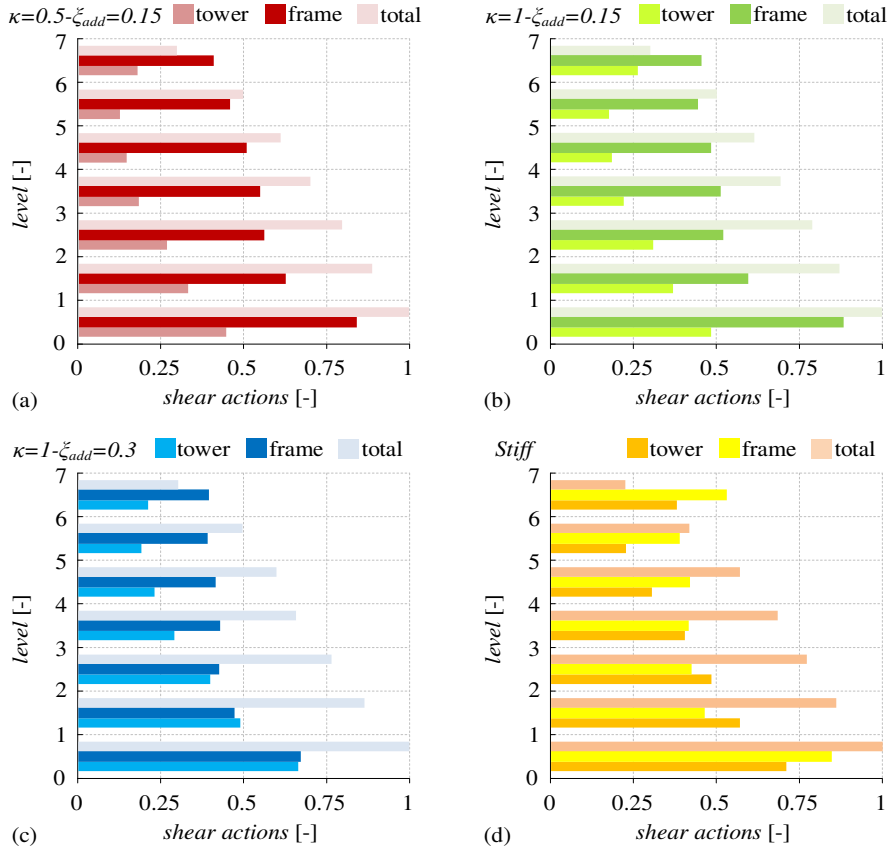

Figure 5-4 Van Nuys building: shear actions resisted by the tower and the frame compared to the total one in all the retrofit cases

The complex mode superposition is also employed to estimate the contribution of the higher modes of vibration on the shear actions before and after the retrofit. Subsequent tables report the distribution of the shear actions in the frame (Table 5-4), in the tower (Table 5-5) and the global (Table 5-6) for the *As is* case and for different retrofit configurations. The results are obtained by considering the contribution of the first mode only and the full response. Differently from the case of the displacements, the contribution of higher order modes is important as the values of both the frame and tower shear responses and the total shear response are significantly higher than the corresponding values obtained by considering the first mode only. Moreover, the contribution of the first mode to the total response of the frame increases due to the coupling with the dissipative tower, compared to the *As is* configuration. In any case, the building response is dominated by the first mode of vibration also in the coupled case, especially for configurations with $\kappa = 1$.

Table 5-4 Van Nuys building: higher order modes influence on the shear actions resisted by the frame

level	*As is*		$\kappa = 0.5$-ξ_{add} =0.15		$\kappa = 1$-ξ_{add} =0.15		$\kappa = 1$-ξ_{add} =0.3	
	V_{frame_full} [kN]	V_{frame_1} [kN]	V_{frame_full} [kN]	V_{frame_1} [kN]	V_{frame_full} [kN]	V_{frame_1} [kN]	V_{frame_full} [kN]	V_{frame_1} [kN]
1	25498	23620	16796	16773	17214	17247	13129	13619
2	22910	22340	12523	12449	11590	11505	9237	9099
3	20925	20490	11206	11039	10145	10036	8292	8168
4	19136	17722	10954	10642	9954	9745	8346	8297
5	16472	14113	10165	9454	9408	8914	8105	7750
6	12621	9815	9154	8042	8636	7922	7614	6944
7	7145	5022	8177	7183	8843	8196	7707	7029

Table 5-5 Van Nuys building: higher order modes influence on the shear actions resisted by the tower

level	$\kappa = 0.5$-ξ_{add} =0.15		$\kappa = 1$-ξ_{add} =0.15		$\kappa = 1$-ξ_{add} =0.3	
	V_{tower_full} [kN]	V_{tower_1} [kN]	V_{tower_full} [kN]	V_{tower_1} [kN]	V_{tower_full} [kN]	V_{tower_1} [kN]
1	8900	9024	9379	7731	12972	16898
2	6598	6656	7156	6530	9575	12594
3	5338	5688	5994	5929	7769	10624
4	3649	3734	4284	4094	5667	7817
5	2876	2254	3556	2590	4475	5492
6	2483	1291	3406	1730	3702	3202
7	3570	3325	5096	4565	4109	3595

Table 5-6 Van Nuys building: higher order modes influence on the total shear actions

level	$\kappa=0.5-\xi_{add}=0.15$		$\kappa=1-\xi_{add}=0.15$		$\kappa=1-\xi_{add}=0.3$	
	V_{total_full} [kN]	V_{total_1} [kN]	V_{total_full} [kN]	V_{total_1} [kN]	V_{total_full} [kN]	V_{total_1} [kN]
1	19970	18130	19417	17259	19547	19160
2	17750	17099	16950	16220	16882	18065
3	15907	15688	15360	14845	14944	16591
4	14012	13641	13496	12895	12866	14466
5	12219	10977	11953	10388	11700	11691
6	9960	7748	9730	7354	9688	8299
7	5948	4033	5826	3843	5898	4346

Figure 5-5 reports the graphic comparison between the frame shear distribution due to the first mode and the overall one, for the bare building (a), the $\kappa=0.5-\xi_{add}=0.15$ (b), the $\kappa=1-\xi_{add}=0.15$ (c), and the $\kappa=1-\xi_{add}=0.3$ (d) configurations.

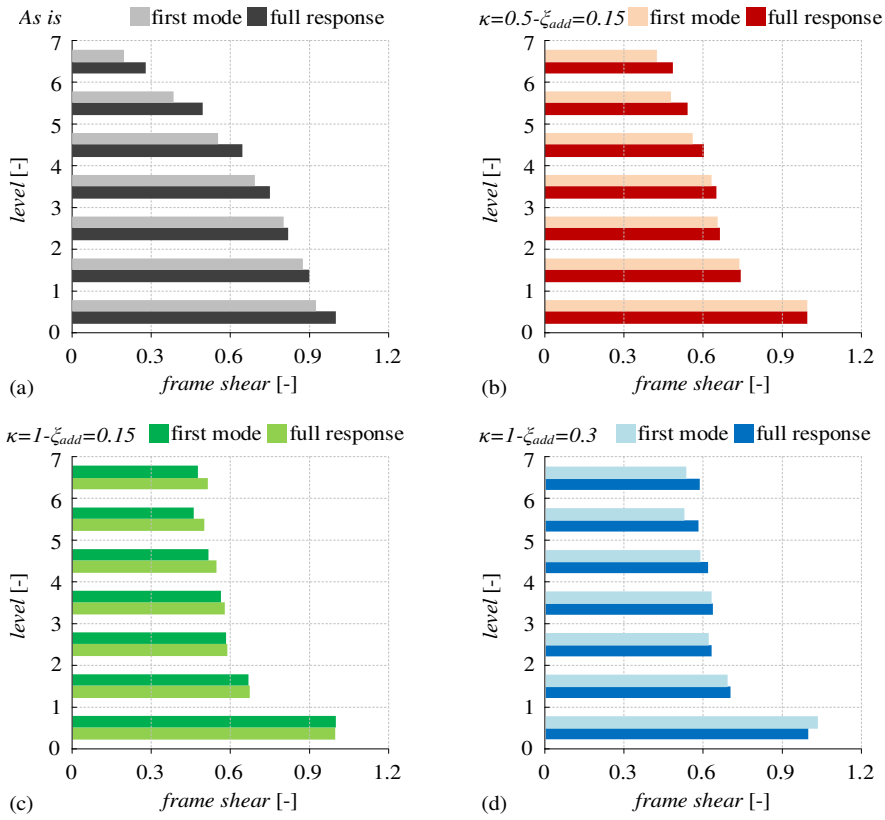

Figure 5-5 Van Nuys building: first mode contribution on the shear response of the frame, due to all modes, for different analyzed configurations

Figure 5-6 depicts the distribution of the shear acting on the tower for the κ=0.5-ξ_{add} =0.15 (a), the κ=1-ξ_{add} =0.15 (b) and the κ=1-ξ_{add} =0.3 (c) cases.

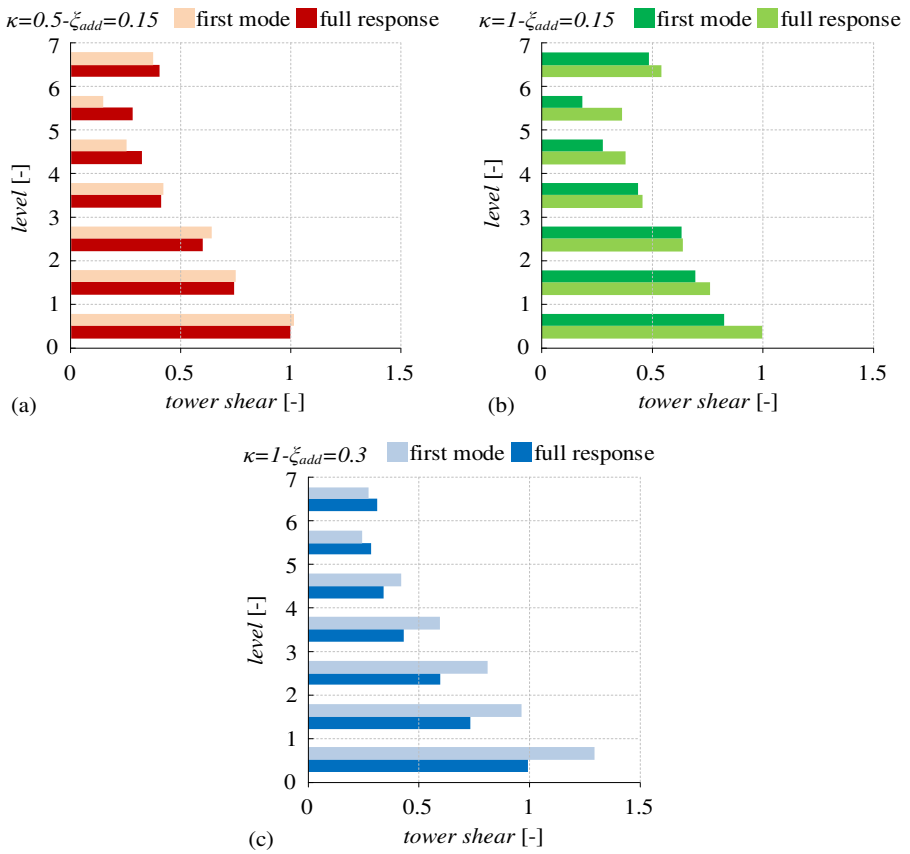

Figure 5-6 Van Nuys building: first mode contribution on the total shear response of the tower for different retrofit analyzed configurations

Table 5-7 reports the maximum values of the exchange forces ($F_{e,i}$) observed at the various levels of the building, for the different retrofit cases investigated. These actions result from the mutual actions between the tower and the existing building during the seismic event and they control the design of the connections between the tower and the frame. Figure 5-7 shows the values of the exchange forces distribution, normalized by the value attained at the first floor for the *Stiff* case. The highest values of these exchange forces are observed at the first and at the last two storeys for all the configurations and are representative of the different signs on the shear action resisted by the frame and by the tower, as explained previously.

Table 5-7 Van Nuys building: exchange forces results between frame and tower

level	$\kappa=0.5-\xi_{add}=0.15$	$\kappa=1-\xi_{add}=0.15$	$\kappa=1-\xi_{add}=0.3$	*Stiff*
	$F_{e,i}$ [kN]	$F_{e,i}$ [kN]	$F_{e,i}$ [kN]	$F_{e,i}$ [kN]
1	5111	6312	5671	7042
2	2658	2868	3328	2239
3	2678	2989	3409	2115
4	2034	2472	2723	2248
5	2102	2427	2562	2017
6	3196	4273	4039	5041
7	3570	5096	4109	5869

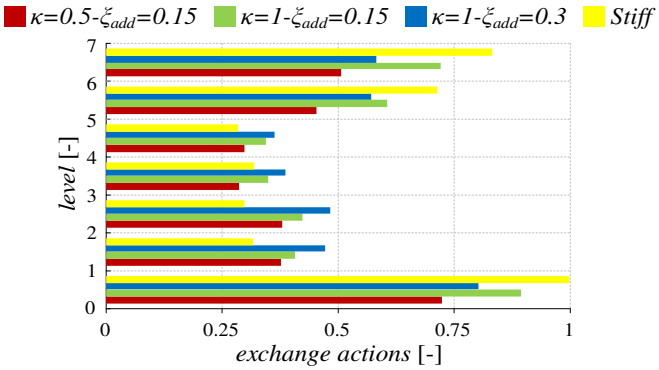

Figure 5-7 Van Nuys building: exchange forces distribution along the height of the building

Table 5-8 contains the velocities values observed at the various levels of the building for the configurations investigated. The relative reduction of the maximum velocity, with respect to the value registered at the 7th floor of the bare building, is nearly 46% for the *Stiff* case and 36% for the $\kappa=1-\xi_{add}=0.3$ one; the $\kappa=0.5-\xi_{add}=0.15$ and $\kappa=1-\xi_{add}=0.15$ configurations provides a reduction of 26% and 28%, respectively. Figure 5-8 shows the values of the floor velocities distribution normalized by the value observed at the last elevation for the *As is* case.

Table 5-8 Van Nuys building: floor velocities results

level	*As is*	$\kappa=0.5-\xi_{add}=0.15$	$\kappa=1-\xi_{add}=0.15$	$\kappa=1-\xi_{add}=0.3$	*Stiff*
	$\dot{x}_i$ [m/s]	$\dot{x}_i$ [m/s]	$\dot{x}_i$ [m/s]	$\dot{x}_i$ [m/s]	$\dot{x}_i$ [m/s]
1	0.430	0.208	0.260	0.249	0.191
2	0.724	0.353	0.435	0.418	0.314
3	0.997	0.506	0.615	0.591	0.437
4	1.197	0.652	0.787	0.756	0.560
5	1.350	0.787	0.946	0.905	0.683
6	1.531	0.944	1.117	1.077	0.806
7	1.715	1.092	1.272	1.237	0.927

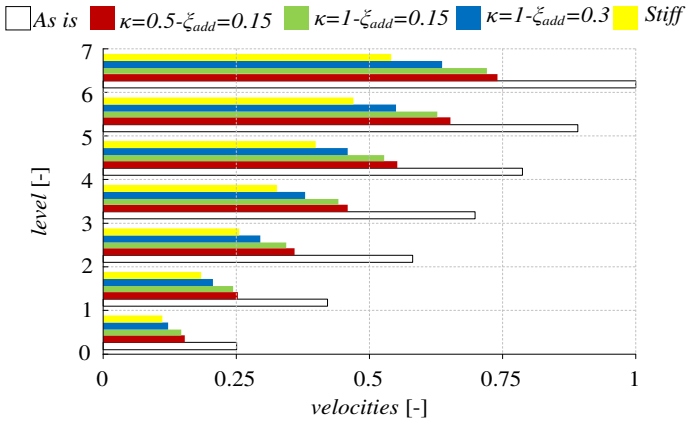

Figure 5-8 Van Nuys building: comparison of the velocities distribution along the height

Table 5-9 contains the absolute acceleration values observed at the various levels of the building for the configurations investigated. The coupling of the frame with the external dissipative system induces a reduction of the maximum absolute acceleration values with respect to those observed in the *As is* case. This result is of particular importance for the performance evaluation of acceleration-sensitive non structural components. Figure 5-9 shows the values of the floor absolute accelerations normalized by the value observed at the 7th floor in the *As is* case. The relative reduction of accelerations, measured at the last elevation, is nearly 18% for the $\kappa = 1 - \xi_{add} = 0.3$ case, 49% for the *Stiff* one, and 17% and 19%, respectively, for the cases corresponding to $\kappa = 0.5 - \xi_{add} = 0.15$ and for $\kappa = 1 - \xi_{add} = 0.15$. Moreover, the values of the accelerations are very similar for all the cases involving a finite stiff tower, whereas in the *Stiff* case they are generally lower.

Table 5-9 Van Nuys building: absolute accelerations

level	*As is*	$\kappa = 0.5 - \xi_{add} = 0.15$	$\kappa = 1 - \xi_{add} = 0.15$	$\kappa = 1 - \xi_{add} = 0.3$	*Stiff*
	$\ddot{x}_i$ [m/s^2]	$\ddot{x}_i$ [m/s^2]	$\ddot{x}_i$ [m/s^2]	$\ddot{x}_i$ [m/s^2]	$\ddot{x}_i$ [m/s^2]
1	6.239	5.658	5.299	5.457	4.487
2	7.742	6.795	6.109	6.443	3.959
3	8.321	6.857	6.272	6.581	3.640
4	8.286	6.523	6.161	6.356	3.642
5	7.879	6.201	5.814	5.724	4.047
6	9.336	6.829	6.609	6.536	4.950
7	11.772	9.770	9.535	9.618	5.986

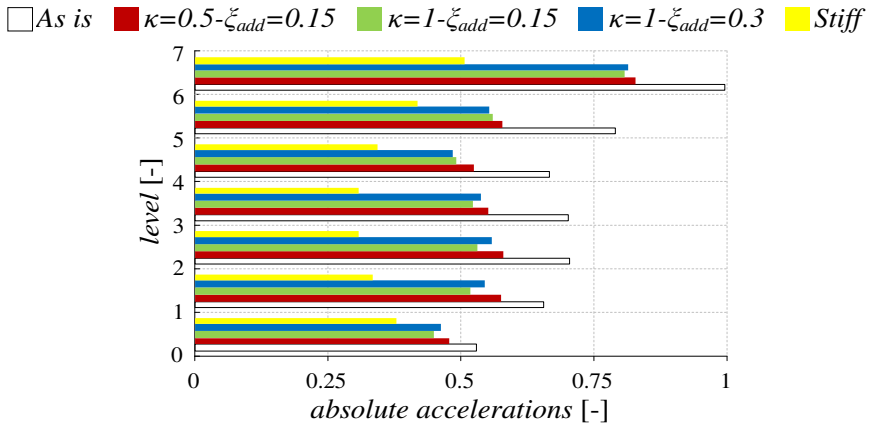

Figure 5-9 Van Nuys building: absolute acceleration distribution along the height

Table 5-10 highlights the displacements (y_i), velocities ($\dot{y}_i$), axial forces (N) and base viscous bending moment, related to damper axial actions (M_v), for all the retrofit configurations considered. These quantities are strictly related to the added damping value. In fact, the *Stiff* and retrofit configurations corresponding to ξ_{add} =0.30, give very similar results. It is also noteworthy that the case of $\kappa = 0.5\text{-}\xi_{add}$ =0.15, provides similar results, even if with half damping added; this can be explained with the fact that this configuration is achieved with only two towers, therefore a reduced number of FVDs. Finally the case of $\kappa = 1\text{-}\xi_{add}$ =0.15 provides the lower axial action on the FVDs and consequently, the lower viscous bending moment. The viscous bending moment is a very important parameter used to design the external bracing foundation, which, normally, is realized by means of drilled piles that should be able to support both the tension and compression forces induced by the rocking motion.

Table 5-10 Van Nuys building: viscous dampers results

$\kappa = 0.5\text{-}\xi_{add}$ =0.15				$\kappa = 1\text{-}\xi_{add}$ =0.15				$\kappa = 1\text{-}\xi_{add}$ =0.3				*Stiff*			
y_i	$\dot{y}_i$	N	M_v	y_i	$\dot{y}_i$	N	M_v	y_i	$\dot{y}_i$	N	M_v	y_i	$\dot{y}_i$	N	M_v
[m]	[m/s]	[kN]	[kNm]	[m]	[m/s]	[kN]	[kNm]	[m]	[m/s]	[kN]	[kNm]	[m]	[m/s]	[kN]	[kNm]
0.0213	0.121	3773	33183	0.0216	0.127	1987	17482	0.0163	0.099	3101	27298	0.0158	0.102	3197	28131

5.2 Camerino building

This section reports the results, in terms of EDPs, expressed as the mean of the maximum values obtained for each of the seven time-histories considered. The total number of analyzed configuration is four, herein briefly recall:

1 the bare existing frame (*As is*);
2 the r.c. frame coupled with two dissipative structures connected with the frame at every elevation, except the roof (*Retrofit*);
3 the same features of the previous case, connected to the existing building only at the fifth floor (*Retrofit 1F*);
4 the case of two infinitely stiff rocking structures (*Stiff*).

It is useful to remember that the design criterion for the external dissipative bracings is the reduction and regularization of the interstorey drifts (θ_i), with respect to the bare frame at the Ultimate Limit State having a return period of 475 years. The results related to upgrading arrangements (Retrofit, Retrofit 1F and Stiff cases) correspond to a total added damping multiplier c=1, which means $\xi_{add} = 0.20$.

Table 5-11 reports the floor displacements and the interstorey drifts (θ_i), expressed also in terms of IDR, for the four configurations analyzed. The reduction of the maximum top displacements, normalized with respect to that of the bare frame, is 51% for the external bracings connected only at the last elevation (*Retrofit 1F*), 54% for the *Retrofit* case and 58% for the *Stiff* one. Figure 5-10 (a) and (b) show the distribution along the height of the building displacements x_i and IDR for i=1, 2, .., 5. The reported values are normalized with respect to the corresponding ones obtained at the 5th level in the *As is* case.

It is noteworthy that the coupling with an infinitely stiff tower leads to a linear distribution of the displacements along the height. Moreover, the displacement demand at the first level is higher in the *Stiff* case than in the other two retrofit arrangements analyzed, while an opposite trend is observed at the top. This means that the regularization of the displacement distribution is achieved with the tower interacting with opposite forces at the base and at the top of the frame. It is also observed that the bracings connected only at last elevation (*Retrofit 1F*) provide higher values of IDR, but always smaller or equal than the value 0.5% allowed for the Operational Limit State (OLS) by seismic codes such as FEMA.

Table 5-11 Camerino building: floor displacements and drifts results

level	*As is*			*Retrofit 1F*			*Retrofit*			*Stiff*		
	x_i [m]	θ_i [m]	*IDR* [%]	x_i [m]	θ_i [m]	*IDR* [%]	x_i [m]	θ_i [m]	*IDR* [%]	x_i [m]	θ_i [m]	*IDR* [%]
1	0.013	0.013	0.5	0.007	0.007	0.2	0.008	0.008	0.3	0.009	0.009	0.3
2	0.040	0.028	0.9	0.021	0.014	0.5	0.019	0.011	0.4	0.018	0.009	0.3
3	0.068	0.029	1.0	0.035	0.015	0.5	0.029	0.011	0.4	0.027	0.009	0.3
4	0.092	0.026	0.9	0.045	0.013	0.4	0.040	0.011	0.4	0.036	0.009	0.3
5	0.109	0.019	0.6	0.053	0.010	0.3	0.050	0.010	0.3	0.046	0.009	0.3

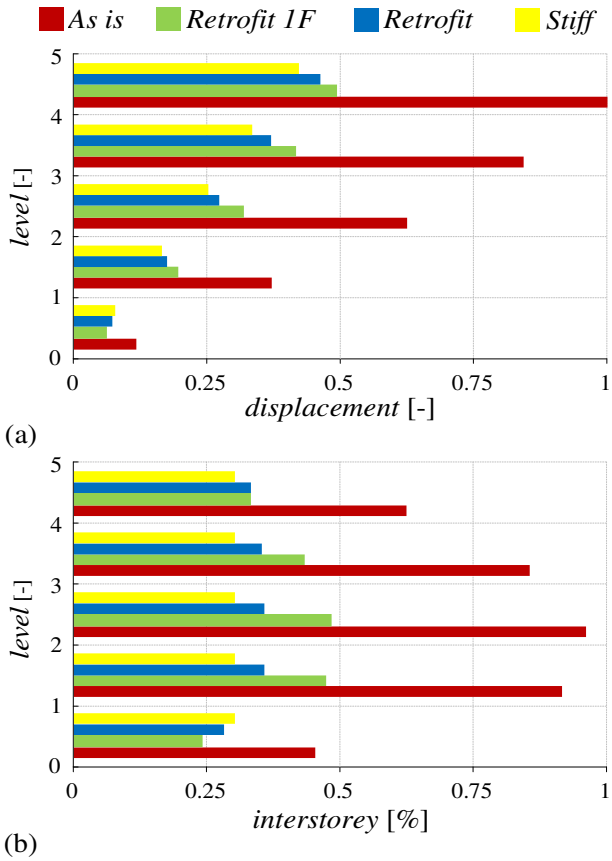

Figure 5-10 Camerino building: displacements (a) and interstorey drifts distributions (b) for the analyzed configurations

Having employed the complex mode superposition approach to solve the seismic problem, the contribution of the higher vibration modes to the response can be estimated by comparing the full response ($x_{i,full}$), accounting for all the modes, to the response obtained by considering the contribution of the first mode only ($x_{i,1}$). Table 5-12 reports the displacement response for the *As is* and the two retrofit cases characterized by finite stiffness of the towers. Figure 5-11 compares the displacement responses of the three analyzed configurations. In all the cases, the first mode contribution nearly controls the total response, while the effect of higher order modes is negligible.

Table 5-12 Camerino building: higher order modes contribution on floor displacements

level	*As is*		*Retrofit 1F*		*Retrofit*	
	$x_{full,i}$ [m]	$x_{1,i}$ [m]	$x_{full,i}$ [m]	$x_{1,i}$ [m]	$x_{full,i}$ [m]	$x_{1,i}$ [m]
1	0.013	0.012	0.007	0.006	0.008	0.008
2	0.040	0.039	0.021	0.019	0.019	0.019
3	0.068	0.068	0.035	0.034	0.029	0.029
4	0.092	0.092	0.045	0.045	0.040	0.040
5	0.109	0.108	0.053	0.052	0.050	0.05

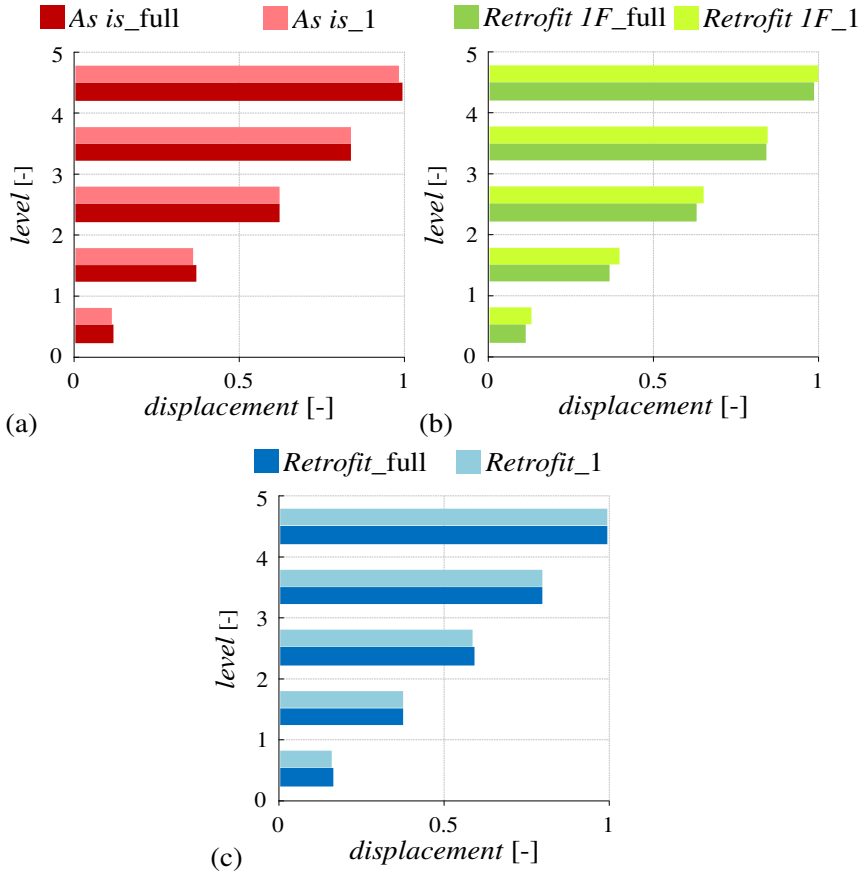

Figure 5-11 Camerino building: contribution of the first mode to the full response of the (a) *As is*, (b) *Retrofit 1F* and (a) *Retrofit* cases

Table 5-13 reports the shear actions resisted by the frame for all the cases, while, for the three retrofit configurations the shear actions resisted by the tower and the total shear actions are also reported. It is noteworthy that the maximum shear for the tower and the frame may not occur at the same instant of time for all the records considered. As already discussed for the displacements, also the global shear demand decreases, but in a less

significant way for all the retrofit configurations, with the exception of the case in which the towers are connected only at the last floor (*Retrofit 1F*). The relative reduction of the maximum base shear acting on the frame, with respect to the bare frame, is nearly 19% for the *Retrofit* case, 6% for the *Stiff* one, while it is nearly 46% for *Retrofit 1F* configuration. It is also observed that at upper floors the reduction of shear resisted by the frame is more appreciable for all the upgrading configurations.

Figure 5-12 (a) shows the frame shear distributions along the height of the building, normalized after dividing them by the value of the base shear in the *As is* configuration. Figure 5-12 (b), instead, shows the shear forces resisted by the towers for all the three analyzed retrofit cases; the values are normalized with respect to the tower base shear, in the *Stiff* case.

Table 5-13 Camerino building: shear actions results

level	*As is*	*Retrofit 1F*			*Retrofit*			*Stiff*		
	$V_{i,frame}$ [kN]	$V_{i,frame}$ [kN]	$V_{i,tower}$ [kN]	$V_{i,total}$ [kN]	$V_{i,frame}$ [kN]	$V_{i,tower}$ [kN]	$V_{i,total}$ [kN]	$V_{i,frame}$ [kN]	$V_{i,tower}$ [kN]	$V_{i,total}$ [kN]
1	5215.7	2834.2	887.7	3242.7	4232.3	2661.3	3544.6	4887.5	3106.8	2961.7
2	4789.8	2569.7	887.7	2921.4	1348.3	1915.4	3060.0	831.7	1956.7	2630.0
3	4197.0	2167.6	887.7	2556.5	1455.9	1292.9	2543.5	1290.1	1310.1	2346.1
4	3687.0	1924.4	887.7	2212.3	1366.9	1169.5	2336.5	1095.1	1060.0	1970.5
5	2755.0	1595.8	887.7	1703.0	1740.8	1020.6	1819.5	1643.5	777.4	1350.7

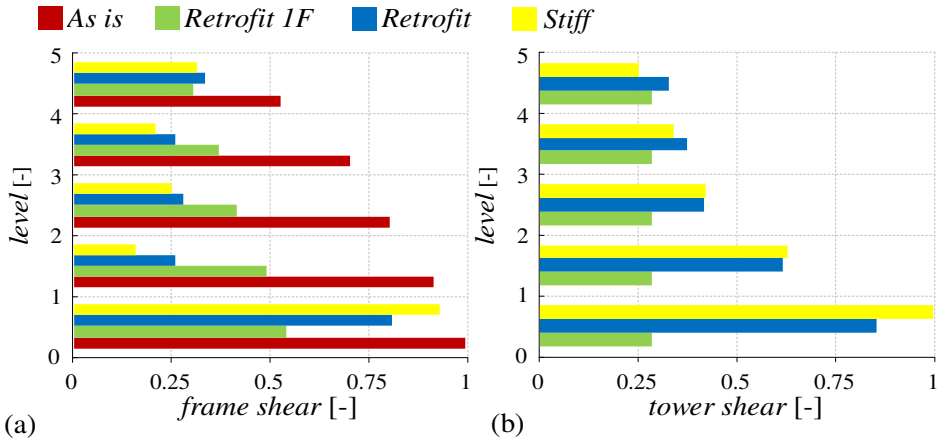

Figure 5-12 Camerino building: (a) shear actions resisted by the frame in all the cases and (b) shear actions resisted by the tower in the three retrofit configurations

Figure 5-13 (a), (b) and (c) report the frame and the tower shear distributions along the height of the building, compared to the total one, for all the retrofit cases. Both the frame and the tower values are normalized to unity with respect to total base shear.

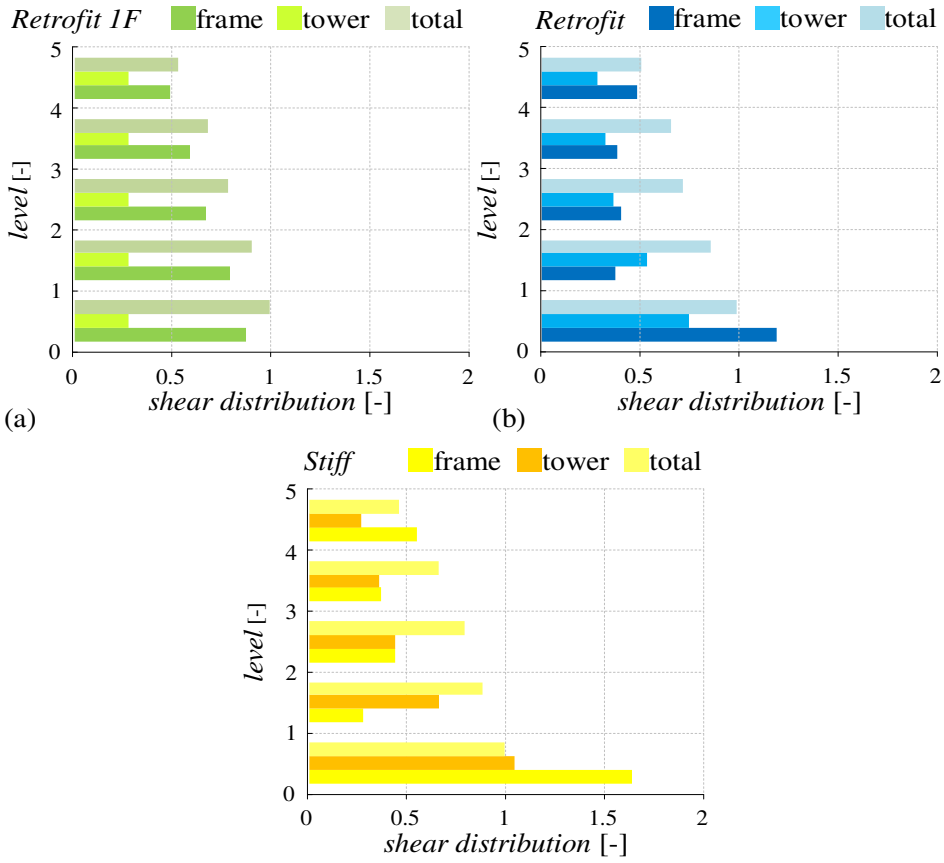

Figure 5-13 Camerino building: shear actions resisted by the tower and the frame, with respect of the total one for (a) *Retrofit 1F*, (b) *Retrofit* and (c) *Stiff* cases

The complex mode superposition is also employed to estimate the contribution of the higher order modes of vibration on the shear actions before and after the retrofit. Table 5-14 reports the shear actions distribution resisted by the frame in the *As is* case and the contributions of both the frame and the tower, due to the full response and the first mode, in the retrofit cases, characterized by a finite stiffness of the bracings. Differently from the case of the displacements, the contribution of higher order modes is important as the values of both the frame shear and the tower shear responses are higher than the corresponding values obtained by considering the first mode only. Consequently also the total shear response is significantly influenced by higher order modes. However, the building response appears to be still dominated by the first mode of the coupled system in the *Retrofit* configuration. These observations, together with the fact that the increase of damping ratio after the retrofit is lower for the higher modes than for the first one, could explain why the reduction of the displacement demand is higher than that of the base shear.

Table 5-14 Camerino building: higher order modes influence on the shear actions

level	*As is*		*Retrofit 1F*					
	$V_{i,frame\_full}$ [kN]	$V_{i,frame\_1}$ [kN]	$V_{i,frame\_full}$ [kN]	$V_{i,frame\_1}$ [kN]	$V_{i,tower\_full}$ [kN]	$V_{i,tower\_1}$ [kN]	$V_{i,total\_full}$ [kN]	$V_{i,total\_1}$ [kN]
1	5215.7	4751.3	2834.2	2370.6	887.7	983.6	3242.7	2815.1
2	4789.8	4600.0	2569.7	2287.1	887.7	983.6	2921.4	2723.2
3	4197.0	4116.0	2167.6	2022.9	887.7	983.6	2556.5	2430.1
4	3687.0	3276.9	1924.4	1584.0	887.7	983.6	2212.3	1924.9
5	2755.0	2142.6	1595.8	1076.1	887.7	983.6	1703.0	1247.4

level	*Retrofit*					
	$V_{i,frame\_full}$ [kN]	$V_{i,frame\_1}$ [kN]	$V_{i,tower\_full}$ [kN]	$V_{i,tower\_1}$ [kN]	$V_{i,total\_full}$ [kN]	$V_{i,total\_1}$ [kN]
1	4232.3	4202.4	2661.3	2204.3	3544.6	2963.0
2	1348.3	1329.6	1915.4	1734.4	3060.0	2825.4
3	1455.9	1440.3	1292.9	1344.5	2543.5	2507.4
4	1366.9	1316.7	1169.5	958.4	2336.5	2007.0
5	1740.8	1665.6	1020.6	687.9	1819.5	1328.4

Figure 5-14 (a), (b) and (c) depicts the first mode contribution to the full shear response of the frame in the three analyzed configurations, normalized by the value of the total base shear.

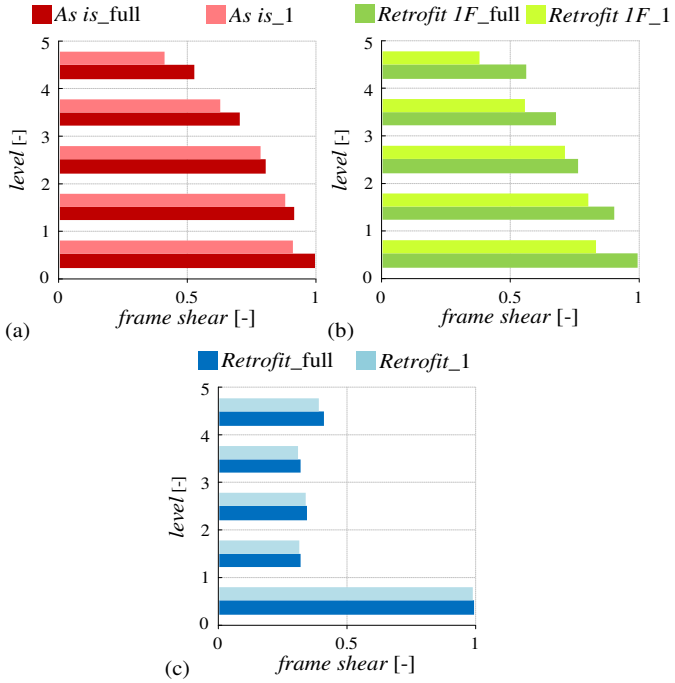

Figure 5-14 Camerino building: first mode contribution on the total frame shear response in the (a) *As is*, (b) *Retrofit 1F* and (c) *Retrofit* cases

Figure 5-15 (a) and (b) shows the first mode contribution on the full tower response for the *Retrofit 1F* and the *Retrofit* configurations, while Figure 5-16 (a) and (b) depicts the first mode contribution to the full response of total shear for the same two cases.

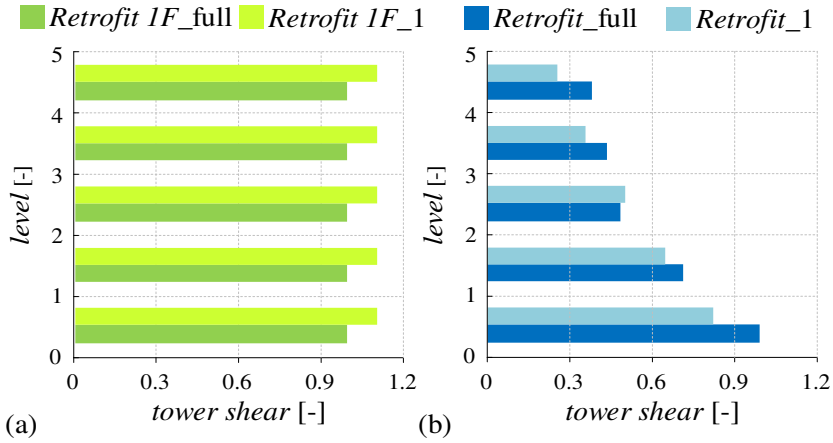

Figure 5-15 Camerino building: first mode contribution on the total tower shear response in the (a) *Retrofit 1F* and (b) *Retrofit* cases

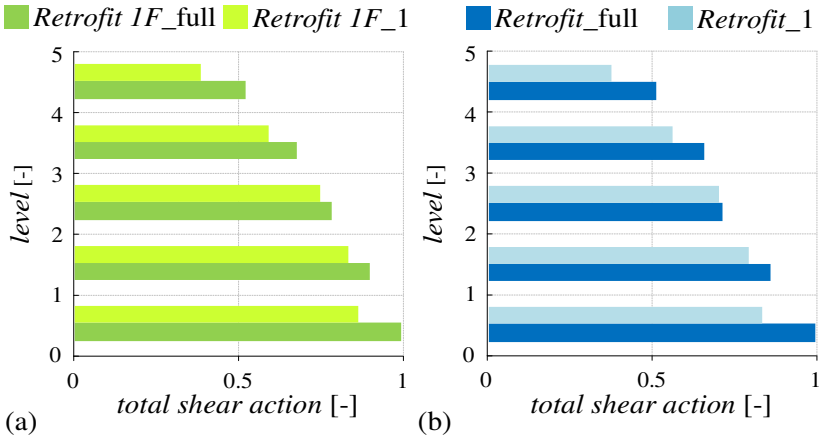

Figure 5-16 Camerino building: first mode contribution on the full response of the total shear in the (a) *Retrofit 1F* and (b) *Retrofit* cases

Table 5-15 reports the maximum values of the exchange forces ($F_{e,i}$) observed at the various levels of the building, for the different retrofit configurations investigated; these actions result from the mutual actions between the towers and the existing building during the seismic event and they control the design of the connections between the external bracings and the frame. Figure 5-17 shows the values of the exchange forces distribution, normalized by the value attained at the first floor for the *Stiff* case. It is observed that the highest value of these forces are observed at the first elevation. The *Retrofit 1F* case

provides mutual actions only at the top, which is the only level in which the bracings and the frame are connected.

Table 5-15 Camerino building: exchange forces results between frame and tower

level	*Retrofit 1F*	*Retrofit*	*Stiff*
	$F_{e,i}$ [kN]	$F_{e,i}$ [kN]	$F_{e,i}$ [kN]
1	-	2909.9	4161.3
2	-	1005.5	899.9
3	-	823.1	409.3
4	-	1061.5	1137.7
5	887.7	1020.6	777.4

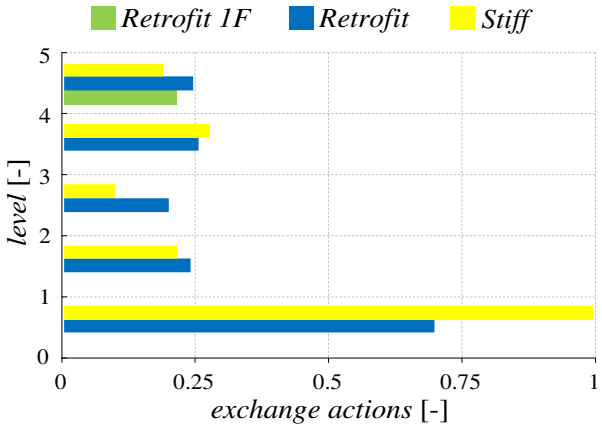

Figure 5-17 Camerino building: tower-frame exchange forces distribution along the height of the building

Table 5-16 reports the maximum values of the velocities ($\dot{x}_i$) observed at the various levels of the building, for the four analyzed cases. Figure 5-18 shows the velocities values normalized with respect of the value recorded at the top of the bare frame. The relative reduction of velocity is nearly 46% for the *Retrofit1F* and *Retrofit* cases and 52% for the *Stiff* one.

Table 5-16 Camerino building: floor velocity distribution

level	*As is*	*Retrofit 1F*	*Retrofit*	*Stiff*
	$\dot{x}_i$ [m/s]	$\dot{x}_i$ [m/s]	$\dot{x}_i$ [m/s]	$\dot{x}_i$ [m/s]
1	0.104	0.070	0.071	0.068
2	0.296	0.184	0.156	0.141
3	0.479	0.277	0.237	0.214
4	0.628	0.341	0.314	0.287
5	0.743	0.399	0.399	0.360

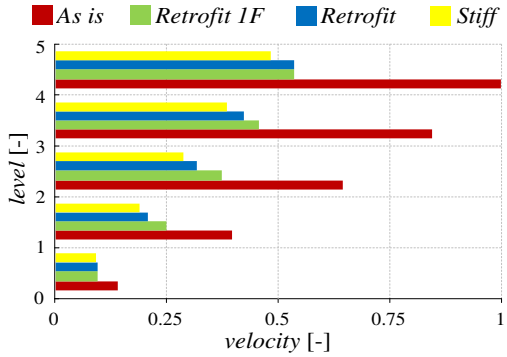

Figure 5-18 Camerino building: velocities distribution along the building height for all the four configurations analyzed

Table 5-17 contains the absolute acceleration values observed at the various levels of the building for the configurations investigated. The coupling with the external dissipative system induces a relative reduction of the maximum absolute accelerations, with respect to the values observed in the *As is* case. This result is noteworthy especially for all the non structural elements (e.g. medical devices) that could be hosted in a structure. Figure 5-19 shows the absolute accelerations distribution, normalized with respect of the value observed at the 5th floor for the *As is* case. The relative reduction of acceleration is nearly 34% for the *Retrofit 1F* case, 39% for the *Retrofit* one and 49% for the *Stiff* configuration.

Table 5-17 Camerino building: floor absolute accelerations distribution

level	*As is*	*Retrofit 1F*	*Retrofit*	*Stiff*
	$\ddot{x}_i$ [m/s^2]	$\ddot{x}_i$ [m/s^2]	$\ddot{x}_i$ [m/s^2]	$\ddot{x}_i$ [m/s^2]
1	2.98	2.88	2.77	2.10
2	3.86	3.24	3.36	1.80
3	4.58	3.16	3.02	1.70
4	4.14	2.65	2.34	1.97
5	5.27	3.22	3.49	2.69

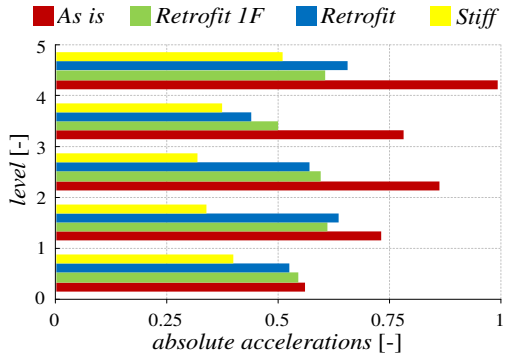

Figure 5-19 Camerino building: absolute accelerations distribution along the building height for all the four configurations analyzed

Table 5-18 highlights the displacements (y_i), velocities ($\dot{y}_i$), axial forces (N) and base viscous bending moment (M_v), related to damper axial actions, for all the retrofit configurations considered. These quantities are strictly related to the added damping value, in fact, all the cases provide an added damping ξ_{add} =0.20, giving, thereby very similar results. Finally the viscous bending moment, depending on the axial actions on the FVDs and on the towers bases dimension, is used to design the foundations of the external bracings. Normally the foundation is realized by means of drilled piles, which should be able to support both the tension and compression forces induced by the rocking motion.

Table 5-18 Camerino building: viscous dampers results

Retrofit 1F				*Retrofit*				*Stiff*			
y_i [m]	$\dot{y}_i$ [m/s]	N [kN]	M_v [kNm]	y_i [m]	$\dot{y}_i$ [m/s]	N [kN]	M_v [kNm]	y_i [m]	$\dot{y}_i$ [m/s]	N [kN]	M_v [kNm]
0.007	0.053	802	6576	0.007	0.049	834	6840	0.006	0.050	842	6904

Chapter 6

Frequency Domain Analysis

This chapter illustrates a frequency domain analysis of the seismic problem. This type of analysis is particularly useful for the problem at hand because it allows to work with an algebraic system rather than a differential one. Moreover, it permits to obtain a reduced formulation of the problem by exploiting the condensation technique, which is not possible in the time domain.

Another advantage of working in the frequency domain is that by representing the seismic input in terms of a stationary stochastic process, a relation can be established between the Power Spectral Density (PSD) of the input and that of the response parameters of interest (e.g. displacement, velocity, ...) via harmonic analysis of the system (Clough and Penzien 2003, Lutes and Sarkani 2004). This way, it is possible to perform extensive parametric studies for different properties of the system and of the seismic input by monitoring only the response variance function, σ^2, that is strictly related to the magnitude of the investigated EDP and to the probability of exceedance of different threshold values.

6.1 A stationary stochastic representation of the input

In Chapter 2, a solution for the dynamic problem of the existing building coupled with a dissipative rocking system through frequency domain analysis was presented. The main advantages of working with the problem transformed through the Fourier Transfer Function are represented by the fact that one has to deal with an algebraic system rather than a differential one. Moreover, the problem dimension can be reduced by exploiting the condensation technique, which allows considering first only the active degrees of freedom of the system (**x**), while the displacements related to deformation and damping of the bracings (**y**) can be successively determined.

If the loading is represented in terms of a stochastic process, a stochastic dynamic analysis of the system is required to evaluate the properties of the stochastic process describing the response. While it is very difficult to perform this analysis in the time domain, under certain assumptions (e.g. linear building behaviour, stationary response) in the frequency domain simple closed form expression are available to relate the input and the output.

In the following, some notions of stochastic dynamics of linear systems are recalled. A common representation of the seismic input is that in terms of a stationary random Gaussian process, i.e. a process whose statistics are invariant under time shifts. This process is completely defined either by the pair mean value μ_X and autocorrelation function $R_X(t)$ or by the mean value μ_X and the Power Spectral Density (PSD) $S_X(\omega)$. In the seismic case, μ_X =0. The autocorrelation function represents the frequency content of a stationary process. Thus, the PSD, which is its Fourier transform, also gives indirectly information about the frequency contents of the random process. The PSD function of a random process $X(t)$ can be defined as:

$$S_X(\omega) = \frac{1}{2\pi} \int_{-\infty}^{\infty} e^{-i\omega\tau} R_X(\tau) d\tau \qquad (6\text{-}1)$$

and since the autocorrelation function is even also the PSD function $S_X(\omega)$ is even and real valued, therefore $S_X(-\omega) = S_X(\omega)$.

An important property of the PSD is that:

$$R_X(0) = E\left[X(t)^2\right] = \sigma^2 = \int_{-\infty}^{\infty} S_X(\omega) d\omega \qquad (6\text{-}2)$$

and with reference to zero-mean stationary process, as the Gaussian one, $E\left[X(t)^2\right]$ is the process variance and it gives a measure of the power of the process; therefore the area enclosed under $S_X(\omega)$ gives a measure of the power of the process and the PSD gives also the distribution of the mean-square value of the process, that is the average energy, over the frequency domain.

As said before, the PSD is defined as the Fourier transform of a random process, therefore, by introducing the cross-correlation $R_{X_1X_2}(t_1t_2)$ of two random processes, as the function which gives information about the degree at which two processes tend to move together, similarly the cross-spectral density can be seen as its Fourier transform defined as:

$$S_{XY}(\omega) = \frac{1}{2\pi} \int_{-\infty}^{\infty} e^{-i\omega\tau} R_{XY}(\tau) d\tau \qquad (6\text{-}3)$$

As seen in Chapter 2, the system response in terms of displacements is achieved through the knowledge of its harmonic transfer function $\overline{\mathbf{H}}(\omega)$, if $S_f(\omega)$ is the PSD of the seismic action, the relation between the input and output PSD, expressed in terms of

displacement PSD $S_d(\omega)$, can be expressed by multiplying the excitation PSD $S_f(\omega)$ by the square of the harmonic transfer function, as shown in Eqn. (6-4) (Lutes and Sarkani 2004):

$$S_d(\omega) = S_f(\omega)\overline{\mathbf{H}}^*(\omega)\overline{\mathbf{H}}(\omega) \qquad (6\text{-}4)$$

Moreover, the PSD of velocity $S_v(\omega)$ and the PSD of the relative acceleration $S_a(\omega)$ are related to the PSD of displacement $S_d(\omega)$ as shown in Eqn. (6-5)

$$\begin{aligned} S_v(\omega) &= \omega^2 S_d(\omega) \\ S_a(\omega) &= \omega^4 S_d(\omega) \end{aligned} \qquad (6\text{-}5)$$

Similarly, the part of Eqn. (6-5) related to the acceleration can be also seen in terms of the displacement response variance

$$\sigma_d^2 = \int_{-\infty}^{\infty} S_d(\omega)d\omega \rightarrow \int_{-\infty}^{\infty} \omega^{-4} S_f(\omega) = \frac{1}{\omega^4}\sigma_a^2 = \frac{1}{\omega^4}\sigma_f \qquad (6\text{-}6)$$

where it can be observed that the acceleration response variance is strictly related to the variance of the input acceleration.

In stochastic dynamic analysis, the seismic input is often represented as a white-noise process, which is characterized by a constant value of $S_X(\omega)$ over all the frequencies. This concept is useful because the stationary response to wide-band input can often be approximated by assuming that the input is a white-noise random process with a PSD equal to the value corresponding to the natural circular frequency of the system $S(\omega) = S(\omega_0)$. This approximation is the consequence of the fact that the earthquake excitation PSD function often varies relatively smoothly closely to the system's natural frequency ω_0, while the system harmonic transfer function, $\overline{\mathbf{H}}^*(\omega)\overline{\mathbf{H}}(\omega)$, exhibits a peak in correspondence of the natural frequency (Figure 6-1).

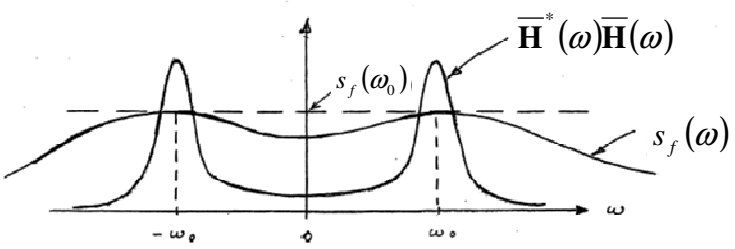

Figure 6-1 Harmonic transfer function behaviour compared with the input approximated as a white noise random process from Barbato 2010

It is noteworthy that the PSD of the seismic action differs from that of a stationary white noise process. However, since the structure acts as a filter which amplifies the excitation components close to resonance, only the values of excitation process close to resonance are

important, while the behaviour away from the latter becomes irrelevant. It is thus an acceptable approximation to use results for the response to a white noise process in analyzing the response to seismic action.

A more accurate representation of the seismic input can be obtained by considering the Kanai-Tajimi spectrum and its extension proposed by Clough and Penzien for the seismic input PSD. The Kanai-Tajimi spectrum is obtained by passing a white process, representing the input motion at the bedrock, through a soil filter frequency ω_g and damping ξ_g; its expression is:

$$S_{KT}(\omega) = S_0 \frac{\omega_g^4 + 4\xi_g^2\omega_g^2\omega^2}{\left[\omega^2 - \omega_g^2\right]^2 + 4\xi_g^2\omega_g^2\omega^2} = S_0 \frac{1 + 4\xi_g^2\left(\frac{\omega}{\omega_g}\right)^2}{\left[1 - \left(\frac{\omega}{\omega_g}\right)^2\right] + 4\xi_g^2\left(\frac{\omega}{\omega_g}\right)^2} \quad (6\text{-}7)$$

where S_0 is the PSD amplitude of the bedrock excitation spectrum, considered to be a white process.

It can be shown that the velocity and displacement spectra of the Kanai-Tajimi acceleration spectrum are not defined as $\omega \to 0$. In order to overcome this drawback, Clough and Penzien passed the Kanai-Tajimi spectrum through an additional filter with parameters ω_f and ξ_f. The equation of motion corresponding to the two filters and the structure are:

$$S_{CP}(\omega) = S_0 \frac{1 + 4\xi_g^2\left(\frac{\omega}{\omega_g}\right)^2}{\left[1 - \left(\frac{\omega}{\omega_g}\right)^2\right] + 4\xi_g^2\left(\frac{\omega}{\omega_g}\right)^2} \cdot \frac{\left(\frac{\omega}{\omega_f}\right)^4}{\left[1 - \left(\frac{\omega}{\omega_f}\right)^2\right]^2 + 4\xi_f^2\left(\frac{\omega}{\omega_f}\right)^2} \quad (6\text{-}8)$$

which yields finite variances for velocities and displacements.

6.1.1 *Analysis of the Van Nuys building subjected to random excitations*

In this section the results of frequency-domain analysis, by means of the PSD function $S(\omega)$ and of the variance of the response σ^2 are reported for the Van Nuys building case study coupled with the external dissipative rocking system. The retrofit configuration analyzed is the one characterized by a unitary tower-to-frame stiffness ratio, providing an added damping of 0.3 ($\kappa = 1 - \xi_{add} = 0.3$).

Let the vector $\overline{\mathbf{x}}$ contain the seismic displacements of the building floors. The matrix $\mathbf{\Phi}_{\overline{\mathbf{x}}\overline{\mathbf{x}}}(\omega)$ represents the corresponding PSD. Given the PSD of the seismic input, $\Phi_{\bar{a}_g\bar{a}_g}(\omega)$, it is possible to express $\mathbf{\Phi}_{\overline{\mathbf{x}}\overline{\mathbf{x}}}(\omega)$ as:

$$\mathbf{\Phi}_{\overline{\mathbf{x}}\overline{\mathbf{x}}}(\omega) = \left(\overline{\mathbf{H}}(\omega)\mathbf{P}\right)^{*} \Phi_{\bar{a}_g\bar{a}_g}(\omega)\left(\overline{\mathbf{H}}(\omega)\mathbf{P}\right)^{T} = \overline{\mathbf{H}}_t^{*}(\omega)\Phi_{\bar{a}_g\bar{a}_g}(\omega)\overline{\mathbf{H}}_t^{T}(\omega) \quad (6\text{-}9)$$

where $\overline{\mathbf{H}}_t$ is a nxm vector, 7x1 in the Van Nuys case, representing the relation between the input, expressed in terms of seismic ground acceleration, and the output, expressed in terms of the floor displacements.

The response variance for the displacement of the *i*-th floor, which is a measure of the response amplitude, can be obtained as:

$$\sigma_{\bar{x}_i}^2 = \int_{-\infty}^{\infty} \left[\mathbf{\Phi}_{\overline{\mathbf{x}}\overline{\mathbf{x}}}(\omega)\right]_{ii} d\omega \quad (6\text{-}10)$$

where $\left[\mathbf{\Phi}_{\overline{\mathbf{x}}\overline{\mathbf{x}}}(\omega)\right]_{ii}$ denotes the element of matrix $\mathbf{\Phi}_{\overline{\mathbf{x}}\overline{\mathbf{x}}}(\omega)$ in correspondence of row *i* and column *i*. It is noteworthy that the function $\left[\mathbf{\Phi}_{\overline{\mathbf{x}}\overline{\mathbf{x}}}(\omega)\right]_{ii}$ is even, i.e., $\left[\mathbf{\Phi}_{\overline{\mathbf{x}}\overline{\mathbf{x}}}(\omega)\right]_{ii} = \left[\mathbf{\Phi}_{\overline{\mathbf{x}}\overline{\mathbf{x}}}(-\omega)\right]_{ii}$. Thus, the response variance can be computed as:

$$\sigma_{\bar{x}_i}^2 = 2\int_{0}^{\infty} \left[\mathbf{\Phi}_{\overline{\mathbf{x}}\overline{\mathbf{x}}}(\omega)\right]_{ii} d\omega \quad (6\text{-}11)$$

As previously introduced, a white noise input is characterized by a flat PSD, i.e., $\Phi_{\bar{a}_g\bar{a}_g}(\omega) = 1$, while the PSD of the Kanai-Tajimi input was expressed as reported in Eqn. (6-7). The root mean square σ_{KT}, associated to the Kanai-Tajimi spectrum, read as follows:

$$\sigma_{KT} = \left[\pi\omega_g\left(\frac{1}{2\xi_g} + 2\xi_g\right)\right]^{1/2} S_0^{1/2} \quad (6\text{-}12)$$

By assuming a peak factor equal to 3 (Lutes Sarkani 2004), the peak ground acceleration can be expressed as:

$$PGA = 3\sigma_{KT} = 3\left[\pi\omega_g\left(\frac{1}{2\xi_g} + 2\xi_g\right)\right]^{1/2} S_0^{1/2} \quad (6\text{-}13)$$

which provides an approximate relation between the PGA and S_0.

The PSD of other response parameters of interest related linearly to the floor displacements through the operator $\mathbf{B}$ can be easily derived by knowing the PSD of the floor displacements $S_{\overline{xx}}$ and $\mathbf{B}$.

For example, the storey drift can be expressed as follows:

$$\boldsymbol{\theta} = \begin{bmatrix} \theta_1 \\ \theta_2 \\ \cdots \\ \theta_7 \end{bmatrix} = \begin{bmatrix} 1 & 0 & 0 & 0 \\ -1 & 1 & 0 & 0 \\ \cdots & \cdots & \cdots & \cdots \\ 0 & 0 & -1 & 1 \end{bmatrix} \begin{bmatrix} \bar{x}_1 \\ \bar{x}_2 \\ \cdots \\ \bar{x}_7 \end{bmatrix} = \mathbf{B}_{\boldsymbol{\theta}} \bar{\mathbf{x}} \qquad (6\text{-}14)$$

Thus, the PSD of the interstorey drifts can be written as $S_{\boldsymbol{\theta}\boldsymbol{\theta}} = \mathbf{B}_{\boldsymbol{\theta}} S_{\bar{\mathbf{x}}\bar{\mathbf{x}}} \mathbf{B}_{\boldsymbol{\theta}}^{\mathbf{T}}$. Similarly, the bare frame floor forces can be expressed as:

$$\mathbf{F} = \begin{bmatrix} F_1 \\ F_2 \\ \cdots \\ F_7 \end{bmatrix} = \mathbf{K}\bar{\mathbf{x}} \qquad (6\text{-}15)$$

and the building storey shear can be expressed as:

$$\mathbf{V} = \begin{bmatrix} V_1 \\ V_2 \\ \cdots \\ V_7 \end{bmatrix} = \begin{bmatrix} 1 & \cdots & 1 & 1 \\ 0 & 1 & \cdots & 1 \\ 0 & \cdots & 1 & 1 \\ 0 & 0 & 0 & 1 \end{bmatrix} \begin{bmatrix} F_1 \\ \cdots \\ F_6 \\ F_7 \end{bmatrix} = \mathbf{T}\mathbf{K}\bar{\mathbf{x}} = \mathbf{B}_{\mathbf{V}} \bar{\mathbf{x}} \qquad (6\text{-}16)$$

Thus, the PSD of the bare frame storey shears can be written as $S_{\mathbf{V}\mathbf{V}} = \mathbf{B}_{\mathbf{V}} S_{\bar{\mathbf{x}}\bar{\mathbf{x}}} \mathbf{B}_{\mathbf{V}}^{\mathbf{T}}$.

$$\mathbf{F} = \begin{bmatrix} F_1 \\ F_2 \\ \cdots \\ F_7 \end{bmatrix} = (\mathbf{K} + i\omega\mathbf{C})\bar{\mathbf{x}} = \mathbf{K}_{dyn}\bar{\mathbf{x}}$$

$$\mathbf{V}_{dyn} = \begin{bmatrix} V_1 \\ V_2 \\ \cdots \\ V_7 \end{bmatrix} = \begin{bmatrix} 1 & \cdots & 1 & 1 \\ 0 & 1 & \cdots & 1 \\ 0 & \cdots & 1 & 1 \\ 0 & 0 & 0 & 1 \end{bmatrix} \begin{bmatrix} F_1 \\ \cdots \\ F_6 \\ F_7 \end{bmatrix} = \mathbf{T}\mathbf{K}_{dyn}\bar{\mathbf{x}} = \mathbf{B}_{\mathbf{V}_{dyn}} \bar{\mathbf{x}} \qquad (6\text{-}17)$$

Thus, the PSD of the bare frame storey shears taking also into account the damping contribution, can be written as $S_{\mathbf{V}_{dyn}\mathbf{V}_{dyn}} = \mathbf{B}_{\mathbf{V}_{dyn}} S_{\bar{\mathbf{x}}\bar{\mathbf{x}}} \mathbf{B}_{\mathbf{V}_{dyn}}^{\mathbf{T}}$.

Finally, the PSD of the absolute floor accelerations $\bar{\mathbf{a}}$ of the bare frame is obtained by manipulating the equation of motion:

$$\mathbf{M}\ddot{\mathbf{x}}(t)+\mathbf{C}\dot{\mathbf{x}}(t)+\mathbf{K}\mathbf{x}(t)=-\mathbf{M}\mathbf{R}a_g(t)$$
$$\left(\ddot{\mathbf{x}}(t)+\mathbf{R}a_g(t)\right)=-\mathbf{M}^{-1}\left[\mathbf{C}\dot{\mathbf{x}}(t)+\mathbf{K}\mathbf{x}(t)\right] \qquad (6\text{-}18)$$
$$\bar{\mathbf{a}}=-\mathbf{M}^{-1}\left(i\omega\mathbf{C}+\mathbf{K}\right)\bar{\mathbf{x}}=\mathbf{B}_{\mathbf{a}}\bar{\mathbf{x}}$$

Thus, the PSD of the absolute floor accelerations can be written as $S_{\bar{\mathbf{a}}\bar{\mathbf{a}}}=\mathbf{B}_{\mathbf{a}}S_{\bar{\mathbf{x}}\bar{\mathbf{x}}}\mathbf{B}_{\mathbf{a}}^{T}$. Finally Table 6-1 reports the parameters of the Kanai-Tajimi and Clough-Penzien spectra, i.e. $\omega_g,\xi_g,\omega_f,\xi_f$, for various soil conditions, proposed by Der Kiuregwan and Neuenhofer (1992).

Table 6-1 Parameters of the Kanai-Tajimi spectra for various soil conditions

Soil type	ω_g [rad/s]	ξ_g	ω_f [rad/s]	ξ_f
soft	5.0	0.2	0.5	0.6
medium	10.0	0.4	1.0	0.6
firm	15.0	0.6	1.5	0.6

Analyses for 20 sample time histories generated based on the assumed PSD, are carried out. The mean values of the maximum floor displacements have been evaluated and compared with the approximate estimate of the floor displacement maxima obtained by using the peak factor η_p. The peak factor is evaluated as

$$\eta_p=\left[2\ln\left(\frac{\frac{\omega_c}{2\pi}t_L}{-\ln p}\right)\right]^{1/2} \qquad (6\text{-}19)$$

where $\omega_c=\sigma_{\dot{\bar{x}}_i}\big/\sigma_{\bar{x}_i}$, p is the probability of exceedance and t_L is the time interval. The actual maximum amplitude corresponding to a confidence level p is thus given by $\bar{x}_{\max,p}=\eta_p\sigma_{\bar{x}}$. The obtained results are quite similar and this provide a validation to the use of the peak factor. Thus, in the subsequent analyses, only the maxima evaluated by using the peak factor of 3.5 will be considered.

For the successive analysis only the response standard deviation of the different response parameter of interest will be shown, thus avoiding time consuming time history analyses.

Table 6-2 reports the results in terms of floor displacements of a parametric analysis involving different soil conditions. The parameters used for soft, medium and firm soil are those of Table 6-1. The results are related to the Van Nuys building in the retrofit configuration and are the mean of the maximum values obtained for the 20 samples. Figure 6-2 displays the displacements normalized to unity with respect of the value obtained at the seventh floor with a soft soil.

Table 6-2 Van Nuys building: displacements results for different soil conditions

level	*firm*	*medium*	*soft*
	$\bar{x}_i$ [m]	$\bar{x}_i$ [m]	$\bar{x}_i$ [m]
1	0.016	0.019	0.027
2	0.028	0.032	0.046
3	0.040	0.046	0.065
4	0.052	0.060	0.083
5	0.063	0.073	0.101
6	0.074	0.085	0.117
7	0.083	0.096	0.131

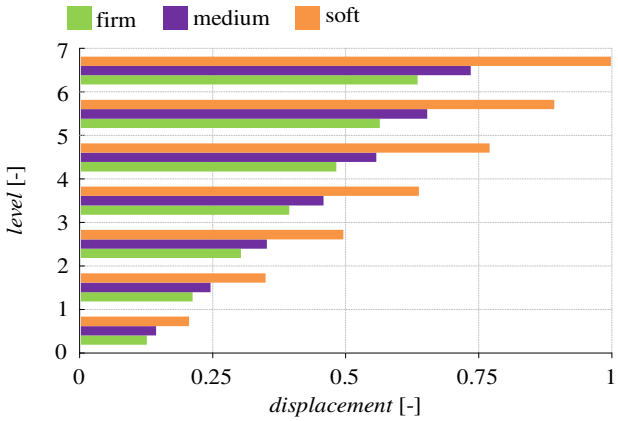

Figure 6-2 Van Nuys building: floor displacements resulting from a parametric analysis involving different soil conditions

Chapter 7

Open Problems

In this chapter other aspects that still require further investigation are discussed and briefly analyzed, with preliminary results. First of all, a comparison is made between the performances obtained by employing nonlinear viscous dampers rather than linear viscous ones. The Camerino building case study is considered and the damping coefficient of the non-linear devices is evaluated through the dissipated energy criterion proposed by Lin et Chopra (2002). The performance comparison, between linear and non-linear FVDs, at different Limit States, is made in terms of forces and strokes.

Successively, with the aim to evaluate the efficiency of the external dissipative rocking system, with respect to another external arrangement, a performance comparison is proposed. The alternative solution deals with the coupling of an existing frame with an external stiff contrasting structure, by using viscous dampers at each floor level. Assuming the external structure as infinitely rigid, the dampers are activated by the absolute floor displacements. This type of system is known in the literature as mass proportional damping system (MPD) (Trombetti and Silvestri 2007, Tubaldi et al. 2014, Tubaldi 2015); first the performance of an infinitely stiff MPD system is investigated and compared with that of the bare building and with the case of a finite stiff MPD. Successively, a performance comparison is made between the external dissipative rocking system and the so called MPD. In both cases, the external structures are considered infinitely stiff.

Finally, a first insight into the soil-structure interaction (SSI) problem is given by means of the substructure approach. This gives the opportunity to evaluate the problem by decomposing the superstructure-foundation-soil into two subsystems, whose responses are determined independently. The overall response is then obtained by performing both kinematic and inertial interaction; frequency domain analysis allows the knowledge of the dynamic impedance matrix and the foundation input motion (kinetic interaction), while the inertial interaction is choose to be performed through time-domain, for the analyzed case study. The dynamic response of the superstructure on compliant base, subjected to the foundation input motion, is evaluated by means of the Lumped Parameter Model (LPM) proposed by Carbonari et al. (2012), while the foundations impedances are determined in accordance to the model proposed by Dezi et al. (2009).

7.1 Non-linear viscous dampers

The investigation of the dynamic response of the system existing frame-external dissipative rocking system, is based on the assumption of the linear elastic behaviour of both the two components. As a consequence, the fluid viscous dampers, located at bracings base, are linear too; this leads to a unitary value of the exponent α in the devices constitutive law.

The use of non-linear fluid viscous dampers (FVDs), characterized by a value of the exponent α smaller than unity, is extremely diffuse and many industries produce only this type of devices, for civil engineering applications. Hence the performance comparison of the external dissipative rocking system, equipped with both linear and non linear FVDs, is evaluated for the two analyzed case studies (Van Nuys and Camerino buildings). For this purpose the FEM models available are exploited to perform non-linear time histories analysis by means of SAP2000.

Even if the performance of non-linear time history analysis is no more a limit, thanks to the enhanced features of many personal computers, which are able to execute this kind of analysis, the use of linear equivalent parameters is still diffuse to solve dynamic problem relating to non-linear FVDs. There are different methods to estimate equivalent linear properties, among them: equating power consumption in the two systems; replacing the non-linear viscous damping by an array of frequency- and amplitude-dependent linear viscous models; random vibration theory and the energy dissipated criterion, which is also the most used. Lin and Chopra (2002) provide a detailed explanation of the latter method, which is based on the equivalence of dissipated energy in a harmonic motion cycle, done by the linear FVD and the non-linear one, for a given value of the exponent α and for a specific Limit State (LS).

It has been observed that, once determined the features of the equivalent non-linear FVD, it provides almost the same performance in terms of the overall system response for the given LS, but with different behaviours for the others. If the equivalence of dissipated energy is done for the Life Safety, it is expected that the non-linear FVD shows almost the same displacements of the equivalent linear device, with smaller forces. At the Collapse Prevention Limit State (CPLS), instead, the forces on the non-linear FVD are still significantly smaller, but the displacements are expected to be higher. The opposite situation is expected, for the Immediate Occupancy Limit State (IOLS), where the non-linear FVD shows higher axial actions and lower displacements. Figure 7-1 provides a comparison of the linear and non linear FVDs behaviour for IOLS and CPLS.

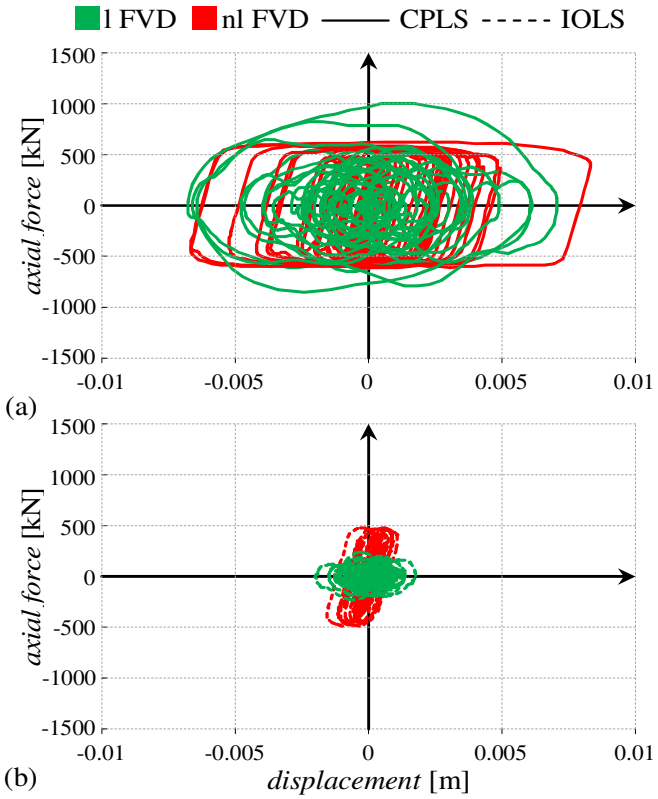

Figure 7-1 Linear and non-linear FVDs force-displacement loops for the CPLS (a) and IOLS (b)

7.1.1 *Equivalence of dissipated energy*

The energy dissipated by a damper during a cycle of harmonic motion $u(t) = u_0 sen(\omega t)$ is

$$E_D = \oint F_d du = \int_0^{2\pi} F_d \dot{u} dt = \int_0^{2\pi} c_\alpha |\dot{u}|^{1+\alpha} dt \qquad (7\text{-}1)$$

where F_d is the constitutive law for a FVD, already shown in Eqn. (1-2). The solution of the integer was found by Symans and Constantinou (1998) and results in

$$E_D = \pi \beta_\alpha c_\alpha \omega^\alpha u_0^{\alpha+1} \qquad (7\text{-}2)$$

where the constant β_α is

$$\beta_\alpha = \frac{2^{2+\alpha}\Gamma^2(1+\alpha/2)}{\pi\Gamma(2+\alpha)} \quad (7\text{-}3)$$

and $\Gamma(\cdot)$ is the gamma function. In the case of a linear FVD the constant β_α has a unitary value and the dissipated energy becomes

$$E_D = \pi c_1 \omega u_0^2 \quad (7\text{-}4)$$

By equating Eqn. (7-2) and Eqn. (7-4) the damping coefficient c_α, for a non-linear FVD, can be found as a function of the linear damping coefficient c_1 and vice versa.

$$c_\alpha = \frac{(\omega u_0)^{1-\alpha}}{\beta_\alpha} c_1 \quad (7\text{-}5)$$

The equivalence of energy dissipated between linear and non-linear FVDs, can be evaluated for a generic input by substituting ω with the natural frequency of the system ω_n, this leads to the conclusion that the dissipated energy criterion in resonance condition can be valid generally.

The main results provided by Lin and Chopra for a single degree of freedom system are:

- the influence of damper non-linearity on harmonic response is very small over the entire range of excitation frequencies for smaller values of damping; this influence increases for larger values of damping and smaller values of the exponent α, in part because damper non-linearity shifts the resonant frequency;
- dampers non-linearity essentially has no influence on the peak responses (deformations, relative velocities and accelerations) of the system in the velocity-sensitive spectral region.

Due to the fact that the retrofit with an external dissipative rocking system leads to a displacements response governed essentially by the first mode, the dissipated energy criterion can be valid for the evaluation of the dynamic response of the system equipped with non-linear FVDs. Moreover, thanks to the fact that dissipative devices are all concentrated at the base and activated by its rotation, Eqn. (7-5) expresses a direct relationship for all the viscous dampers.

7.1.2 *Comparison between linear and non-linear fluid viscous dampers*

The damping coefficient c_α, is determined for both the two case studies and the equivalence of dissipated energy is done for the Ultimate Limit State (ULS). The maximum displacement of the FVD, u_0, is assumed as the mean of the maximum values obtained for the twenty time histories for the Van Nuys building, and for the seven time histories in the case of Camerino building. The exponent chosen for the non-linear fluid viscous dampers is α=0.15, which leads to a constant $\beta_{0.15}$, equal to 1.218.

The performance comparison is evaluated through monitoring strokes, velocities, forces and viscous bending moments of the FVDs and through the displacements distributions control along the height of the coupled systems. For the operational Limit States the distribution of absolute accelerations is also reported, because their evaluation is particularly significant for the protection of acceleration-sensitive non structural components.

Van Nuys building:

For the Van Nuys building the damping coefficient of each of the sixteen dampers in the FEM model, is determined only for one of the retrofit configurations considered, that is the $\kappa = 1 - \xi_{add} = 0.30$ case, where the linear damping coefficient is $C_1 = 31296 kNs/m$.

The amplitude of displacement needed in Eqn. (7-5) is 0.0163 m, the fundamental period in the horizontal direction of the FEM model is $T = 1.179 s$, hence the natural frequency results in $\omega_n = 2\pi/T = 5.329 rad$, therefore the non linear damping coefficient results equal to $C_{0.15} = 3219 kNs/m^{\alpha}$.

The performance comparison is evaluated only for two of the twenty time histories performed at the ULS, that is records n. 12 and n. 15. The reason is due to the fact that only records related to the over mentioned Limit State were available and the use of artificial earthquakes would have led to a seismic hazard non coherent to the previous one used.

Table 7-1 reports the results in terms of displacement y, velocity $\dot{y}$, axial force N and viscous bending moment M_v of both linear and non-linear FVDs for the record n. 12, while Figure 7-2 depicts the force-displacement loops for linear devices (green line) and non-linear ones (red line). Table 7-2, instead, shows the results in terms of displacements distribution along the height of the building.

It is observed that, as expected, the displacements of the devices are similar, while the axial action is smaller in the case of non-linear behaviour. The displacements of the coupled system are higher (4%) in the case of non-linear FVDs.

Table 7-1 Van Nuys building: FVDs results for the record n.12

acc12							
linear FVD				*Non-linear FVD*			
y_i [m]	$\dot{y}_i$ [m/s]	N [kN]	M_v [kNm]	y_i [m]	$\dot{y}_i$ [m/s]	N [kN]	M_v [kNm]
0.0083	0.092	2859	25437	0.0073	0.134	2377	20917

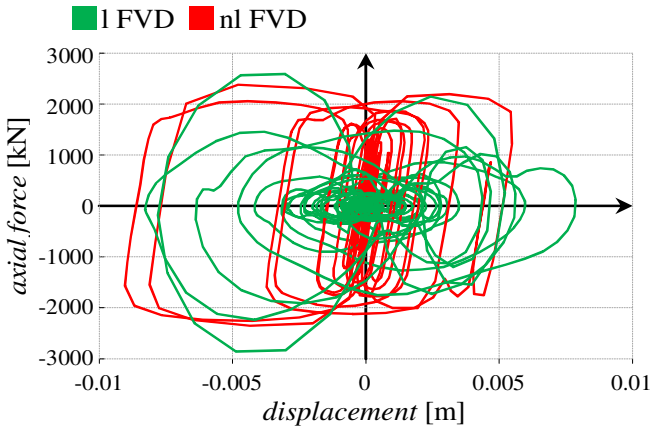

Figure 7-2 Van Nuys building: FVDs force-displacement loops for record n. 12

Table 7-2 Van Nuys building: floor displacements for the record n.12

	acc12	
level	*linear FVD*	*non-linear FVD*
	x_i [m]	x_i [m]
1	0.0166	0.0207
2	0.0305	0.036
3	0.0454	0.0514
4	0.0577	0.0648
5	0.0648	0.0757
6	0.0774	0.0848
7	0.0892	0.0934

Table 7-3, Figure 7-3 and Table 7-4 show the same results for the record n. 15; also in this case it is observable that use of non-linear FVDs leads to almost equal displacements in the devices, with smaller axial actions and higher displacements distribution, along the height of the building (nearly 10%).

Table 7-3 Van Nuys building: FVDs results for the record n.15

acc15							
linear FVD				*Non-linear FVD*			
y_i [m]	$\dot{y}_i$ [m/s]	N [kN]	M_v [kNm]	y_i [m]	$\dot{y}_i$ [m/s]	N [kN]	M_v [kNm]
0.0221	0.133	4174	36747	0.0198	0.154	2430	21386

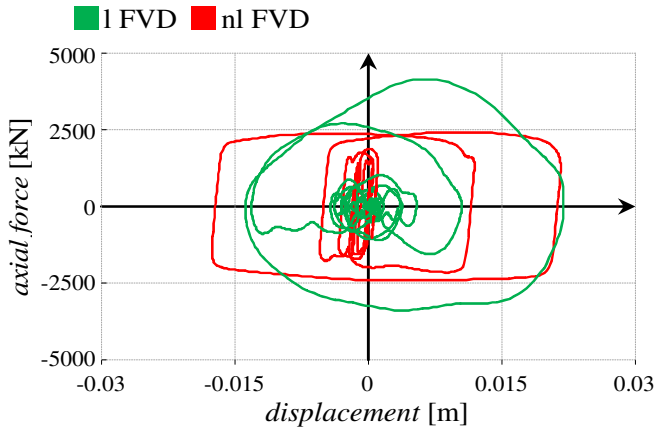

Figure 7-3 Van Nuys building: FVDs force-displacement loops for record n. 15

Table 7-4 Van Nuys building: floor displacements for the record n.15

level	*acc15*	
	linear FVD	*non-linear FVD*
	x_i [m]	x_i [m]
1	0.0413	0.0423
2	0.071	0.073
3	0.1015	0.1054
4	0.1316	0.139
5	0.1602	0.1726
6	0.1876	0.2045
7	0.2118	0.2328

Camerino building:

For the Camerino building case study seven groups of artificial earthquakes, generated in accordance with Italian Standards, were already available for the SLV. Therefore seven groups of artificial earthquakes have been generated for the other three Limit States provided by the Code NTC 2008, that is SLO, SLD and SLC. The related pseudo-acceleration response spectra are depicted in Figure 7-4.

The reported results are the mean of the maximum values obtained for each one of the four analyzed LS. Moreover the comparison of the force-displacement loop, between linear and non-linear FVDs is reported for all the seven artificial earthquakes of the investigated LS. The force-displacement loop is determined as the mean, time instant per time instant, of each one of the eight dampers (four per external dissipative structure) of the FEM model.

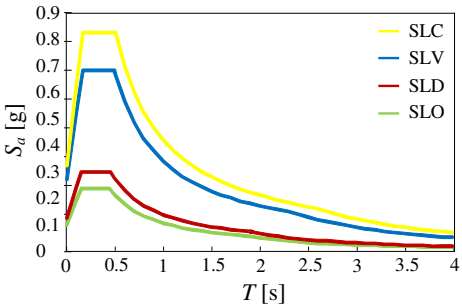

Figure 7-4 Camerino building: pseudo-acceleration response spectra describing the seismic hazard

The linear damping coefficient of each one of the dampers is $C_1 = 16877 kNs/m$, while the displacement amplitude in the longitudinal direction is $u_0 = 0.00654m$ (mean of the maximum values at the SLV). The natural period of the coupled system is $T = 0.96s$, hence the natural frequency results in $\omega_n = 2\pi/T = 6.52 rad$, therefore the non linear damping coefficient is $C_{0.15} = 948 kNs/m^{\alpha}$.

The non-linear FVDs are dimensioned with the energy dissipated criterion to provide almost equal displacements with respect to the linear ones for a given LS, that is the SLV. As expected at the SLV, non-linear devices produce similar displacements with smaller axial actions. Successively different situations are analyzed, producing some differences among the two kind of dampers. At the SLO and SLD, non-linear FVDs show smaller displacements, together with higher axial forces. Looking, instead, to rarer seismic events, as in the case of SLC, the non-linear behaviour is not properly the expected one. Axial actions are always smaller in comparison to those of the linear devices, while the displacements result higher only in some cases. A possible explanation can lie in an apparent initial stiffness displayed by the non-linear devices, which leads to smaller displacements.

Table 7-5 reports the results in terms of displacement y, velocity $\dot{y}$, axial force N and viscous bending moment M_v of both linear and non-linear FVDs for the SLO, while Figure 7-5 depicts for every time history analysis, a force-displacement cycle for both linear (green line) and non-linear (red line) FVDs.

Table 7-5 Camerino building: FVDs results for the SLO

SLO							
linear FVD				*Non-linear FVD*			
y_i [m]	$\dot{y}_i$ [m/s]	N [kN]	M_v [kNm]	y_i [m]	$\dot{y}_i$ [m/s]	N [kN]	M_v [kNm]
0.00203	0.0157	267	2172	0.0013	0.0136	495	4058

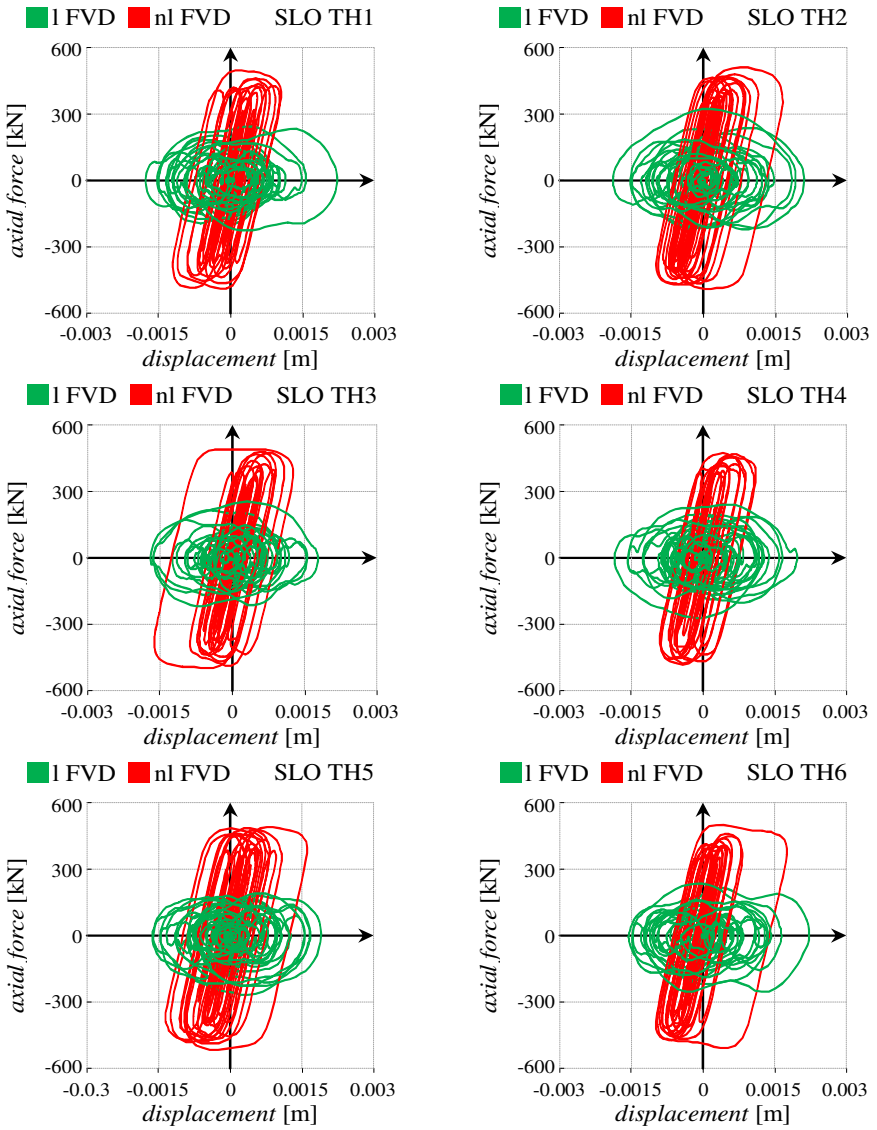
l FVD
nl FVD
SLO TH1
SLO TH2
SLO TH3
SLO TH4
SLO TH5
SLO TH6
axial force [kN]
displacement [m]
600
300
0
-300
-600
-0.003
-0.0015
0
0.0015
0.003
-0.0.3

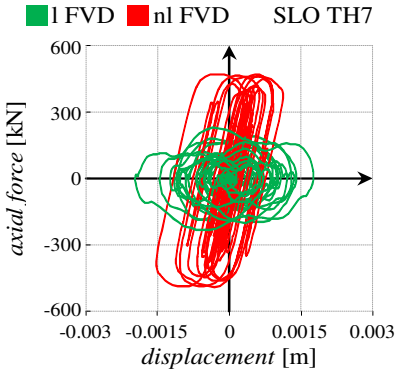

Figure 7-5 Camerino building: FVDs force-displacement loops for the seven earthquakes at the SLO

Table 7-6 reports the distribution of displacements and absolute accelerations along the height of the building for the SLO limit state obtained with linear and non-linear devices. It is observed that the performance is almost equal, in terms of displacements, while there is an increase of the absolute accelerations in the case of non-linear behaviour, in the range +20% - +36%, which is particularly significant for all the acceleration-sensitive contents.

Table 7-6 Camerino building: floor displacements for the SLO

	SLO			
level	*linear FVD*	*non-linear FVD*	*linear FVD*	*non-linear FVD*
	x_i [m]	x_i [m]	$\ddot{x}_i$ [m/s^2]	$\ddot{x}_i$ [m/s^2]
1	0.0025	0.0022	0.98	1.18
2	0.0059	0.0054	1.21	1.49
3	0.0092	0.0088	1.07	1.39
4	0.0124	0.0122	0.77	1.04
5	0.0155	0.0154	1.18	1.60

Table 7-7 reports the results related to the SLD, while Figure 7-6 depicts for every time history analysis, a force-displacement cycle for both linear (green line) and non-linear (red line) FVDs.

Table 7-7 Camerino building: FVDs results for the SLD

SLD							
linear FVD				*Non-linear FVD*			
y_i [m]	$\dot{y}_i$ [m/s]	N [kN]	M_v [kNm]	y_i [m]	$\dot{y}_i$ [m/s]	N [kN]	M_v [kNm]
0.00263	0.0201	340	2785	0.00175	0.0184	519	4254

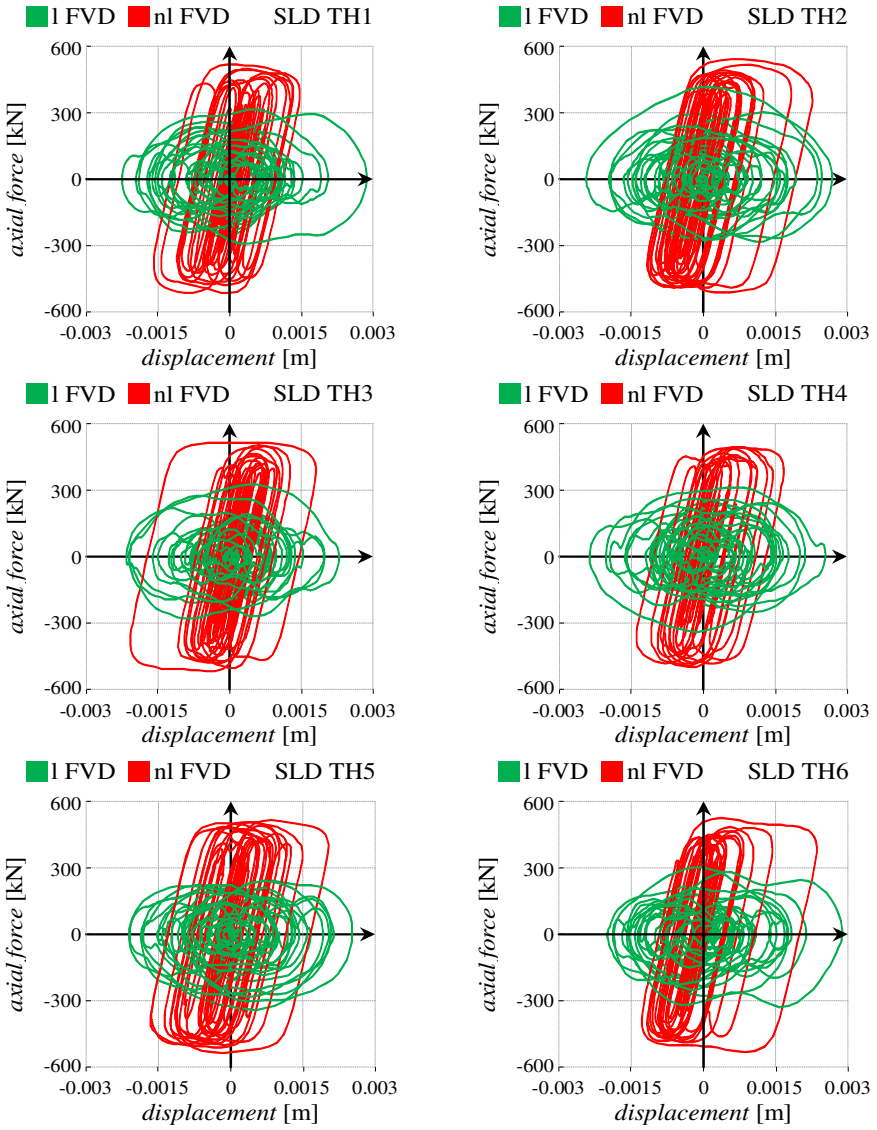
l FVD
nl FVD
SLD TH1
SLD TH2
SLD TH3
SLD TH4
SLD TH5
SLD TH6
axial force [kN]
displacement [m]
600
300
0
-300
-600
-0.003
-0.0015
0
0.0015
0.003

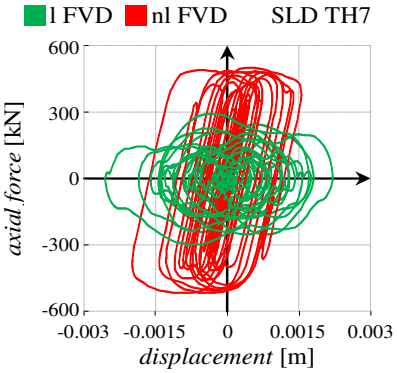

Figure 7-6 Camerino building: FVDs force-displacement loops for the seven earthquakes at the SLD

Table 7-8 reports the displacements distribution along the height of the building for the SLD limit state obtained with linear and non-linear FVDs. It is observed that the performance is very similar, with higher displacements in the case of linear behaviour (4%). For what concerns absolute accelerations, the use of non-linear devices leads to an increase of the values, recorded at every level, in the range +18% - +28%, which is particularly significant for all the acceleration-sensitive contents, as already seen for the SLO.

Table 7-8 Camerino building: floor displacements for the SLD

	SLD			
level	*linear FVD*	*non-linear FVD*	*linear FVD*	*non-linear FVD*
	x_i [m]	x_i [m]	$\ddot{x}_i$ [m/s^2]	$\ddot{x}_i$ [m/s^2]
1	0.0032	0.0029	1.23	1.45
2	0.0076	0.0069	1.50	1.80
3	0.0119	0.0111	1.34	1.66
4	0.0160	0.0153	0.97	1.21
5	0.0200	0.0192	1.49	1.91

Table 7-9 reports the results related to both linear and non-linear FVDs for the SLV, while Figure 7-7 depicts for every time history analysis, a force-displacement cycle for both linear (green line) and non-linear (red line) FVDs.

Table 7-9 Camerino building: FVDs results for the SLV

SLV							
linear FVD				*Non-linear FVD*			
y_i [m]	$\dot{y}_i$ [m/s]	N [kN]	M_v [kNm]	y_i [m]	$\dot{y}_i$ [m/s]	N [kN]	M_v [kNm]
0.00654	0.0494	834	6840	0.00556	0.0481	600	4923

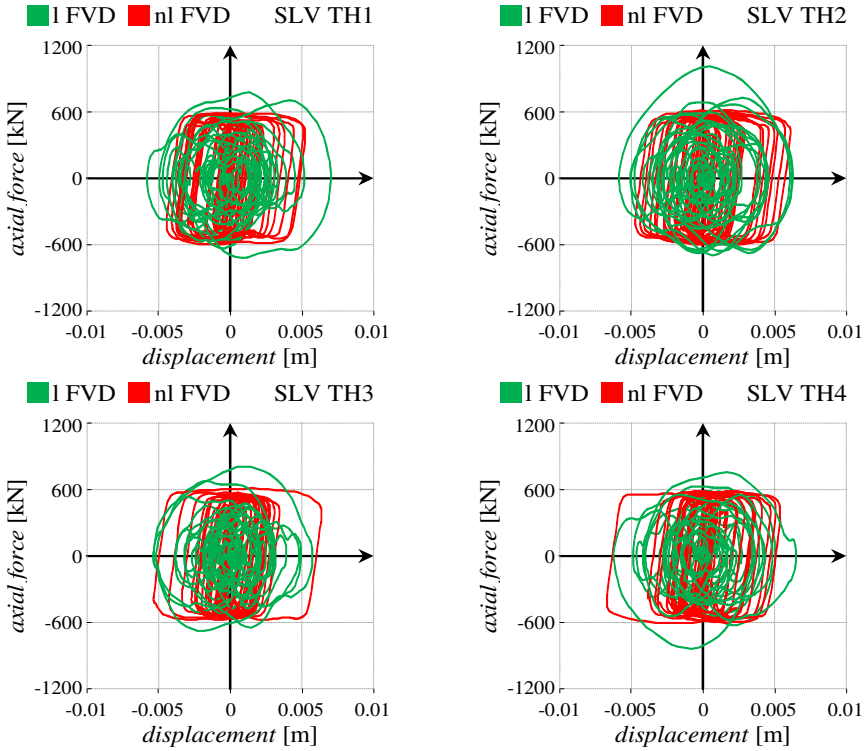

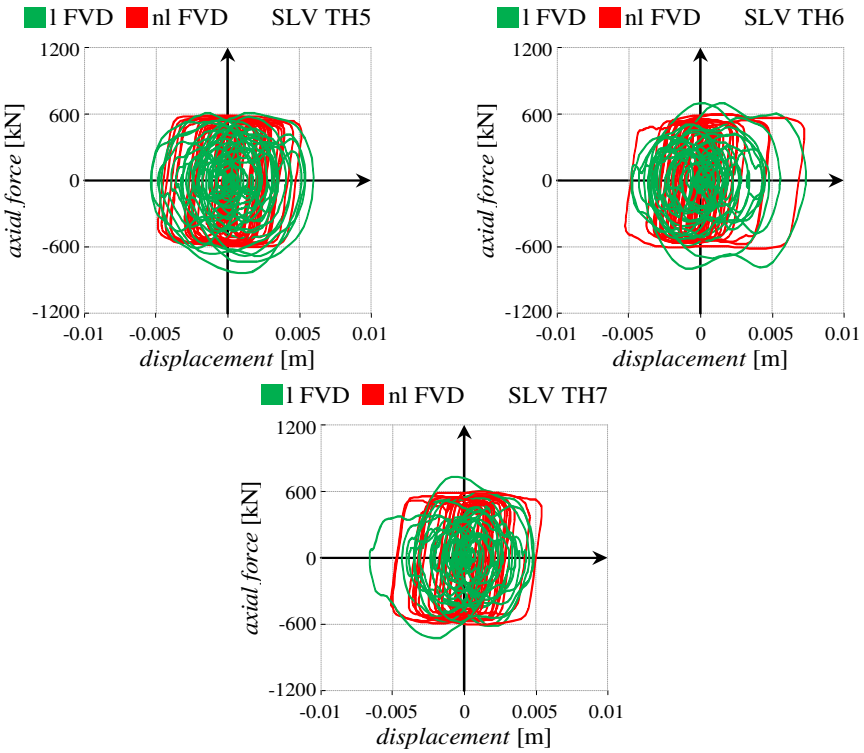

Figure 7-7 Camerino building: FVDs force-displacement loops for the seven earthquakes at the SLV

Table 7-10 reports the displacements distribution along the height of the building for the SLV limit state. It is observed that the performance obtained with the two kind of devices is the same, as expected, due to the fact that the equivalence of dissipated energy is done for this specific limit state.

Table 7-10 Camerino building: floor displacements for the SLV

level	***SLV***	
	linear FVD	*non-linear FVD*
	x_i [m]	x_i [m]
1	0.008	0.008
2	0.0188	0.0187
3	0.0295	0.0292
4	0.0399	0.0396
5	0.0497	0.0495

Table 7-11 reports the results related to both linear and non-linear FVDs for the SLC, while Figure 7-8 depicts for every time history analysis, a force-displacement cycle for both linear (green line) and non-linear (red line) FVDs.

Table 7-11 Camerino building: FVDs results for the SLC

SLC							
linear FVD				*Non-linear FVD*			
y_i [m]	$\dot{y}_i$ [m/s]	N [kN]	M_v [kNm]	y_i [m]	$\dot{y}_i$ [m/s]	N [kN]	M_v [kNm]
0.00812	0.0611	1032	8459	0.00758	0.0619	624	5114

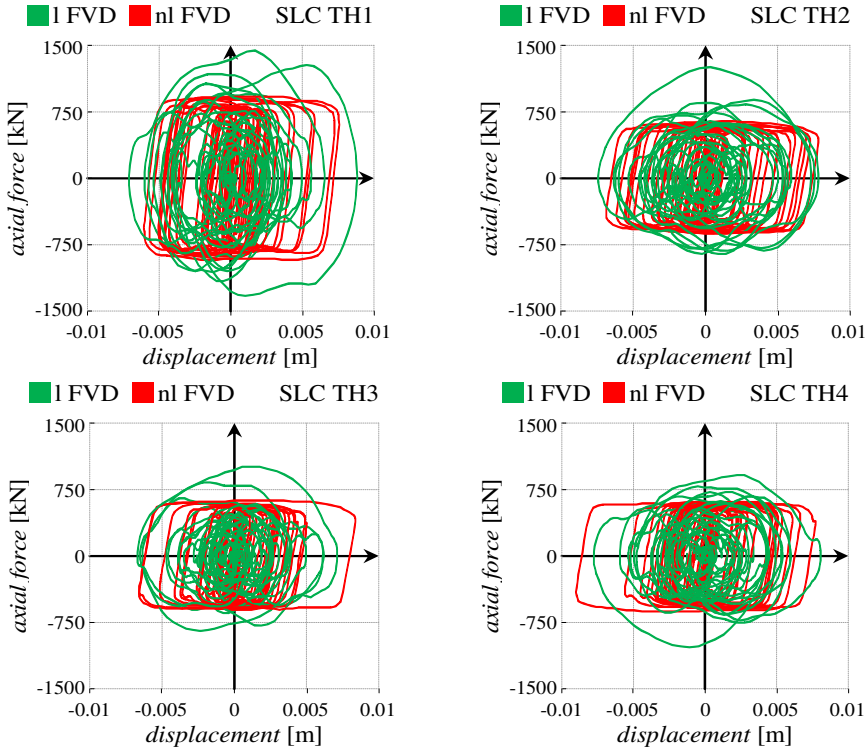

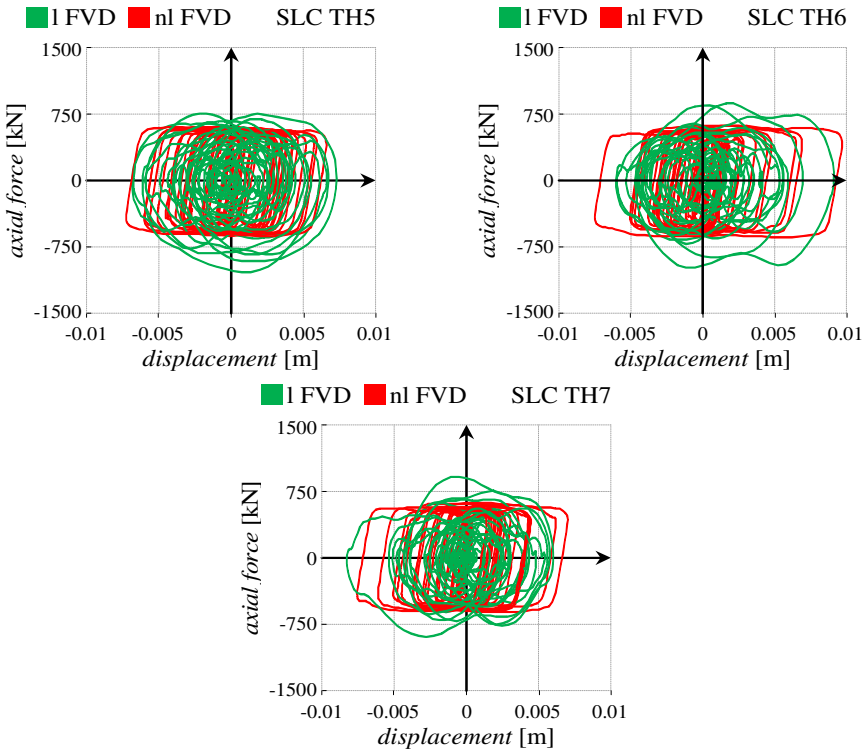

Figure 7-8 Camerino building: FVDs force-displacement loops for the seven earthquakes at the SLC

Table 7-12 reports the displacements distribution along the height of the building for the SLC limit state obtained with linear and non-linear FVDs. It is observed that the performance is similar, with higher displacements in the case of non-linear behaviour (6%).

Table 7-12 Camerino building: floor displacements for the SLC

level	***SLC***	
	linear FVD	*non-linear FVD*
	x_i [m]	x_i [m]
1	0.010	0.0105
2	0.0233	0.0247
3	0.0366	0.0387
4	0.0495	0.0526
5	0.0617	0.0658

7.2 Comparison with other retrofitting schemes

In Chapter 1 the state of the art of possible arrangements based on the use of passive control system was introduced; among them there is the case of FVDs used for the coupling of two adjacent structural systems. In the recent past many studies (Westermo 1989, Xu et al. 1999, Yang et al. 2003, Bhaskararao and Jangid 2007 and Roh et al. 2011) have investigated both the dynamic and the seismic behaviour of such systems and, in general, it was shown that the interaction between two systems with different dynamic properties reduces the magnitude of structural seismic response, when compared to the unconnected structure. Moreover this kind of solutions also permits to avoid the potentially catastrophic consequences of pounding.

Figure 7-9 (a) depicts the ideal case where dampers are placed horizontally at the storey level, between the frame and an external stiff contrasting structure; this way, the links are activated by the floor absolute displacements and the system can be analyzed as a mass proportional damping system (MPD) (Trombetti and Silvestri 2007). Figure 7-9 (b), instead, depicts the more realistic case in which dampers are placed between adjacent buildings, characterized by different dynamic properties, therefore the solution can be efficient (Gattulli et al. 2013, Tubaldi et al. 2014, Tubaldi 2015).

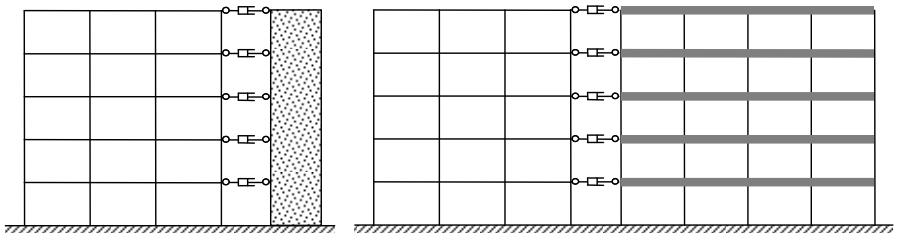

Figure 7-9 FVDs used for the coupling with external stiff contrasting structure (a) and for the coupling of adjacent buildings (b)

Differently from the case of the external dissipative rocking system, the coupling with an external MPD system does not modify the dynamic behaviour of the existing frame which still deforms as its own vibration modes.

In this section the seismic response of the Van Nuys building coupled with an infinitely stiff contrasting structure (MPD system), providing an added damping of 30% $(\xi_{add} = 0.30)$ is analyzed. Successively its performance is compared with a second arrangement in which the coupling is done with a MPD system characterized by a finite stiffness, providing the same damping contribution. In this latter case the external MPD system has the same members and dimension of the external rocking system used in the $\kappa = 1 - \xi_{add} = 0.30$ retrofit configuration. It is important to specify that in both the two MPD arrangements analyzed, the added damping contribution is obtained taking into account the masses of the Van Nuys building only.

Finally the seismic performance of the bare Van Nuys building is compared with both the two external configurations, that is an infinitely stiff external rocking system and the infinitely stiff MPD system.

The seismic response is investigated in the transverse direction only.

7.2.1 *Equation of motion of a finite stiffness MPD system*

The equation of motion of an existing frame coupled with an external contrasting structure (MPD system), characterized by finite stiffness, can be expressed as:

$$\mathbf{M}\ddot{\mathbf{u}}(t)+\mathbf{C}\dot{\mathbf{u}}(t)+\mathbf{K}\mathbf{u}(t)=\mathbf{M}\mathbf{p}a_g(t) \qquad (7\text{-}6)$$

where $\mathbf{u}(t)=\begin{vmatrix}\mathbf{u}_F(t)\\ \mathbf{u}_D(t)\end{vmatrix}$, is the vector collecting the $N=m+n$ nodal displacements at the various floors of both the existing building, denoted as *"F"* with *m* degrees of freedom, related to active inertial forces, and of the MPD system, denoted as *"D"* with *n* degrees of freedom, involved in the bracings deformation. The dot (·) denotes time-derivative; $\mathbf{p}$ is the load distribution vector and $a_g(t)$ is the external scalar loading function describing the seismic base acceleration. The time invariant matrices $\mathbf{M}=\begin{vmatrix}\mathbf{M}_F & \mathbf{0}\\ \mathbf{0} & \mathbf{0}\end{vmatrix}$, $\mathbf{K}=\begin{vmatrix}\mathbf{K}_F & \mathbf{0}\\ \mathbf{0} & \mathbf{K}_D\end{vmatrix}$, $\mathbf{C}=\begin{vmatrix}\mathbf{C}_F+\mathbf{C}_d & -\mathbf{C}_d\\ -\mathbf{C}_d & \mathbf{C}_d\end{vmatrix}$ describe the mass, stiffness and damping operators of the coupled system, respectively. It is noteworthy that the damping operator $\mathbf{C}$ is obtained as the sum of the contributions due to the inherent damping of the bare frame $(\mathbf{C}_F)$, modelled as Rayleigh damping matrix; plus the mass proportional damping contribution provided by the FVDs $\mathbf{C}_d$, related to the masses of the existing frame $\mathbf{C}_d=\alpha\mathbf{M}_F$. The dynamic behaviour of the coupled system is studied through time-domain analysis by means of the proposed formulation, described in Chapter 2, stated in the state-space form.

7.2.2 *Seismic response of a MPD system*

This section reports and compares the seismic response of three configurations:

- the bare Van Nuys building (*As is*);
- the existing frame coupled with an infinitely stiff MPD system providing an added damping equal to 0.3 (*MPD stiff*);
- the existing frame coupled with a MPD stiffness providing the same damping contribution and characterized by a finite stiffness (*MPD*).

Both the two retrofit configurations can be achieved with the insertion of four external structures, each one equipped with two FVDs per floor. The number of external structures is defined for feasibility limit related to the stresses on the foundation system.

Table 7-13 reports the floor displacements and the interstorey drifts for the three configurations analyzed. It is observed that the reduction of the frame displacements is nearly 48% in the *MPD* case and nearly 54% in the infinitely stiff configuration.

Figure 7-10 (a) reports distribution of the displacements (x_i) along the height of the building, for i=1, 2 ,.., 7, normalized with respect to the value observed at the top of the bare frame; the orange lines represent the displacements of the external structures in the retrofit case *MPD*. Figure 7-10 (b) reports the distribution of the IDRs (θ_i), as expected, the MPD system does not affect the shape of the interstorey drifts distribution, which remains the same after the retrofit. The *MPD stiff* configuration yields a reduction of 53% with respect to the bare frame, while the other retrofit case, *MPD*, to a reduction of 48%, even though the highest interstorey drift is bigger than 1%. The performances of the two retrofit cases are very similar, either in terms of displacements, either in terms of interstorey drifts.

Table 7-13 MPD systems: floor displacements and drifts results

level	*As is*		*MPD*				*MPD stiff*	
	x_i	θ_i	$x_{i,frame}$	$\theta_{i,frame}$	x_{i,ext_str}	θ_{i,ext_str}	x_i	θ_i
	[m]	[%]	[m]	[%]	[m]	[%]	[m]	[%]
1	0.063	1.52	0.033	0.80	0.004	0.09	0.030	0.72
2	0.113	1.90	0.059	0.99	0.010	0.24	0.053	0.89
3	0.165	2.07	0.085	1.08	0.020	0.39	0.077	0.97
4	0.213	1.98	0.110	1.02	0.034	0.51	0.098	0.94
5	0.253	1.72	0.131	0.87	0.049	0.57	0.117	0.83
6	0.285	1.35	0.147	0.68	0.064	0.59	0.132	0.66
7	0.306	0.91	0.158	0.46	0.079	0.58	0.142	0.46

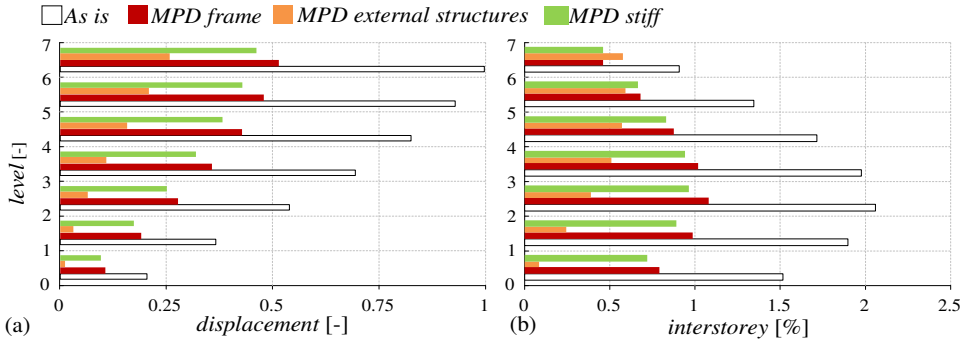

Figure 7-10 MPD systems: displacements (a) and interstorey drifts (b) distributions

Table 7-14 reports the shear actions resisted by the frame and by the external structures, together with the total shear. As already discussed for the displacements, the connection with MPD systems results in a reduction of the global shear demand on the frame and the performances of the two retrofit cases are very close one to each other. In particular, the infinitely stiff system provides better results in terms of shear reduction along the height of the building, with the exception of the last storey. The relative reduction of the maximum base shear acting on the frame, with respect to the bare building, is nearly 47% for the *MPD* case and 52% for the stiff system.

Table 7-14 MPD systems: shear actions results

level	*As is*	*MPD*			*MPD stiff*		
	$V_{i,\text{frame}}$ [kN]	$V_{i,\text{frame}}$ [kN]	V_{i,str_ext} [kN]	$V_{i,total}$ [kN]	$V_{i,\text{frame}}$ [kN]	V_{i,str_ext} [kN]	$V_{i,total}$ [kN]
1	25498	13446	7687	18334	12283	7893	16511
2	22910	12016	7317	16277	10903	7459	13728
3	20925	11066	6778	14778	9939	6827	11478
4	19136	9929	5955	13001	9230	5897	9947
5	16472	8359	4831	10968	8046	4706	8522
6	12621	6368	3450	8224	6340	3307	6536
7	7145	3686	1809	4564	3793	1719	3776

Figure 7-11 (a) reports distribution of the shear actions along the height of the frame, normalized after dividing them by the value of the base shear in the *As is* configuration, while Figure 7-11 (b) reports the distribution of the shear action in the external structures; normalized with respect to base shear in the case of infinitely stiff external structure. It is also observable, that, in the case *MPD stiff* the shear action on the external structure is due only to the axial actions on the FVDs.

Figure 7-12 (a) and (b) provides a graphic insight on the shear actions distribution between external contrasting structure and frame, compared to the total one, for the retrofit configurations, that is *MPD* (a) and *MPD stiff* (b).

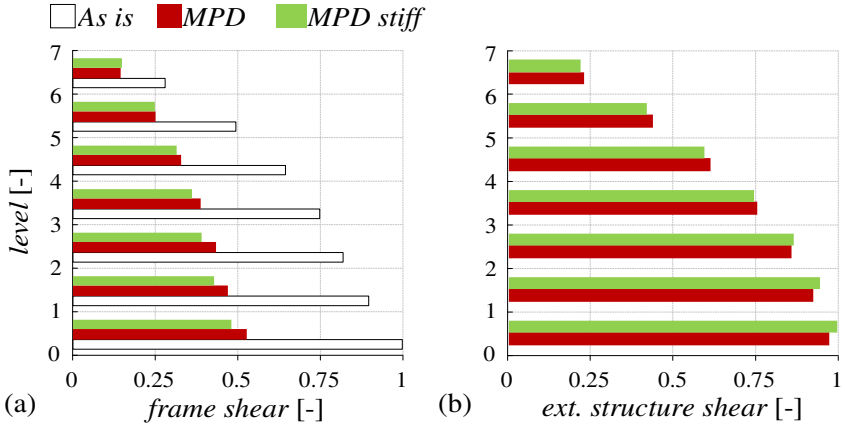

Figure 7-11 MPD systems: shear actions resisted by the frame (a) and by the external structures (b)

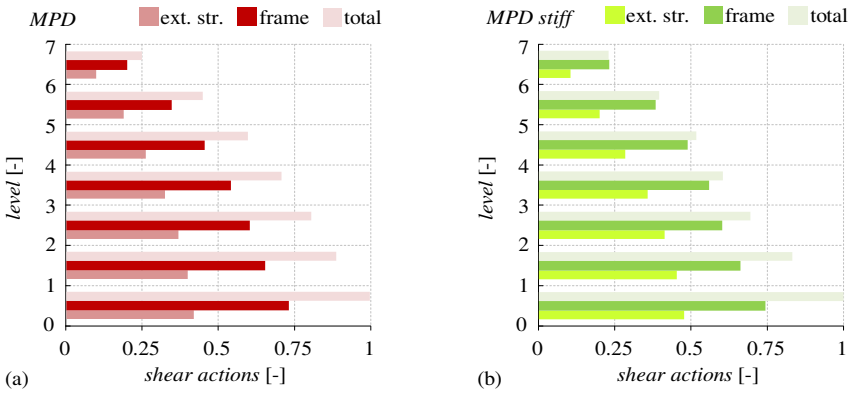

Figure 7-12 MPD systems: shear actions resisted by the external structure and the frame compared to the total one

Table 7-15 contains the velocities values observed at the various levels of the building for the configurations investigated. The relative reduction of the maximum velocity, with respect to the value registered at the 7th floor of the bare building, is nearly 48% for the *MPD stiff* case and 39% for the *MPD* one. Figure 7-13 shows the values of the floor velocities distribution normalized by the value observed at the last elevation for the *As is* case.

Table 7-15 MPD systems: floor velocities results

level	*As is*	*MPD*		*MPD stiff*
	$\dot{x}_i$ [m/s]	$\dot{x}_{i,frame}$ [m/s]	$\dot{x}_{i,str.ext.}$ [m/s]	$\dot{x}_i$ [m/s]
1	0.430	0.254	0.058	0.244
2	0.724	0.429	0.092	0.406
3	0.997	0.601	0.160	0.544
4	1.197	0.750	0.259	0.651
5	1.350	0.866	0.380	0.741
6	1.531	0.961	0.511	0.823
7	1.715	1.040	0.637	0.897

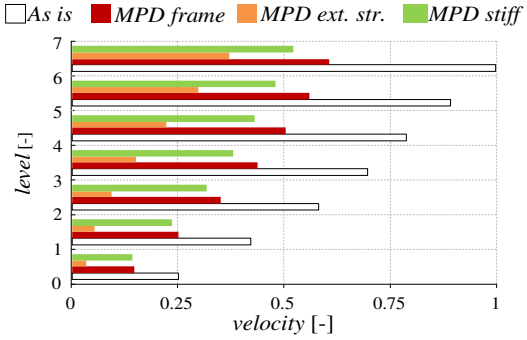

Figure 7-13 MPD systems: comparison of the velocities distribution along the height

Table 7-16 contains the absolute acceleration values observed at the various levels of the building for the configurations investigated. It is observable that also the coupling with MPD systems induces a reduction of the maximum absolute acceleration values with respect to bare frame. This result is of particular importance for the performance evaluation of acceleration-sensitive non structural components. Figure 7-14 shows the values of the floor absolute accelerations normalized by the value observed at the 7th floor in the *As is* case. The relative reduction of accelerations, measured at the last elevation, is nearly 35% *MPD* case, 46% for the *MPD stiff* one. Moreover, the values of the accelerations at floors from 5 to 7 are sensibly lower in the stiff retrofit case.

Table 7-16 MPD systems: absolute accelerations

level	*As is*	*MPD*		*MPD stiff*
	$\ddot{x}_i$	$\ddot{x}_{i,frame}$	$\ddot{x}_{i,str.ext.}$	$\ddot{x}_i$
	[m/s^2]	[m/s^2]	[m/s^2]	[m/s^2]
1	6.239	5.201	2.162	5.286
2	7.742	5.535	1.696	5.559
3	8.321	5.611	2.516	5.533
4	8.286	5.513	4.239	5.194
5	7.879	5.557	6.034	4.574
6	9.336	6.313	6.913	5.031
7	11.772	7.621	7.149	6.371

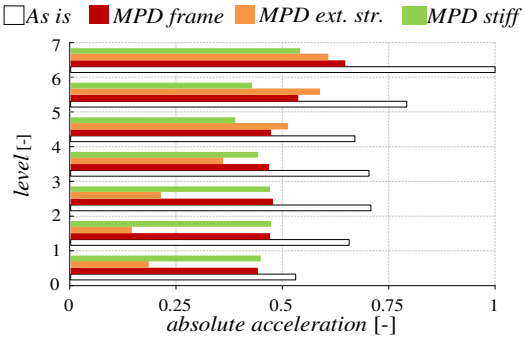

Figure 7-14 MPD systems: absolute acceleration distribution along the height

Table 7-17 highlights the displacements (y_i), velocities $(\dot{y}_i)$, axial forces (N) and base viscous bending moment (M_v), related to damper axial actions, for the two retrofit configurations considered. These quantities are strictly related to the added damping value, in fact, both the *MPD stiff* and the *MPD* configurations corresponding to $\xi_{add} = 0.30$, give very similar results. The axial actions reported are related to a single FVD, while the viscous bending moment is evaluated at the base and the value reported refers to one of the four external structures. It is also useful to remember that the viscous bending moment is a very important parameter used to design the external structures foundation, which, should be realized by means of drilled piles, able to support both the tension and compression forces induced by the axial actions of the FVDs distributed along the height. Figure 7-15

depicts the axial actions distribution along the height of the building for the two retrofit cases, the values are normalized to unity with respect to the value observed at the 7th floor in the stiff configuration.

Table 7-17 MPD systems: viscous dampers results

	level	1	2	3	4	5	6	7
MPD	y_i [m]	0.031	0.055	0.079	0.100	0.119	0.133	0.142
	$\dot{y}_i$ [m/s]	0.219	0.382	0.518	0.631	0.727	0.823	0.920
	N [kN]	68	93	126	154	177	200	221
	M_v [kNm]	26514	-	-	-	-	-	-
MPD stiff	y_i [m]	0.030	0.053	0.077	0.098	0.117	0.132	0.142
	$\dot{y}_i$ [m/s]	0.244	0.406	0.544	0.651	0.741	0.823	0.897
	N [kN]	76	99	133	159	181	200	215
	M_v [kNm]	27718	-	-	-	-	-	-

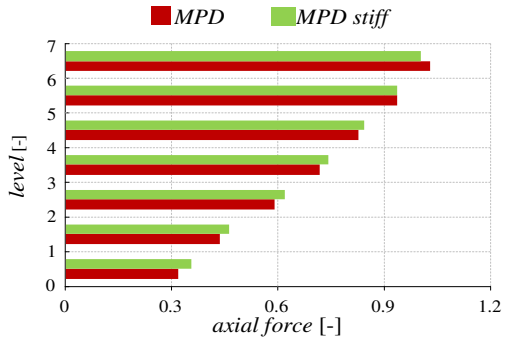

Figure 7-15 MPD systems: FVDs axial actions distribution along the height

7.2.3 *Systems comparison: MPD and dissipative rocking bracing*

This section reports and compares the seismic response of the external systems, that is a dissipative rocking bracing and a MPD system. Both the two systems are applied to the Van Nuys building case study, providing an added damping $\xi_{add} = 0.30$, and both of them are considered as infinitely stiff external passive systems.

Three configurations are analyzed and they are:

- the bare Van Nuys building (*As is*);
- the existing frame protected with an infinitely stiff MPD system (*MPD stiff*);
- the existing frame protected by means of an infinitely stiff dissipative rocking system (*tower stiff*).

Table 7-18 reports the floor displacements and the interstorey drifts for the three configurations analyzed. It is observed that the reduction of the frame displacements is nearly 54% in the *MPD stiff* case and nearly 53% in the *tower stiff* configuration. Figure 7-16 (a) reports the displacements distribution (x_i) along the height of the building, for i=1, 2, .., 7, normalized with respect to the value observed at the top of the bare frame; while Figure 7-16 (b) reports the distribution of the IDRs (θ_i). It is noteworthy that the coupling with an infinitely stiff tower leads to a linearization of the frame displacements and to a constant distribution of IDRs equal to 0.0072; the coupling with an infinitely stiff MPD system, instead, do not affect the shape of both displacements and IDRs distribution. Nevertheless the *MPD stiff* configuration yields a reduction of IDRs, even though they are close to 1% at intermediate elevations.

Table 7-18 External stiff systems comparison: floor displacements and drifts results

level	*As is*		*MPD stiff*		*tower stiff*	
	x_i [m]	θ_i [%]	x_i [m]	θ_i [%]	x_i [m]	θ_i [%]
1	0.063	1.52	0.030	0.72	0.030	0.72
2	0.113	1.90	0.053	0.89	0.049	0.72
3	0.165	2.07	0.077	0.97	0.068	0.72
4	0.213	1.98	0.098	0.94	0.087	0.72
5	0.253	1.72	0.117	0.83	0.106	0.72
6	0.285	1.35	0.132	0.66	0.125	0.72
7	0.306	0.91	0.142	0.46	0.144	0.72

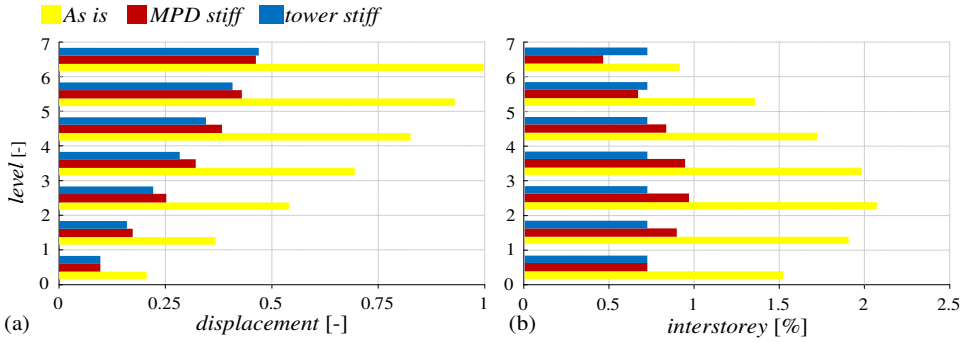

Figure 7-16 External stiff systems comparison: displacements (a) and interstorey drifts (b)

Table 7-19 reports the shear actions resisted by the frame and by the external structures, together with the total shear, for all the analyzed configurations. As already discussed for the displacements, the addition of the two external dissipative systems results in a reduction of the global shear demand on the frame, with respect to the bare frame, but it is observable

that the addition of infinitely stiff rocking bracings, that leads to a displacements linearization, results also in higher shear actions on the frame at some levels. Moreover, for both the retrofit configurations, the maximum shear for the dissipative structures and the frame may not occur at the same instant of time for all the records considered. The relative reduction of the maximum base shear acting on the frame, with respect to the bare building, is nearly 52% for the *MPD stiff* case and 49% for the *tower stiff* one.

Table 7-19 External stiff systems comparison: shear actions results

level	*As is*	*MPD stiff*			*tower stiff*		
	$V_{i,frame}$ [kN]	$V_{i,frame}$ [kN]	$V_{i,tower}$ [kN]	$V_{i,total}$ [kN]	$V_{i,frame}$ [kN]	$V_{i,tower}$ [kN]	$V_{i,total}$ [kN]
1	25498	12283	7893	16511	13126	11008	15511
2	22910	10903	7459	13728	7197	8846	13350
3	20925	9939	6827	11478	6575	7505	11965
4	19136	9230	5897	9947	6425	6261	10586
5	16472	8046	4706	8522	6514	4703	8828
6	12621	6340	3307	6536	6018	3513	6481
7	7145	3793	1719	3776	8234	5869	3486

Figure 7-17 (a) reports distribution of the shear actions along the height of the frame, normalized after dividing them by the value of the base shear in the *As is* configuration, while Figure 7-17 (b) reports the distribution of the shear action in the external structures along their heights; the values are normalized with respect to the base shear in the case of infinitely stiff tower. It is noteworthy that in the case of *MPD stiff* the shear action on the external contrasting structures is due only to the axial actions on the FVDs, while in the case of coupling with infinitely stiff tower there are also the exchange forces produced by the mutual interaction between the bracings and the existing frame.

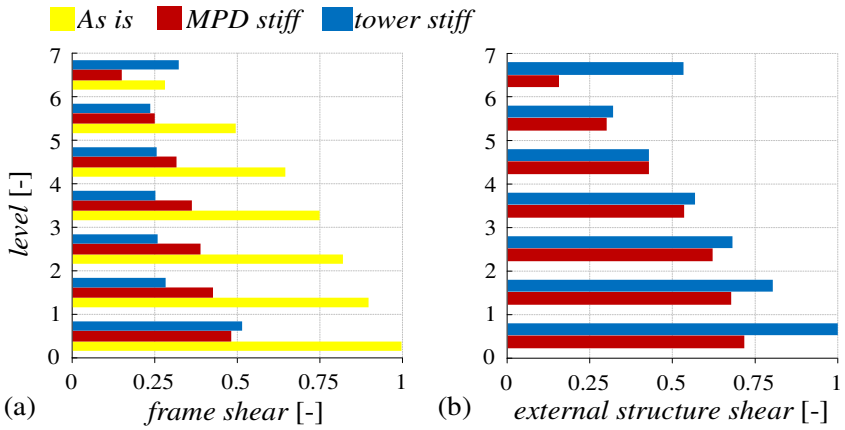

Figure 7-17 External stiff systems comparison: shear actions resisted by the frame (a) and by the external dissipative structures (b)

Figure 7-18 (a) and (b) provide a graphic insight on the shear actions distribution between external dissipative systems and existing frame, compared to the total one. In both cases the shear actions are normalized with respect to the total base shear.

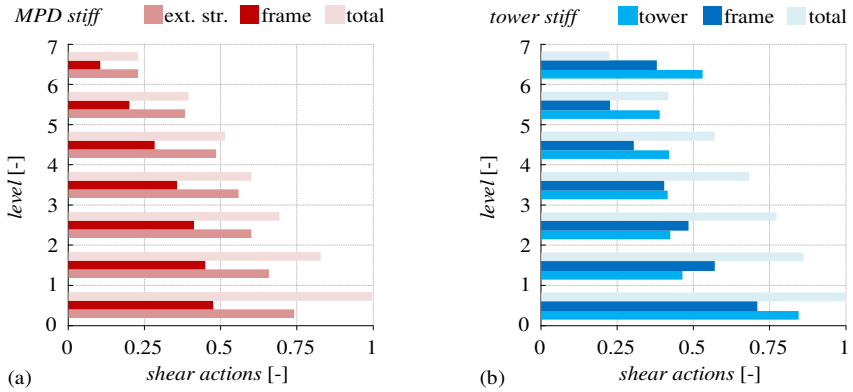

Figure 7-18 External stiff systems comparison: shear actions resisted by the external structure and the frame compared to the total one in the two retrofit analyzed cases

Table 7-20 contains the velocities values observed at the various levels of the building for the configurations investigated. The relative reduction of the maximum velocity, with respect to the value registered at the 7th floor of the bare building, is nearly 48% for the *MPD stiff* case and 46% for the *tower stiff* one. Figure 7-19 shows the values of the floor velocities distribution normalized by the value observed at the last elevation for the *As is* case.

Table 7-20 External stiff systems comparison: floor velocities results

level	*As is*	*MPD stiff*	*tower stiff*
	$\dot{x}_i$ [m/s]	$\dot{x}_i$ [m/s]	$\dot{x}_i$ [m/s]
1	0.430	0.244	0.191
2	0.724	0.406	0.314
3	0.997	0.544	0.437
4	1.197	0.651	0.560
5	1.350	0.741	0.683
6	1.531	0.823	0.806
7	1.715	0.897	0.927

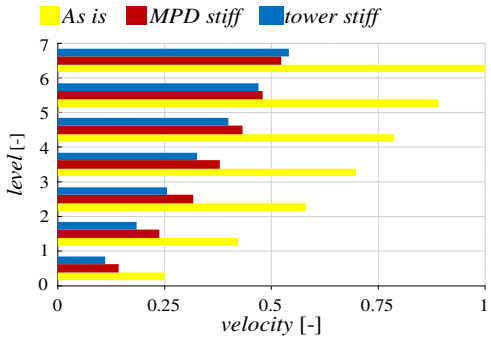

Figure 7-19 External stiff systems comparison: velocities distribution along the height

Table 7-21 contains the absolute acceleration values observed at the various levels of the building for the configurations investigated. It is observable that both the two retrofit configurations induces a reduction of the maximum absolute acceleration values with respect to bare frame. A better result is achieved with the addition of infinitely stiff rocking bracings, which leads to a reduction of nearly 39%, while the infinitely stiff MPD case provides a reduction of nearly 35%. This result is of particular importance for the performance evaluation of acceleration-sensitive non structural components. Figure 7-20 shows the values of the floor absolute accelerations normalized by the value observed at the 7th floor in the *As is* case.

Table 7-21 External systems comparison: absolute accelerations

level	*As is*	*MPD stiff*	*tower stiff*
	$\ddot{x}_i$ [m/s^2]	$\ddot{x}_i$ [m/s^2]	$\ddot{x}_i$ [m/s^2]
1	6.239	5.286	4.487
2	7.742	5.559	3.959
3	8.321	5.533	3.640
4	8.286	5.194	3.642
5	7.879	4.574	4.047
6	9.336	5.031	4.950
7	11.772	6.371	5.986

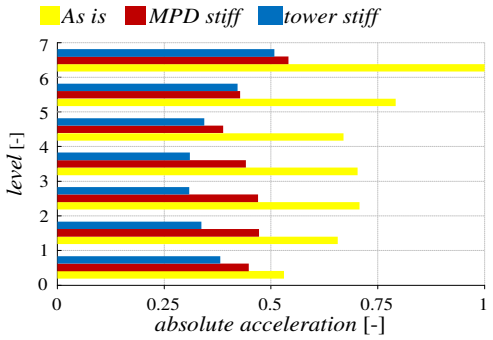

Figure 7-20 External stiff systems comparison: absolute acceleration distribution along the height

Table 7-22 highlights the displacements (y_i), velocities $(\dot{y}_i)$, axial forces (N) and base viscous bending moment, related to damper axial actions (M_v), for the two retrofit configurations considered. The axial actions reported are related to a single FVD, while the viscous bending moment is evaluated at the base and the value reported refers, in both cases, only to one of the four external dissipative structures. Both the retrofit configurations provide a damping contribution of $\xi_{add} = 0.30$, therefore they give very similar results in terms of viscous bending moment, parameter used to design the external dissipative structures foundation. It can be observed that the retrofit configurations analyzed provide, in general, very similar results. The coupling with infinitely stiff tower leads to a

displacements linearization and IDRs distribution regularization, with the drawback of high exchange actions and higher shear actions at some levels of the frame. On the other hand the coupling with an infinitely stiff MPD system do not modify the IDRs distribution, but to be effective need a very high number of FVDs with respect of the other system. In both the two cases the foundations are designed with almost the same value of viscous bending moment.

Table 7-22 External systems comparison: viscous dampers results

	level	1	2	3	4	5	6	7
MPD stiff	y_i [m]	0.030	0.053	0.077	0.098	0.117	0.132	0.142
	$\dot{y}_i$ [m/s]	0.244	0.406	0.544	0.651	0.741	0.823	0.897
	N [kN]	76	99	133	156	181	200	215
	M_v [kNm]	27718	-	-	-	-	-	-
tower stiff	y_i [m]	0.0158	-	-	-	-	-	-
	$\dot{y}_i$ [m/s]	0.102	-	-	-	-	-	-
	N [kN]	3197	-	-	-	-	-	-
	M_v [kNm]	28131	-	-	-	-	-	-

Table 7-23 reports, for the external dissipative rocking bracings, the overall exchange actions related to each floor ($F_{e,i}$). These forces are used for the design of the bracings-frame connections and are representative of their mutual interaction. In the case of MPD system these interaction correspond to the FVDs axial actions.

Table 7-23 Existing frame-external rocking bracings exchange actions

level	*Tower stiff*
	$F_{e,i}$ [kN]
1	7042
2	2239
3	2115
4	2248
5	2017
6	5041
7	5869

7.3 Soil Structure Interaction (SSI)

Among the open problems of this work there is also the one related to the soil-structure interaction (SSI) that may affect sensibly, if not taken into account, the system response in terms of both global stiffness and damping, with consequences on the external dissipative system efficiency.

The topic of soil-structure interaction can be analyzed through two different approaches, the first one is known as a "direct approach", in which the frame and the soil (near field) are modelled simultaneously, together with surrounding constraints able to guarantee the radiation conditions. This approach, which usually requires high computational efforts, allows capturing the soil and structural responses simultaneously and must be used if both systems (soil and structure) behave nonlinearly. A sketch of the direct approach is reported in Figure 7-21, where surrounding constraints consisting of spring-viscous dashpot systems are used to account for the far-field compliance and damping.

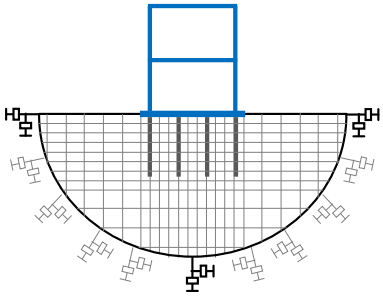

Figure 7-21 SSI direct approach scheme

The second approach is known as "substructures approach" and it is a technique by which a SSI problem is solved by decomposing the whole superstructure-foundation-soil system into two subsystems (the soil-foundation system and the structural system). The response of the soil-foundation system subjected to the seismic excitation is firstly determined, obtaining the system compliance and the foundation input motion; then the structural response on compliant restraints subjected to the foundation motion is evaluated. The approach allows adopting specific analysis methodologies and tools to study the soil-foundation system (kinematic interaction analysis and impedances determination) and the superstructure system (inertial interaction analysis). The substructure approach is based on the superposition principle (Kausel et al. 1978), valid for linear systems but can be also adopted to include structural nonlinearities.

The global response is fully determined through the following three steps:

1 Solution of the kinematic interaction problem. This step allows capturing the soil-foundation interactions and leads to the evaluation of the foundation input motion (FIM), namely the motion experienced by the foundation subjected to the seismic wave field. Due to the soil-foundation system linearity the problem is solved in the frequency domain in order to easily account for the frequency-dependent behaviour of the system.

2 Evaluation of the soil-foundation system dynamic stiffness. This step leads to the evaluation of the frequency-dependent dynamic impedance matrix of the soil-foundation system, detached from the superstructure. The real part of the impedance matrix, reflects the compliance of the soil-foundation system and it may be represented by a spring with a frequency-dependent coefficient, while the imaginary part captures the energy dissipation occurring in the soil as the foundation vibrates (mainly due to the radiation damping).

3 Calculation of the dynamic response of the structural system subjected to the FIM. Inertial interaction is taken into account in this step. In order to evaluate inertial effects in the soil-foundation system, the inertial contribution to the foundation motion, which may be determined at this step by subtracting the FIM to the inertial foundation displacement, needs to be evaluated and applied to the soil-foundation system at the foundation level. The global soil-foundation response is finally determined superimposing the latter results to those determined in step 1.

The inertial interaction analysis can be performed either through time- and frequency-domain analyses. Frequency-domain analyses are carried out by implementing the frequency-dependent dynamic impedance matrix previously computed in the finite element model (FEM) of the superstructure, at the foundation level. This generally presents difficulties since commercial structural analysis programs does not include library elements able to introduce fully coupled frequency-dependent matrices. In time-domain analyses, otherwise, it is possible to account for the linear or non-linear behaviour of the superstructure. However, the frequency dependent impedance matrix of the soil-foundation system cannot be used directly and an implementation strategy must be adopted. Generally, dynamic Lumped Parameter Models (LPMs) having frequency independent parameters are used; parameters are calibrated so that the dynamic impedance of the LPM approximates the soil-foundation one in the frequency range of interest. Figure 7-22 reports a scheme of the "sub-structures approach".

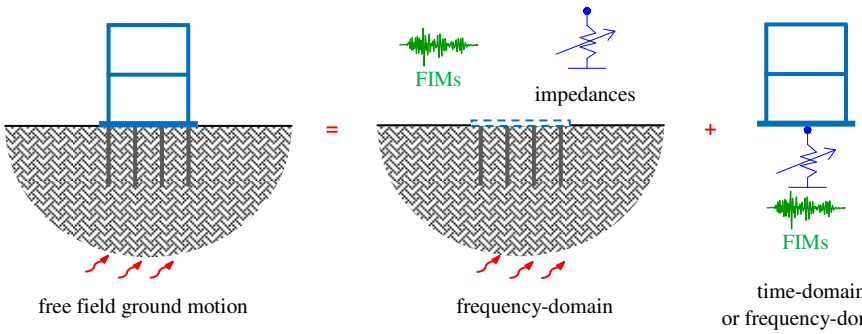

Figure 7-22 SSI substructures approach

For the Van Nuys building case study, in the retrofit configuration, the foundation input motion and the dynamic impedance matrix are evaluated in frequency-domain (kinematic interaction), while the inertial interaction is evaluated in time-domain, by implementing a

lumped parameter model in the FEM model already available in order to account for the soil-foundation compliance. Both the superstructure and piles are assumed to behave linearly, while for the soil a linear equivalent behaviour is assumed. The seismic action is described in section 3.1.3 (twenty time histories having a probability of exceedance of 10% in 50 years) and the relevant foundation input motions (seismic input affected by the foundation filtering effects) are determined by means of kinematic interaction analyses of the soil-foundation systems, starting from the free-field soil displacements, determined through a deconvolution analysis. The soil-foundation system does not include tie beams, which are, instead, incorporated in the superstructure model.

7.3.1 *Lumped parameter model for time-domain analysis*

The analysis of the soil-foundation system allows evaluating the soil-foundation dynamic impedances, namely the complex-valued forces-displacements relationships which define the compliant restraints of the superstructure in the subsequent inertial interaction analysis. Different models have been developed over the years to this purpose, however, since foundation impedances are frequency-dependent functions, all procedures furnish results that may be adopted directly only if the inertial interaction analysis of the superstructure is performed in the frequency-domain. If time-domain inertial interaction analyses are performed, as in this case, suitable Lumped Parameter Models (LPMs) have to be introduced to reproduce the foundation dynamic behaviour. LPMs are constituted by frequency-independent springs, dashpots and masses, suitably assembled and calibrated in order to reproduce the dynamic behaviour of the soil-foundation system. The numerical model of Dezi et al. (2009), in which piles are modelled with beam elements and the soil is schematized with independent horizontal infinite layers, is used for the definition of the foundation impedances, while the LPM parameters are determined in accordance to the model proposed by Carbonari et al. (2012).

A LPM model was determined for each kind of pile, composing the foundation system. Every LPM is characterized by 24 parameters, in the case of spatial analysis, which are translational (m_x, m_y and m_z) and rotational masses (I_x, I_y and I_z), lumped at the external node of the LPM, elastic (k_x, k_y, k_{rx}, k_{ry}, k_z and k_{rz}) and viscous (c_x, c_y, c_{rx}, c_{ry}, c_z and c_{rz}) constants that define the relevant spring-dashpot elements and two additional eccentric masses (m_{xh}, m_{yh}) connected to the external node by a stiff link (of length h_x, h_y) and to the ground by spring-dashpot elements (c_{xh}, c_{yh}). Figure 7-23 depicts a sketch of a deep foundation layout and the related LPM scheme.

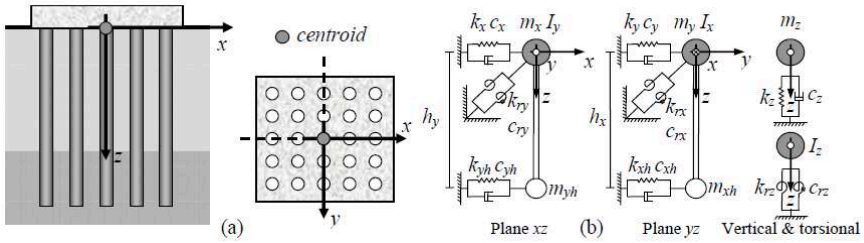

Figure 7-23 Deep foundations layout (a) and related LPMs scheme (b) as proposed by Carbonari et al. (2012)

7.3.2 *Soil and foundations characteristics*

Since the Van Nuys building was investigated through many studies, both the building foundation system and the site conditions are almost known.

The existing foundation system consists of drilled piles of diameter 61 cm and depth of about 12 m. Piles are collected in groups of two, three or four piles and connected by concrete caps about 97 cm high. Single piles are used for the stairwells. Groups of three piles are used for the perimeter columns, while groups of four pile are used for inner columns; in both cases columns are located in the centre of the caps. All pile caps are connected by a grid of tie beams. Each pile has a design capacity greater than 450 kN vertical load and up to 90 kN lateral load. The foundations of the retrofitting system refers to the $\kappa = 1 - \xi_{add} = 0.30$ case, in which the building is equipped with four external bracings and stress resultants used for the design of piles are derived from the fixed-base model. Each rocking bracing is founded on nine drilled piles of diameter 100 cm, depth 22 m and spacing of three diameters. The foundation cap has a square plan of 8m x 8m, with an height of 1.2 m. A planar view and a transverse section of the foundations of the coupled system are reported in Figure 7-24 and in Figure 7-25, respectively.

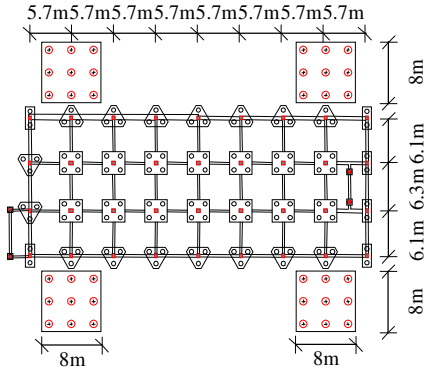

Figure 7-24 Foundations system planar view

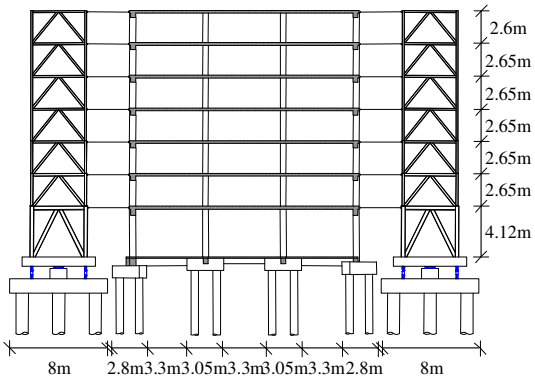

Figure 7-25 Transverse section of the overall structural system

The soil conditions are known through five boring logs (Blume and Associates 1973, Krawinkler 2005), whose results lead to the features reported in Table 7-24. The geological surveys were executed between 1965, the first one, and 1994, after Northridge earthquakes. The shear wave velocity in the area is comprises in the range 200 m/s – 300 m/s (Tinsley and Fumal 1985, Trifunac et al. 2001, Krawinkler 2005) and for the analysis is assumed equal to 250 m/s and constant for the first 30 m.

Table 7-24 Soil site features

depth [m]	description	unit weight [kN/mc]	N_{SPT}	Dr [%]	ϕ [°]	V_s [m/s]
0-2.4	Fill	18.7	45	-	-	-
2.4-5.5	Silty sand	18.3	35	95	41	250
5.5-8.5	Silty sand	18.3	31	90	40	250
8.5-10.1	Silty sand	19.1	19	63	37	250
10.1-13.7	Sandy silt	19.5	11	47	32	250
>13.7	Gravelly sand	20.3	49	82	43	250

7.3.3 *Preliminary results*

This section reports some preliminary results related to the SSI of the Van Nuys building case study, obtained by considering a single time-history planar analysis (acc. 2). Results from the compliant base model subjected to the foundation input motion are compared to those descending from a fixed base model. The monitored parameters are expressed in terms of floor displacements, absolute accelerations and shear actions resisted by the frame. It is observed that, for the analyzed case, the SSI does not sensibly affect the response of the system. The effects of the rocking of the foundation on a system whose efficiency is based on a rocking motion still require an investigation, therefore future developments can be addressed towards this target.

Table 7-25 reports the maximum floor displacements (x_i) and IDR (θ_i) distributions along the height of the Van Nuys building. SSI produces an increment of nearly 10% of the maximum floor displacements measured on a fixed base model. Figure 7-26 reports and compares 15 seconds of the time history of the 7th floor displacement, with and without taking into account the SSI.

Table 7-25 Floor displacements and IDR comparison

level	fixed base		SSI	
	x_i [m]	θ_i [%]	x_i [m]	θ_i [%]
1	0.026	0.63	0.029	0.70
2	0.044	0.69	0.047	0.73
3	0.063	0.70	0.067	0.76
4	0.080	0.72	0.087	0.81
5	0.097	0.72	0.107	0.82
6	0.114	0.71	0.126	0.77
7	0.129	0.64	0.144	0.69

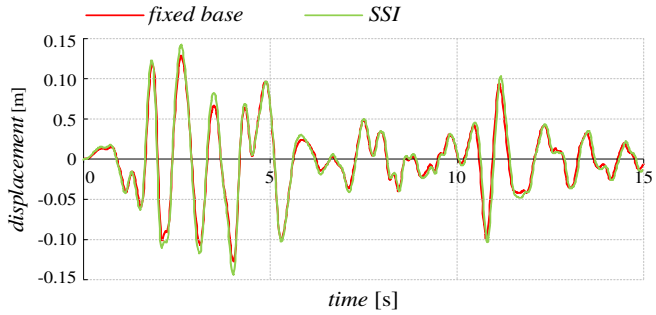

Figure 7-26 Comparison of the 7th floor displacements on a fixed base and on compliant base

Table 7-26 reports the maximum floor absolute accelerations $\left(\ddot{x}_i\right)$ distributions along the height of the Van Nuys building. SSI produces an increment of nearly 12% of the maximum fixed base model accelerations at the first two elevations; at higher floors the percentage is notably reduced. Figure 7-27 reports and compares 15 seconds of the time history of the 7th floor absolute accelerations, with and without taking into account the SSI.

Table 7-26 Floor absolute acceleration comparison

level	fixed base $\ddot{x}_i$ [m/s^2]	SSI $\ddot{x}_i$ [m/s^2]
1	6.02	6.88
2	7.13	8.13
3	7.11	7.85
4	6.28	6.69
5	5.43	5.37
6	7.15	7.37
7	11.5	12.0

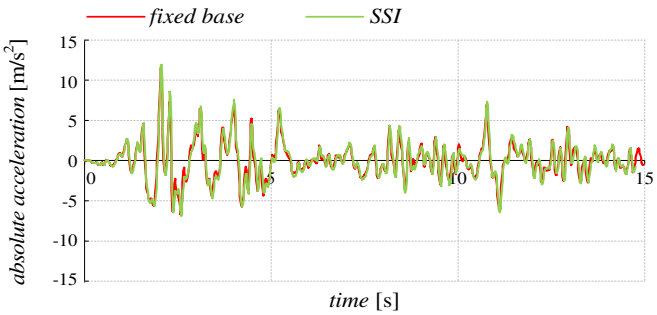

Figure 7-27 Comparison of the 7th floor absolute accelerations on a fixed base and on compliant base

Finally Table 7-27 reports the maximum shear forces acting on the frame $\left(V_{frame,i}\right)$; it can be observed that the base shear is almost equal, while at the second elevation the shear

increases of about 9% for the superstructure on compliant base. Figure 7-28 shows and compares 15 seconds of the time history of the base shear, resisted by the frame, with and without taking into account the SSI.

Table 7-27 Comparison of the shear resisted by frame

level	fixed base	SSI
	$V_{frame,i}$ [kN]	$V_{frame,i}$ [kN]
1	11372	11237
2	9286	10188
3	7203	6972
4	6511	6601
5	5962	6236
6	4459	4671
7	3566	3428

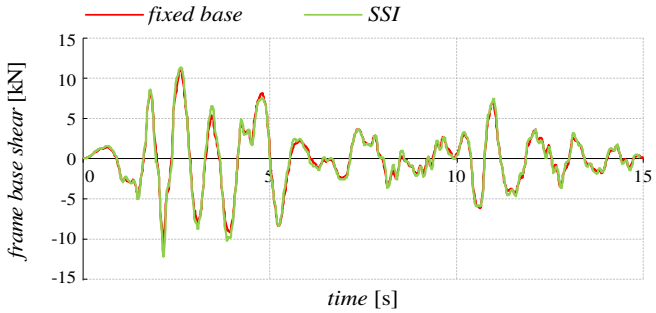

Figure 7-28 Comparison of the base shear resisted by the frame on a fixed base and on compliant base

Conclusion

This work investigates the seismic performance of existing building frames equipped with external dissipative rocking bracing, consisting of a steel truss, hinged at the foundation level, whose rocking motion promotes the dissipation of energy via viscous dampers located at the base.

The system which results from the coupling of frame and external dissipative rocking bracing, is non-classically damped, being the energy dissipation concentrated at the base of the truss. Under the assumption of linear elastic behaviour of both the frame and the damping structure, the equation of motion of the system is presented by splitting the vector of displacements into two contributions. One is related to the so called active degrees of freedom, related to inertial actions, while the other to the dependent degrees of freedom, involved in the deformation and damping of the bracing. The time-domain and frequency-domain formulations are presented, together with a generalized S-DOF approximation of the overall system, for the investigation of the limit case of infinitely stiff external bracing structure.

Time-domain analysis are based on a state space approach which permits the complex modal analysis of the overall system, allowing the evaluation of the influence of the added bracing stiffness, in terms of regularization of interstorey-drifts, and damping on both the dynamic behaviour and the seismic response. In particular, the proposed formulation permits to evaluate separately the contribution of each of the complex vibration modes of the system to the global seismic response. This approach is employed to study the performances of two case studies with different retrofit configurations, involving the external dissipative rocking system, with various bracing-to-frame stiffness ratios and damping properties. Based on the study results the following conclusions can be drawn:

- The addition of the external dissipative rocking system leads to a regularization of the drift demand along the building height. A global stiffness parameter is proposed for the evaluation of the effectiveness of the drift control.
- Nevertheless the investigated retrofit configuration may lead to significant changes in the shear force distribution of the existing frame, as a consequence of the regularization of the interstorey drift demands, and this may reduce the benefits of the retrofit. Furthermore, it is necessary to pay attention to exchange actions resulting

from the mutual action between the bracing and the existing frame during the seismic actions and which control the design of the connections.

- The addition of external dissipative rocking bracing provides also a reduction of floor absolute accelerations, but in a less considerable way, compared to displacements.
- The simplified formula commonly suggested by design codes to estimate the system damping ratio provides a good approximation of the first modal damping ratio ($\xi 1$) in all the retrofit cases considered.
- Higher order modes of vibration influence significantly the internal actions demand in the frame and the bracing, while they do not affect considerably the displacement response.
- The case corresponding to infinitely stiff bracings and added damping ratio in the range 20-30% provides an optimal distribution of absolute accelerations and inter-storey drifts. However the retrofit configurations involving bracings with stiffness similar to that of the frame and equal added damping ratios, provide results quite similar to those observed for the infinitely stiff case. Other retrofit configurations, employing a reduced bracing-to-stiffness ratio and dampers with reduced damping capacity, allow to achieve good performance enhancements while limiting the cost of the retrofit. Moreover the number of external dissipative structure is a question of feasibility related to dampers axial actions, which notably influence the foundation system dimension, usually realized through drilled piles.
- An alternative arrangement in which the bracings are connected only at the last elevation seems to provide good results in terms of global displacements reduction. Besides this solution produces smaller interferences in the shear force distribution of the existing frame, because the shape of the interstorey drift demands do not change significantly.

Frequency-domain analysis is particularly useful for the problem at hand because it allows to work with an algebraic system and it permits to obtain a reduced formulation of the problem, by exploiting the condensation technique, which is not possible in the time domain. Moreover by representing the seismic input in terms of a stationary stochastic process, a relation can be established between the Power Spectral Density (PSD) of the input and the response parameters of interest, via harmonic analysis of the system. This way, extensive parametric studies for different properties of the system and of the seismic input, are permitted by monitoring only the response variance function, σ^2, strictly related to the magnitude of the investigated EDPs. That is, a versatile and quick tool for the investigation of the system.

Further investigations are required for a complete analysis of the system potentialities. An overview of the main open problems are presented in the last part of the thesis. They concern: the response of non-linear viscous dampers, the comparison with alternative external systems, the soil-structure interaction.

References

Ajrab JJ, Peckan G, Asce M, Mander JB. Rocking wall-frame structures with supplemental tendon system. *Journal of Structural Engineering* 2004; **130**(6): 895-203. DOI: 10.1061/(ASCE)0733-9445(2004)130:6(895).

Alavi B, Krawinkler H. Strengthening of moment-resisting frame structures against near-fault ground motion effects. *Earthquake Engineering and Structural Dynamics* 2004; **33**: 707-722. DOI: 10.1002/eqe.370.

Arima F, Miyazaki M, Tanaka H, Yamazaki Y. A study on buildings with large damping using viscous damping walls. *Proceedings of Ninth World Conference on Earthquake Engineering.* Tokyo-Kyoto, Japan, 2-9 August 1988.

ASCE Standard ASCE/SEI 41-13: Seismic Evaluation and Retrofit of Existing Buildings. American Society of Civil Engineers, 2014.

Balducci A, Dissipative Towers. Application n. EP2010074723820100831, WO2010EP62748 20100831, International and European classification E04H9/02 – Italian concession n 0001395591, 2005.

Barbato M. "Lecture notes on CE 7700-Random Vibrations Spring 2010. Instructor: Michele Barbato" Louisiana State University.

Bazzurro P, Park J, Tothong P, Luco N. Multidirectional seismic excitations effects in building response excitation: collaborative research with USGS (Dr. Luco) and AIR. USGS Report.

Beck JL, Porter KA, Shaikhudtinov RV, Au SK, Mizukoshi K, Miyamura M, Ishida H, Moroi T, Tsukada Y, Masuda M. *Impact of seismic risk on lifetime property values*. EERL Report 2002-04, California Institute of Technology, Earthquake Engineering Research Laboratory, Pasadena, California December 2002.

Bhaskararao AV, Jangid Rs. Optimum viscous damper for connecting adjacent SDOF structures for harmonic and stationary white-noise random excitations. *Earthquake Engineering and Structural Dynamics* 2007; **36**: 563-571.

Blume J A & Associates. *Holiday Inn (Chapter 29), San Fernando Earthquake of February 9, 1971*. Vol. I, Part A. U.S. Department of Commerce, National Oceanic and Atmospheric Administration: Washington, DC, 1973.

Christopoulos C, Filiatrault A, Folz B. Seismic response of self-centering hysteretic SDOF systems. *Earthquake Engineering and Structural Dynamics* 2002; **31**(5), 1131-1120. DOI: 10.1002/eqe.152

Christopoulos C, Filiatrault A. *Principles of Passive Supplemental Damping and Seismic Isolation*. IUSS Press: Pavia, Italy, 2006.

Christopoulos C, Tremblay R, Kim HJ, Lacerte M. Self-Centering Energy Dissipative Bracing System for the Seismic Resistance of Structures: Development and Validation. *Journal of Structural Engineering* 2008; **134**: 96-107.

Christopoulos C. Self-Centering Post-Tensioned Energy Dissipating (PTED) Steel Frames for Seismic Regions. PhD Thesis, Department of Structural Engineering, University of California, San Diego, CA, 2002.

Chu Y-L, Song J, Lee G C. *Modal Analysis of Arbitrarily Damped Three-Dimensional Linear Structures Subjected to Seismic Excitations.* Technical Report MCEER-09-0001, University at Buffalo, State University of New York, January 2009.

Clough RW, Penzien J. *Dynamics of structures*. Computers and Structures Inc.: USA, 2003.

Craig RR Jr, Kurdila AJ. *Fundamentals of Structural Dynamics*. John Wiley and Sons Inc., New Jersey 2006.

Dall'Asta A, Tubaldi E, Ragni L. Influence of the nonlinear behaviour of viscous dampers on the seismic demand hazard of building frames. *Earthquake Engineering and Structural Dynamics* 2016. **45**(1): 149-169.

Der Kiuregwan A, Neuenhofer A. Response spectrum method for multi-support seismic excitations. *Earthquake Engineering and Structural Dynamics* 1992; **21**: 713-740.

Dezi F, Carbonari S, Leoni G. Empirical formulas to define LPMS for time-domain analysis of structures on pile foundations. *Proceedings of the International Conference on Earthquake Geotechnical Engineering in honour of Prof. Kenji Ishihara*. Istanbul, Turkey, 17-19 June 2013.

Di Cesare A, Ponzo FC, Nigro D, Dolce M, Moroni C. Experimental and numerical behaviour of hysteretic and visco-recentring energy dissipating bracing systems. *Bulletin of Earthquake Engineering* 2012; **10**(5): 1585-1607.

Di Cesare A, Ponzo FC, Nigro D. Assessment of the performance of hysteretic energy dissipation bracing systems. *Bulletin of Earthquake Engineering* 2014; **12**(6): 2777-2796.

Doulatabadi P R. Three-dimensional nonlinear dynamic seismic behaviour of a seven storey reinforced concrete building. University of British Columbia, Canada, 1997.

EN 1993 Eurocode 3 – Design of steel structures.

Freddi F, Tubaldi E, Ragni L, Dall'Asta A. Probabilistic performance assessment of low-ductility reinforced concrete frames retrofitted with dissipative braces. *Earthquake Engineering and Structural Dynamics* 2012; **42**(7): 993-1011.

Fumal TE, Tinsley JC. Mapping shear-wave velocities of near-surface geologic materials. *Evaluating Earthquake Hazards in the Los Angeles Region – An Earth-Science Perspective*. US Geological Survey Professional Paper 1360. United States Government Printing Office, Washington 1985.

Gattulli V, Potenza F, Lepidi M. Damping performance of two simple oscillators coupled by a dissipative connection. *Journal of Sound and Vibration* 2013; **332**(26): 6934-6948.

Hwang JS, Lin WC, Wu NJ. Comparison of distribution methods for viscous damping coefficients to buildings. *Structure and Infrastructure Engineering: Maintenance, Management, Life-Cycle Design and Performance* 2013; **9**(1): 28-41.

Islam M S. Analysis of the Northridge earthquake response of a damaged non-ductile concrete frame building. *The Structural Design of Tall Buildings* 1996; **5**: 151-182.

Kausel E, Whitman RV, Morray JP, and Elsabee F. The spring method for embedded foundations. *Nuclear Engineering and Design* 1978; **48**: 377–392.

Krawinkler H. *Van Nuys Hotel building testbed report: exercising seismic performance assessment*. PEER Report 2005/11, Department of Civil and Environmental Engineering, Stanford University, October 2005.

Lavan O, Abecassis D. Seismic behavior and design of wall-EDD-frame systems. *Frontiers in Built Environment* 2015. DOI: 10.3389/fbuil.2015.00007

Lavan O, Avishur M. Seismic behaviour of viscously damped yielding frames under structural and damping uncertainties. *Bulletin of Earthquake Engineering* 2013; **11**(6): 2309-2332.

Lavan O. On the efficiency of viscous dampers in reducing various seismic responses of wall structures. *Earthquake Engineering and Structural Dynamics* 2012; **41**: 1673-1692. DOI: 10.1002/eqe.1197.

Lin W-H, Chopra AK. Earthquake response of elastic SDF system with non-linear fluid viscous dampers. *Earthquake Engineering and Structural Dynamics* 2002; **31**: 1623-1642. DOI: 10.1002/eqe.179

Lutes LD, Sarkani S. *Random vibrations: Analysis of Structural and Mechanical Systems*. Elsevier Butterworth-Heinemann, Burlington, Mass., 2004. ISBN: 0-07506-7765-1.

Marriott D, Pampanin S, Bull D, Palermo A. Dynamic testing of precast, post-tensioned rocking wall systems with alternative dissipating solutions. *Bulletin of the New Zeland Society for Earthquake Engineering* 2008; **41**(2): 90-103.

MATLAB, The MathWorks Inc., 1994.

Nims DK, Richter PJ, Bachman RE. The use of energy Dissipating Restraint for Seismic Hazard Mitigation. *Earthquake Spectra* 1993; **9**(3): 467-489.

Nuove Norme Tecniche per le Costruzioni, D.M. Infrastrutture 14 gennaio 2008, Circolare 02 febbraio 2009 n. 617/C.S.LL.PP. 2009 (in Italian).

Occhiuzzi A. Additional viscous dampers for civil structures: Analysis of design methods based on effective evaluation of modal damping ratios. *Engineering Structures* 2009; **31**(5): 1093-1101. DOI: 10.1016/j.engstruct.2009.01.006

Passoni C, Belleri A, Marini A, Riva P. Existing structures connected with dampers: state of the art and future developments. *2nd European Conference on Earthquake Engineering and Seismology*. Istanbul, Turkey, 25-29 August 2014.

Peng BF, Conte JP. Closed-form solution for the response of linear systems to fully nonstationary earthquake excitation. *Journal of Engineering Mechanics* 1998; **124**(6): 684-694.

Ponzo FC, Di Cesare A, Nigro D, Vulcano A, Mazza F, Dolce M, Moroni C. Jet-Pacs Project: dynamic experimental tests and numerical results obtained for a steel frame equipped with hysteretic damped chevron braces. *Journal of Earthquake Engineering* 2012; **16**(5): 662-685.

Porter K A, Beck J L, Shaikhutdinov R V. *Investigation of sensitivity of building loss estimates to major uncertain variables for the Van Nuys testbed*. PEER Report 2002/03, College of Engineering, University of California, Berkeley August 2002.

Ragni L, Dezi L, Dall'Asta A, Leoni G. HDR devices for the seismic protection of frame structures: Experimental results and numerical simulation. *Earthquake Engineering and Structural Dynamics* 2009; **38**(10): 1199-1217. DOI:10.1002/eqe891

Roh H, Cimellaro GP, Lopez-Garcia D. Seismic response of adjacent steel structures connected by passive device. *Advances in Structural Engineering* 2011; **14**(3): 499-517.

Roia D, Gara F, Balducci A, Dezi L. Ambient vibration tests on a reinforced concrete school building before and after retrofitting works with external steel" dissipative towers". *Proceedings of the 9th International Conference on Structural Dynamics, EURODYN 2014*. Porto, Portugal, 30 June - 2 July 2014.

Roia D, Gara F, Balducci A, Dezi L. Dynamic tests on an existing r.c. school building retrofitted with "dissipative towers". *11th International Conference on Vibration Problems*, Lisbon, Portugal, 9-12 September 2013.

SAP2000, Structural Analysis Program, Computers and Structures, Inc., 1995 University Ave., Berkeley, CA.

SEAOC, Vision 2000: Performance Based Seismic Engineering of Buildings. Structural Engineers Association of California, San Francisco, April 1995.

Somerville P, Smith N, Punyamurthula S, Sun J. *Development of Ground Motion Time Histories for Phase II of the FEMA/SAC Steel Project*. SAC Background Document Report, Report No. SAC/BD-97/04, 1997.

Soong TT, Constantinou MC. *Passive and active structural vibration control in civil engineering*. State University of New York, Buffalo, 1994.

Soong TT, Dargush GF. *Passive Energy Dissipation Systems in Structural Engineering*. Wiley: New York, 1997.

Soong TT, Spencer BF. Supplemental energy dissipation: state-of-the art and state-of-the practice. *Engineering Structure* 2002; **24**: 243–259.

Symans MD, Constantinou MC. Passive fluid viscous damping systems for seismic energy dissipation. *Journal of Earthquake Technology* 1998; **35**(4): 185-206

Taghavi S, Miranda E. *Response assessment of nonstructural building elements*. PEER Report 2003/05, College of Engineering, University of California, Berkeley September 2003.

Tinsley JC, Fumal TE. Mapping quaternary sedimentary deposits for areal variations in shaking response. *Evaluating Earthquake Hazards in the Los Angeles Region – An Earth-Science Perspective.* US Geological Survey Professional Paper 1360. United States Government Printing Office, Washington 1985.

Trifunac M D, Ivanovic S S, Todorovska M I. Apparent periods of a building. I: Fourier Analysis. *Journal of Structural Engineering* 2001; **127**(5): 517-526.

Trifunac MD, Ivanovic SS, Todorovska MI. *Instrumented 7-storey reinforced concrete building in Van Nuys, California: description of the damage from the 1994 Northridge earthquake and strong motion data.* Report CE 99-02, Department of Civil Engineering, University of California, Los Angeles, California, July 1999.

Trombetti T, Silvestri S. Novel Schemes for Inserting Seismic Dampers in Shear-Type Systems Based Upon the Mass Proportional Component of the Rayleigh Damping Matrix. *Journal of Sounds and Vibrations* 2007; **302:** 486-526.

Tubaldi E, Barbato M, Dall'Asta A. Efficient approach for the reliability-based design of linear damping devices for seismic protection of buildings. *ASCE-ASME Journal of Risk and Uncertainty if Engineering Systems, Part A: Civil Engineering, special issue on Stochastic Dynamics and Reliability Analysis of Structural and Mechanical Systems Subject to Environmental Excitations* 2015; DOI: 10.1061/AJRUA6.0000858.

Tubaldi E, Barbato M, Dall'Asta A. Performance-based seismic risk assessment for buildings equipped with linear and nonlinear viscous dampers. *Engineering Structures* 2014: **78**: 90-99.

Tubaldi E, Ragni L, Dall'Asta A. Probabilistic seismic response assessment of linear systems equipped with nonlinear viscous dampers. *Earthquake Engineering and Structural Dynamics* 2014; DOI: 10.1002/eqe.2462.

Tubaldi E. Dynamic behavior of adjacent buildings connected by linear viscous/visco-elastic dampers. *Structural Control and Health Monitoring* 2015; **22**(8): 1086-1102.

Westermo BD. The dynamics of interstructural connection to prevent pounding. *Earthquake Engineering and Structural Dynamics* 1989; **18**(5): 687-699. DOI: 10.1002/eqe.4290180508.

Whittle JK, Williams MS, Karavasilis TL, Blakeborough A. Comparison of Viscous Damper Placement Methods for Improving Seismic Building Design. *Journal of Earthquake Engineering* 2012; **16**(4): 540-560.

Wiebe L, Christopoulos C, Tremblay R, Leclerc M. Mechanism to limit higher mode effects in a controlled rocking steel frame. 1: Concept, modelling, and low-amplitude shake table testing. *Earthquake Engineering and Structural Dynamics* 2013; **42**: 1053-1068. DOI: 10.1002/eqe.2259.

Wiebe L, Christopoulos C. Mitigation of higher mode effects in base-rocking systems by using multiple rocking sections. *Journal of Earthquake Engineering* 2009; **13**(1): 83-108.

Wu D, Lu X L. Structural performance evaluation of a new energy-dissipation and light-weight rocking frame by numerical analysis and experiment. *Proceedings of the 10th Pacific Conference on Earthquake Engineering Building and Earthquake-Resilient*. Sidney, Australia, 6-8 November 2015.

Xu YL, He Q, Ko JM. Dynamic response of damper-connected adjacent buildings under earthquake excitation. *Engineering structures* 1999; **21**(2): 135-48.

Appendix A

Case studies FEM models

A.1 Van Nuys building

The FEM models describe both the bare Van Nuys building and the coupled system (existing frame plus external dissipative rocking bracing) by using three-dimensional linear elastic elements for the frame as well as for the interior slabs, which are modelled as equivalent beams by adopting the general criteria used in ASCE Standard (ASCE/SEI 41-13). The shell elements are used only to assign loads and they do not interfere with others structural members neither in terms of mass, nor stiffness.

Slabs are 25.4 cm deep at the 2nd floor, 22 cm at the 3rd through 7th floors, and 20.3 cm at the roof. The roof also has lightweight concrete topping varying in thickness between 8.2 cm and 20.3 cm. Figure A-1 shows a view of the three dimensional FEM models, realized by means of SAP2000, of the Van Nuys building as is and in a retrofit configuration.

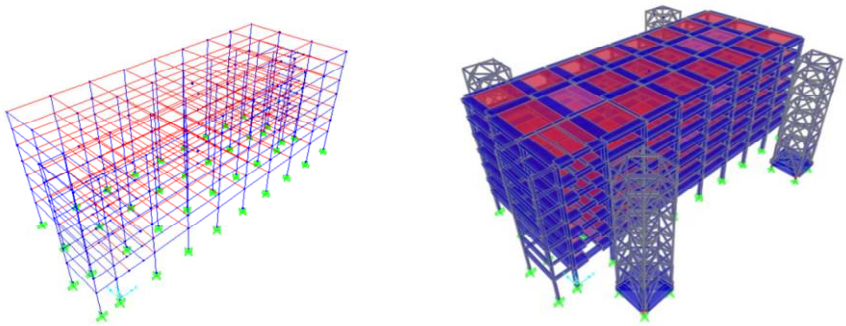

Figure A-1 Van Nuys building FEM models

The planar dimensions and the heights of the building are described in section 3.1.1, while the members size of the external dissipative rocking bracings can be find in section 3.1.5. The properties of the concrete are reported in Table A-1, while Table A-2 shows the members size (beams and columns sections), whose tracking id are reported in Figure A-2.

A three dimensional analysis of the bare frame reveals a period of 1.203 s in the transverse direction and 1.05 s in the longitudinal one.

Table A-1 Van Nuys building concrete properties

element	Compressive strength $f_c^{'}$ [MPa]
columns 1st through 2nd floor	34.5
columns 2nd through 3rd floor	27.6
beams and slabs 2nd floor	27.6
all elements 3rd floor through roof	20.7

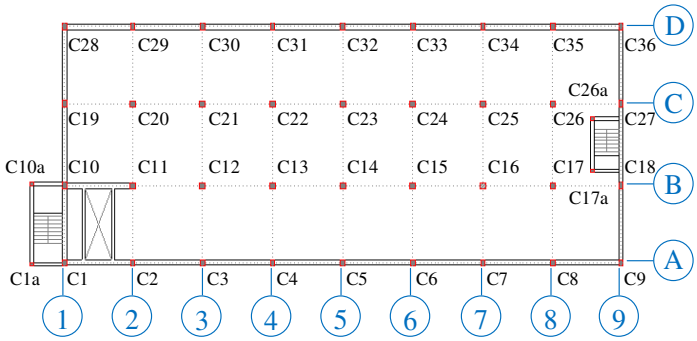

Figure A-2 Van Nuys building members tracking id

Table A-2 Van Nuys building members size

beams tracking id	size [m]	columns tracking id	size [m]
A1 to A9 D1 to D9 2nd floor	0.406x0.762	C11 to C17 C20 to C26 level 1	0.508x0.508
A1 to A9 D1 to D9 3rd through 7th floor	0.406x0.572	C11 to C17 C20 to C26 level 2 trough 7	0.457x0.457
A1 to A9 D1 to D9 roof	0.406x0.559	C1 to C C28 to C36 level 1 trough 7	0.355x0.508
1A to 1D 9A to 9D 2nd floor	0.356x0.762	C10, C18, C19, C27 level 1 trough 7	0.355x0.508
1A to 1D 9A to 9D 3rd through 7th floor	0.356x0.572	C1a, C10a level 1 trough 7	0.305x0.254
1A to 1D 9A to 9D roof	0.356x0.559	C17a, C26a level 1 trough 7	0.305x0.254

A.2 Camerino building

The FEM models of the Camerino building describe both the bare frame and its retrofit configurations by using three-dimensional linear elastic frame elements for beams and columns. The shell elements are used only to assign loads at the roof and they do not interfere with others structural members neither in terms of mass, nor stiffness. Figure A-3 shows a view of the FEM models realized with SAP 2000.

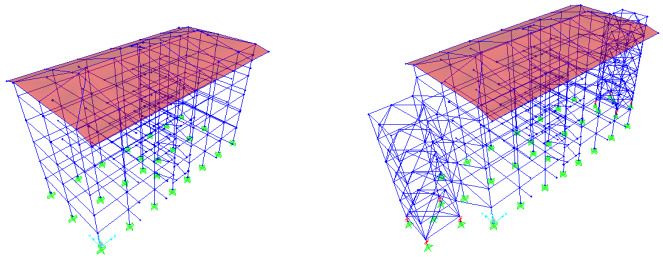

Figure A-3 Camerino building FEM models

The planar dimensions and the heights of the building are described in section 3.2.1, the floors have a thickness of 20 cm (16+4 cm), while the balconies are realized with slabs of equal thickness (20 cm). The perimeter infill walls are realized with a double layer of bricks and a layer of thermal insulator, for a total thickness of 25 cm (8+5+12 cm). The properties of the concrete are reported in Table A-3, while Table A-4 and Table A-5 show the members size of beams and columns, respectively. The members tracking id are reported in Figure A-4. A three dimensional analysis of the bare frame reveals a period of 1.02 s in the longitudinal direction and 0.73 s in the transverse one.

Table A-3 Camerino building concrete properties

level	f_{cm} [MPa]
1st	22.4
2nd through 3rd	18.4
4th through 5th	24.4

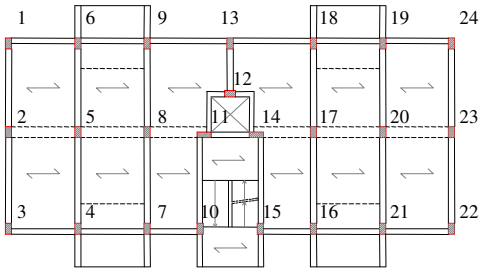

Figure A-4 Camerino building members tracking id

Table A-4 Camerino building beams size

floor	beams tracking id	size [m]
1st	1-2, 5-6, 7-8, 18-17, 19-20, 24-23, 2-3, 5-4, 8-9, 17-16, 20-21, 23-22, 12-13	0.35x0.50
	10-11, 15-14, 11-12, 14-12	0.25x0.50
	1-6, 3-4, 24-19, 22-21, 6-7, 4-9, 19-18, 21-16, 7-13, 18-13, 9-10, 16-15	0.30x0.50
	11-14	0.30x0.20
	2-5, 5-8, 23-20, 20-17, 8-11, 17-14	0.60x0.20
2nd through 5th	1-2, 5-6, 7-8, 18-17, 19-20, 24-23, 2-3, 5-4, 8-9, 17-16, 20-21, 23-22, 12-13	0.30x0.50
	10-11, 15-14, 11-12, 14-12, 1-6, 3-4, 24-19, 22-21, 6-7, 4-9, 19-18, 21-16, 7-13, 18-13, 9-10, 16-15	0.25x0.50
	11-14	0.30x0.20
	2-5, 5-8, 23-20, 20-17, 8-11, 17-14	0.60x0.20
roof	1-2, 24-23, 2-3, 23-22	0.65x0.20
	4-5, 19-20, 9-8, 16-17, 5-6, 20-21, 8-7, 17-18, 12-13	0.30x0.50
	10-11, 15-14, 11-12, 14-12	0.25x1.20
	1-6, 3-4, 24-19, 22-21, 6-7, 4-9, 19-18, 21-16, 2-5, 23-20, 5-8, 20-17, 7-13, 18-13, 9-10, 16-15	0.45x0.20
	8-11, 17-24	0.70x0.20

Table A-5 Camerino building columns size

elevation	columns tracking id	size [m]
1st	1, 2, 3, 4, 5, 6, 7, 8, 9, 13, 16, 17, 18, 19, 20, 21, 22, 23, 24	0.35x0.60
	12	0.60x0.35
	10, 15	0.25x0.60
	11, 14	0.8x0.30
2nd through 5th	1, 2, 3, 4, 5, 6, 7, 8, 9, 13, 16, 17, 18, 19, 20, 21, 22, 23, 24	0.30x0.60
	12	0.60x0.35
	10, 15	0.25x0.60
	11, 14	0.80x0.30
roof	1, 2, 3, 4, 5, 6, 7, 8, 9, 13, 16, 17, 18, 19, 20, 21, 22, 23, 24	0.30x0.60
	12	0.60x0.35
	10, 15	0.25x0.60
	11, 14	0.25x0.30